

Analysis and Synthesis of the Handpan Sound

Eyal ALON

MSc by Research

University of York

Electronics

April 2015

Abstract

Handpan is a term used to describe a group of struck metallic musical instruments, which are similar in shape and sound to the Hang¹, developed by PANArt in January 2000. The Hang is a hand played instrument, which consists of two hemispherical shells of nitrided steel that are fastened together along the circumference. The instrument usually contains a minimum of eight elliptical notes and is played by delivering rapid and gentle strikes to the note areas. Previous studies of the Hang have typically discussed the modes of vibration and sound radiation field when note areas are excited by sinusoidal, hammer, and finger force. It was noted that the manner in which the Hang is played has considerable influence on the spectral content, decay time, and amplitude envelope features produced. This report details the design and implementation of an experimental procedure to record, analyse and synthesise the handpan sound. Four instruments from three different makers were used for the analysis, which gives insight into common handpan sound features, the influence of strike position on spectral content, and the origin of beating phenomena in the signature handpan sound. Subjective listening tests were conducted aiming to estimate the minimum number of vibrational modes required to synthesise the handpan sound.

¹Hang[®] is a registered trademark and should not be used to describe other musical instruments such as handpans [1], nor should the term handpan be used to refer to the Hang[®] [2].

Contents

Abstract	2
Contents	3
List of Figures	6
List of Tables	9
List of Accompanying Material	10
Acknowledgements	11
Declaration of Authorship	12
1 Introduction	13
1.1 Project Aims	15
1.2 Report Structure	15
2 Background	17
2.1 Acoustics of Struck Metallic Percussion Instruments	17
2.1.1 Key Terminologies	18
2.1.1.1 Linear System	18
2.1.1.2 Simple Harmonic Motion	19
2.1.1.3 Beating	20
2.1.1.4 Vibrational Modes	21
2.1.1.5 Wave Propagation	21
2.1.1.6 Periodic and Aperiodic Waveforms	22
2.1.2 Metallophones	24
2.1.3 Cymbals and Gongs	24
2.1.4 Steelpans	28
2.1.5 Hang	32
2.1.6 Handpan Background	35
2.1.7 Summary	39

2.2	Sound Analysis and Synthesis	40
2.2.1	Spectral Techniques in Sound Analysis	40
2.2.1.1	Short-Time Fourier Transform	41
2.2.1.2	Spectrogram	43
2.2.1.3	Peak Detection	46
2.2.2	Decay Rate Estimation	47
2.2.2.1	Energy Decay Relief	48
2.2.3	Synthesis of Musical Instrument Sounds	49
2.2.3.1	Additive and Spectral Modelling Synthesis	50
2.2.3.2	Modal Synthesis	52
2.2.4	Summary	55
2.3	Project Objectives	56
3	Measurement	58
3.1	Experimental Procedure	58
3.1.1	Anechoic Chamber	60
3.1.2	Note-Field Excitation Method	60
3.1.3	Handpan Frame	63
3.1.4	Measurement System	64
3.2	Measuring the Signature Handpan Sound	65
3.3	Summary	68
4	Analysis	70
4.1	Excitation Repeatability	70
4.2	Signature Handpan Sound	74
4.2.1	Signature Vibrational Modes	76
4.2.2	Decay Rates	80
4.2.3	Beating	83
4.3	Note-Field Strike Position	84
4.4	Undamped and Damped Measurements	90
4.4.1	Multiple Instruments	92
4.4.2	Pre-tuned and Post-tuned Instrument	97
4.5	Summary	99
5	Synthesis and Listening Test	101
5.1	Modal Synthesis of the Handpan Sound	101
5.1.1	Estimation of the Impulse Response	103
5.1.2	Estimation of the Excitation Signal	107
5.1.3	Beating Correction	110
5.2	Subjective Listening Test	112
5.2.1	Preparation of Audio	115
5.2.2	Results	115
5.2.3	Discussion	119
5.2.4	Summary	120

6 Conclusion	122
6.1 Project Aims	122
6.2 Project Management	124
6.3 Future Development	124
6.3.1 Further Work	124
6.3.2 Future Work	130
Appendices	132
Appendix A : Data DVD Content	132
Appendix B : Hang Note Analysis	134
Appendix C : Musical Note Frequencies	136
Appendix D : Strike Cross-Correlation	137
Appendix E : Signature Vibrational Modes	138
Appendix F : T60 decay times	143
Appendix G : Beating Rate Estimation	146
Appendix H : Multiple Instruments	148
Appendix I : Listening Test	149
References	155

List of Figures

1.1	Top-side view of a handpan with eight note-fields.	13
2.1	A simple mass-spring vibrating system	19
2.2	Periodic amplitude vibrations due to linear superposition of two simple harmonic vibrations with nearly the same frequency.	20
2.3	Reflection of a transverse pulse on a string with: (a) fixed end; and (b) free end.	22
2.4	Frequency analysis of a string plucked at its centre.	23
2.5	Periodic waveforms of A ₄ (440 Hz) played on a violin, trumpet, flute and oboe.	23
2.6	Vibrational modes of a glockenspiel bar.	25
2.7	Vibrational modes of free edged circular plates.	26
2.8	Harmonic excitation of a gong with increasing force amplitude.	27
2.9	Sections and note placement of a typical tenor steelpan.	28
2.10	Sound spectra of the C ₃ note in the cello steelpan.	31
2.11	A simple Helmholtz resonator.	32
2.12	The Hang. Ding and Gu sides.	33
2.13	Interferograms of the Hang driven at low and high amplitude levels at frequencies near the first three vibrational modes of the F ₃ Ding.	34
2.14	Waveform and spectrogram analysis of a Hang note played at soft and strong levels.	36
2.15	The typical handpan note-field, nodal lines, and sweetspots.	38
2.16	Window functions in the time-domain.	42
2.17	Time and frequency domain analysis of some common window types.	44
2.18	Three spectrograms of a B ₂ handpan note signal.	45
2.19	3D Energy Decay Relief of a B ₂ handpan note signal.	49
2.20	Additive synthesis block diagram.	50
2.21	SMS synthesis block diagram.	52
2.22	Modal synthesis models.	54
3.1	Recording apparatus set-up for the measurement of the signature handpan sound	60
3.2	The torsional spring based Note-Field Excitation Mechanism (NFEM) used for this project's experimental procedure.	61
3.3	Top view of the handpan inside the frame.	64
3.4	Frequency response of the Earthworks M30 measurement microphone.	65

3.5	The magnetic absorbing pads used in the damped configuration.	66
3.6	Time domain waveforms of the undamped and damped F# ₃ signals, struck at the ‘D’ sweetspot.	68
4.1	Alignment of successive strikes delivered to the undamped F# ₃ note-field.	71
4.2	Spectra of time aligned strikes and their difference signal.	73
4.3	Spectrogram and EDR plot of a measured signal.	75
4.4	Peak detection using a single EDR analysis frame for the F# ₃ note-field.	77
4.5	EDCs of detected vibrational modes.	81
4.6	Beating rate estimation.	83
4.7	EDCs of strikes to ‘D’ sweetspot.	85
4.8	EDCs of strikes to ‘O’ sweetspot.	87
4.9	EDCs of strikes to ‘P’ sweetspot.	88
4.10	Undamped and damped spectrogram analysis.	91
4.11	Spectra of the undamped and damped D ₄ note-field signals for Instrument 1, and the D4 difference signal, undamped-damped, Instrument 1.	93
4.12	Spectra of the undamped and damped D ₄ note-field signals for Instrument 3, and the D4 difference signal, undamped-damped, Instrument 3.	95
4.13	Spectra of the undamped A ₄ handpan note-field signals of Instrument 4 struck in the ‘D’ sweetspot, pre and post-tuning.	98
4.14	Spectra of the damped A ₄ handpan note-field signals of Instrument 4 struck in the ‘D’ sweetspot, pre and post-tuning.	99
5.1	Block diagram of the modal synthesis model implemented for this project.	103
5.2	Decay curves of detected peaks, estimated straight line fits, and calculated T60 decay times.	106
5.3	Time domain waveform and spectrum of an NFEM strike delivered to the interstitial area of a handpan.	108
5.4	The attack stage of: (a) the original; (b) the estimated impulse response signal; and (c) the modal synthesis signal.	109
5.5	Spectrograms of the: original, modal synthesis, and modal synthesis with beating correction signals.	111
5.6	The listening test’s interface for a single question showing the question description, reference audio, five audio samples, continuous scales, and text-box for any additional comments.	114
5.7	Boxplots of results for all damped, undamped, and undamped with beating correction synthesised signals.	117
5.8	Boxplots of results for Instrument 3 synthesis.	118
5.9	Boxplots of results for Instrument 1 synthesis.	119
6.1	EDCs of synthesised results with corrected synthesis T60.	126
6.2	‘A’ and ‘C’ frequency weightings.	127
6.3	Waveform and spectrogram analysis of a Hang note played at a strong level.	134
6.4	Waveform and spectrogram analysis of a Hang note played at a soft level.	135
6.5	Musical note names and corresponding frequencies.	136

6.6	Autocorrelation of Strike 1.	137
6.7	Cross-correlation of Strike 1 and Strike 2.	137
6.8	Beating rate of 438 Hz bin for A ₃	146
6.9	Beating rate of 248 Hz bin for B ₃	146
6.10	Beating rate of 373 Hz bin for F# ₃	147
6.11	Beating rate of 374 Hz bin for F# ₄	147
6.12	Spectra of the undamped and damped D ₄ note-field for Instrument 2 struck in the 'D' sweetspot.	148
6.13	Spectra of the undamped and damped D ₄ note-field for Instrument 4 struck in the 'D' sweetspot.	148
6.14	The ethical approval process required prior to commencing the listening tests. Page 1.	149
6.15	The ethical approval process required prior to commencing the listening tests. Page 2.	150
6.16	The ethical approval process required prior to commencing the listening tests. Page 3.	151
6.17	The ethical approval process required prior to commencing the listening tests. Page 4.	152
6.18	The ethical approval process required prior to commencing the listening tests. Page 5.	153
6.19	The subject information statements were filled by each participant prior to completing the listening test. Page 1.	154

List of Tables

3.1	A key of measurements taken for all four instruments investigated in this project.	68
4.1	Highest magnitude peaks, corresponding frequency values, and frequency ratios for all eight note-fields of Instrument 3 (pre-tuned).	78
4.2	All instruments/note groups T60 decay times.	82
4.3	Estimated beating rates for several vibrational modes from undamped Instrument 1. Strikes were delivered to the ‘D’ sweetspot.	84
4.4	Approximate onset times for relevant signature modes from the undamped and damped measurements of the F# ₃ note-field, struck in the ‘D’ sweetspot.	92
4.5	Six identified peaks in the undamped spectrum (above +10 dB in the 115 Hz-1 kHz region), which are not present in the corresponding damped spectrum for the D ₄ note-field of Instrument 1 struck at the ‘D’ sweetspot, as seen in 4.11(b).	94
4.6	Three identified peaks in the undamped spectrum (above +10 dB, in the 130 Hz-1.2 kHz region), which are not present in the corresponding damped spectrum for the D ₄ note-field of Instrument 3 struck in ‘D’ sweetspot, as seen in 4.12(b).	96
4.7	Total energy values in decibel for all D ₄ signals, struck in the ‘D’ sweetspot.	97
6.1	T60 decay times for all three signals displayed in Figure 6.1.	125
6.2	Instrument 1 signature peaks and ratios.	138
6.3	Instrument 2 signature peaks and ratios.	139
6.4	Instrument 3 signature peaks and ratios (post-tuned)	140
6.5	Instrument 4 signature peaks and ratios (pre-tuned).	141
6.6	Instrument 4 signature peaks and ratios (post-tuned).	142
6.7	T60 decay times, Instrument 1	143
6.8	T60 decay times, Instrument 2	143
6.9	T60 decay times, Instrument 3, pre tuning.	144
6.10	T60 decay times, Instrument 3, post tuning.	144
6.11	T60 decay times, Instrument 4, pre tuning.	145
6.12	T60 decay times, Instrument 4, post tuning.	145

List of Accompanying Material

The contents of the accompanying data DVD are as follows:

1. **EyalMSc/EyalMSc.pdf** - A .pdf version of this document.
2. **EyalMSc/README.txt** - This document details the contents of the data DVD, as well as provides key points on how to best review the data.
3. **EyalMSc/Audio/** - A total of 399 audio files including all measurements, listening test audio files, and four audio files of musical compositions performed on the instruments investigated in this project.
4. **EyalMSc/Code/** - Contains all MATLAB code used to complete the analysis, synthesis, and production of thesis figures.
5. **EyalMSc/Listening_test/** - Contains data from all listening test subjects.
6. **EyalMSc/Video/** - Contains a single video, which demonstrates the experimental procedure to record the signature handpan sound in an anechoic chamber.

More detail regarding the content and the best way to review the data DVD is provided in Appendix A, and the **EyalMSc/README.txt** file on the data DVD.

Acknowledgements

To my family, thank you all for the constant love, support, and guidance throughout this project. I am infinitely grateful. Always.

To my supervisor Damian Murphy, thank you for your patience, guidance, understanding, and for providing the best possible conditions for this project's success.

To my thesis advisor, John Szymanski, thank you for our constructive and useful meetings, and for being a source of inspiration to me.

To Maarten van Walstijn, thank you for agreeing to be the external examiner for this project.

To Frank, thank you for the many chats regarding the acoustics of handpans and trees. You have been a great motivator throughout this project and I deeply appreciate your support and friendship.

To Andrew and the AudioLab members, thank you all for the lunch-time entertainment, and assistance with completing the anechoic recordings and listening tests. I will truly miss each and every one of you.

To John, Joe, Alon, and Danielle, thank you for your friendship. We have spent many hours together talking about handpans, life, and the MSc process in general. Thanks for always being there.

Finally, thank you to the inventors of the Hang, and the numerous handpan makers and players that I've communicated with over the course of this project. I am excited and grateful to be able to witness the conception and growth of this instrument and community.

Declaration of Authorship

I, Eyal ALON, declare that this MSc by Research, 'Analysis and Synthesis of the Handpan Sound', and the work presented in it are my own. Any substantial external influences have been attributed in the text. None of the content in this thesis has been published by the author in any form, nor has it previously been presented for an award at this, or any other, university.

Chapter 1. Introduction

Handpan is a term used to describe a group of struck metallic percussion instruments, which are similar in shape and sound to the Hang¹, developed by PANArt Ltd. in Bern, Switzerland in January 2000 [3]. The Hang is a hand played instrument, which consists of two hemispherical shells of nitrated steel that are fastened together along the circumference. The instrument is played by delivering rapid and gentle finger strikes to individual notes. The sound of the Hang has been described as unique, overwhelming, and relaxing, and its worldwide popularity has soared quickly [4]. Due to the extremely high demand and lack of interest in supplying such a demand, PANArt required potential buyers to send hand-written letters, approximately 20,000 of which were received before the cessation of Hang production in December 2013. Despite this, the Hang and handpan instrument family continues to grow. A notable Hang/handpan player is Manu Delago, who has performed with acts such as Björk, Anoushka Shankar, and Shpongle [5].

This report details the design and implementation of an experimental procedure to record, analyse, and synthesise the handpan sound. As seen in Figure 1.1, the handpan typically consists of eight or more notes. Amongst handpan makers and players, the note areas are commonly known as “note-fields” due to the fact that strikes delivered to different areas

¹Hang[®] is a registered trademark and should not be used to describe other musical instruments such as handpans [1], nor should the term handpan be used to refer to the Hang[®] [2].

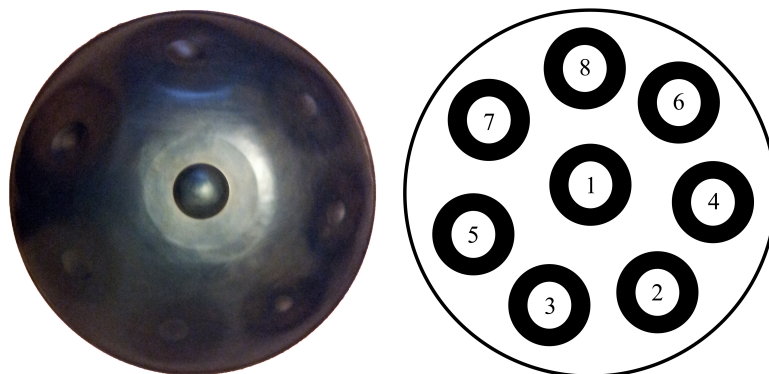


FIGURE 1.1: Top-side view of a handpan with eight note-fields.

of the note-field will emphasize specific harmonics, resulting in a different timbre. In October 2014, there were approximately 80 handpan makers worldwide [6]. Notable handpan makers are Pantheon Steel [7], CFoulke [8], Zen Handpans [9], Saraz Handpans [10], Symphonic Steel [11], and Dave's Island Instruments [12]. An objective standard for classification of handpan quality does not yet exist, however some discussion of this amongst makers and enthusiasts has occurred [13]. Furthermore, no standards exist for handpan making or tuning, so each maker creates instruments with different tools, dimensions, shell and note-field architectures. The accompanying data DVD contains four audio files of musical compositions performed on the instruments investigated in this project².

Previous studies of the Hang have typically discussed the modes of vibration and sound radiation field when note areas were excited by sinusoidal, hammer, and finger force [14, 15]. There are several motivations that justify the research proposed for this project:

- To further the understanding of the handpan's acoustic properties building on this prior work.
- The identification of common handpan sound characteristics. These could be useful for a handpan quality classification scheme. This project investigates a total of four handpans from three different makers. Additionally, two of the four handpans were recorded prior to, and following, tuning by an established handpan maker.
- Highly accurate modelling and virtual prototyping of musical instruments is of interest to physical modelling researchers, instrument makers and musicians [16]. This project does not aim to develop a fully functioning virtual handpan instrument, however the findings may be used as a basis for the development of such a virtual instrument.
- Advancing the field of musical instrument acoustics analysis and synthesis.

²Can be found in the following directory on the DVD: **EyalMSc/Audio/**.

1.1 Project Aims

The aims of this project are as follows:

1. To design and implement an experimental procedure to record the handpan sound, and estimate note coupling.
2. To demonstrate identification of the signature handpan sound including vibrational modes for individual notes, corresponding decay rates, and beating characteristics.
3. To estimate the minimum number of vibrational modes required for synthesis of the handpan sound.

In Section 4.4, some of the amplitude modulation characteristics present in the handpan sound are shown to be due to note coupling. This note coupling results in beating, which manifests as amplitude modulations. Further detail regarding beating is provided in Chapter 2. This report will cover all of the work required to develop a suitable experimental procedure, analysis, and synthesis system to achieve the project aims.

1.2 Report Structure

Chapter 2 starts by providing an overview of common acoustic properties and relevant prior research related to the analysis of struck metallic percussion instruments, followed by the history and background of the handpan. Then the uses of spectral techniques in sound analysis (including the short-time Fourier transform, spectrogram analysis, and peak detection) are detailed. This chapter concludes with an overview of relevant musical instrument synthesis methods, and presentation of the project objectives.

Chapter 3 covers the design and implementation of a suitable experimental procedure for the measurement of the signature handpan sound.

Chapter 4 presents an analysis of the results from the experimental procedure outlined in Chapter 3. Initially, the repeatability of the note-field excitation mechanism is assessed.

Then, the recorded handpan notes are analysed in order to extract the frequencies, decay rates, and beating rates of signature vibrational modes. Finally, spectrograms, EDR plots, and frequency spectra of measurements are displayed and analysed in order to estimate the significance of strike position to a given note-field, and the coupling between individual notes.

Chapter 5 first presents an explanation of the modal synthesis technique used, based on the signature vibrational modes and corresponding decay rates identified in Chapter 4, and an experimentally measured excitation signal. Then, results from a listening test conducted in order to assess the quality of the synthesised handpan sounds are detailed.

Chapter 6 concludes the report with a discussion of the success of meeting the project aims and objectives, a review of the project management process, and detail of potential future development of the project work.

Chapter 2. Background

In order to develop and implement a suitable experimental procedure, and to make use of suitable analysis and synthesis methods it is required to have knowledge of the theories and techniques underlying the available options. Furthermore, it is also necessary to review prior work done in the field of musical instrument analysis and synthesis. This chapter starts by providing an overview of common acoustic properties and relevant prior research related to the analysis of struck metallic percussion instruments, followed by the history and background of the handpan. Then the role of spectral techniques in sound analysis such as the short-time Fourier transform, spectrogram analysis and peak detection are detailed. This chapter concludes with an overview of relevant musical instrument synthesis methods, and presentation of the project objectives.

2.1 Acoustics of Struck Metallic Percussion Instruments

According to the Hornbostel-Sachs classification system, all musical instruments can be grouped into one of the following five categories according to how they produce sound [17]:

- Idiophones: Produce sound by vibration of the instrument body.
- Membranophones: Produce sound by vibration of a membrane.
- Chordophones: Produce sound by vibration of a string.
- Aerophones: Produce sound by vibration of an air column.
- Electrophones: Produce sound electronically.

Instruments in any of these five families can further be classified according to the perceived sensation of pitch [18]. Pitch is a subjective measure related to the periodicity

of a signal. Generally, a periodic signal will convey a stronger sensation of pitch, whereas an aperiodic signal will not [19]. The Hang, which is classified as a percussion vessel of the directly struck idiophone type [20, 21], produces sound mainly by the actual body of the instrument vibrating, rather than a string, membrane, or column of air. Like the Hang, the handpan can also be played in a manner that produces sounds with a weaker sensation of pitch, which will be covered in Section 2.1.6. Instruments like the cymbal, hi-hat, slit gong, steelpan, and udu belong to the same family of percussion. An understanding of the common acoustic properties of struck metallic percussion instruments and knowledge of relevant prior research are crucial for designing and implementing an experimental procedure to produce, measure, and analyse the handpan sound.

2.1.1 Key Terminologies

Before considering the relevant literature, some key concepts that are important to the context of this thesis will be introduced:

2.1.1.1 Linear System

This can be defined as a system, $f(x)$, which satisfies the properties of superposition and homogeneity:

$$f(x_1 + x_2) = f(x_1) + f(x_2) \quad (2.1)$$

$$f(k \cdot x) = k \cdot f(x) \quad (2.2)$$

Equation 2.1 describes the property that a linear system's output can be decomposed into contributions from individual inputs. Equation 2.2 describes the scaling property, which says that if the system's input is scaled by a factor of k , the output will also be scaled by a factor of k . Different mechanical elements constituting a given musical instrument might behave approximately as linear systems [22], however in some instruments such as the steelpan, non-linear processes are required to describe the system accurately [23].

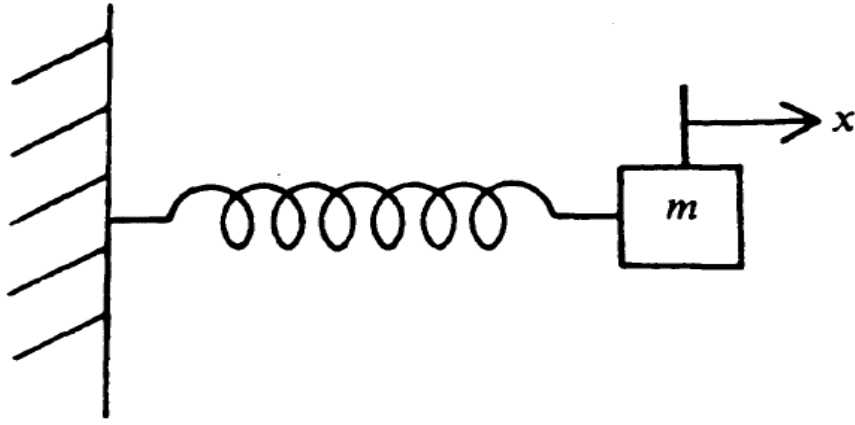


FIGURE 2.1: A simple mass-spring vibrating system. From [22] p. 4, Fig. 1.1.

The output of an linear time-invariant (LTI) system, $y_{li}(t)$, will be identical regardless of the time that the input, $x_{li}(t)$, is applied: If $y_{li}(t) = x_{li}(t)$ then $y_{li}(t - T_{li}) = x_{li}(t - T_{li})$, where T_{li} is a time delay in seconds.

2.1.1.2 Simple Harmonic Motion

Simple harmonic motion can be described as a sinusoidal function of time t [22]:

$$x(t) = A_{shm} \cdot \sin(2\pi f_{shm}t) \quad (2.3)$$

Where A_{shm} is peak amplitude of the motion, and f_{shm} is the vibration frequency. The period of the motion is given by: $T_{shm} = \frac{1}{f_{shm}}$. A mass-spring system can vibrate with simple harmonic motion, assuming that the spring operates within its linear operational limits, and that no energy is lost during vibration [22]. The equation of motion for the mass-spring system displayed in Figure 2.1 can be obtained by combining Hooke's law, $F = -Kx$ with Newton's second law, $F = m\ddot{x}$:

$$m\ddot{x} = -Kx \quad (2.4)$$

Where F is the restoring force, x is displacement, m is the mass, and K is the spring constant or stiffness of the spring. In this case, the system is free to vibrate only in the x direction. The natural frequency of this mass-spring system can be calculated by:

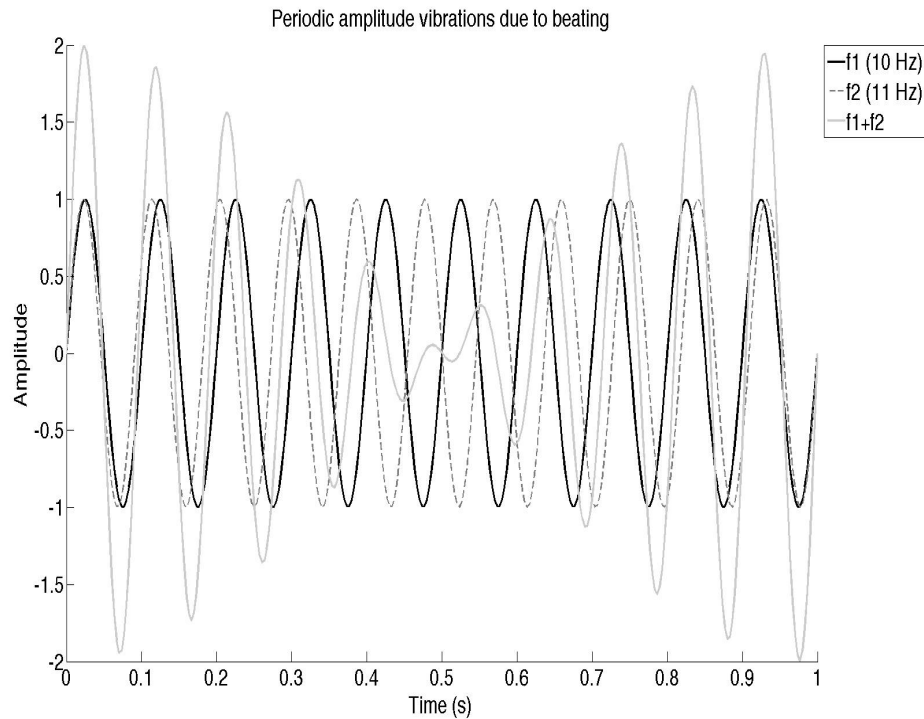


FIGURE 2.2: Periodic amplitude vibrations due to linear superposition of two simple harmonic vibrations with nearly the same frequency ($f_1 = 10$ Hz, $f_2 = 11$ Hz). The amplitude vibration rate of the summation signal ($f_1 + f_2$) is 1 Hz.

$f_0 = \frac{1}{2\pi} \sqrt{\frac{K}{m}}$. Thus, simple harmonic motion of this mass-spring system produces a pure tone. A pure tone consists of a single frequency component, whereas complex tones consist of numerous frequency components. The human hearing system's frequency range is usually quoted as 20 Hz-20 kHz [19].

2.1.1.3 Beating

A linear combination of two simple harmonic vibrations having the same frequency, will result in another simple harmonic vibration with the same frequency. Linear superposition of two simple harmonic vibrations with nearly the same frequency leads to periodic amplitude vibrations or beating, as can be seen in Figure 2.2. The rate of amplitude vibration is equal to the absolute difference between both frequency values [22]. For pure tones, which consist of a single frequency component, beats are usually heard when the frequency difference is less than 12.5 Hz [19].

2.1.1.4 Vibrational Modes

The mass-spring system displayed in Figure 2.1, consists of a single mass and spring and is free to vibrate only in the x direction, producing a single natural mode of vibration with frequency $f_0 = \frac{1}{2\pi} \sqrt{\frac{K}{m}}$ Hz. An additional vibrational mode is added to the system for each mass. Furthermore, if the mass-spring system is allowed to move in a plane, enabling longitudinal and transverse vibrations, an additional mode of vibration is added for each mass. These modes of vibration are known as normal modes in the sense that their vibration is independent of each other and orthogonal [22]. Thus a mass-spring system that is allowed to move in three dimensions, and contains three masses, will have nine normal modes of vibration. For metallic instruments like the steelpan, Hang, and handpan, transverse vibrations are most acoustically relevant [23].

2.1.1.5 Wave Propagation

A vibrating uniform string with linear density can be modelled using a mass-spring system with numerous mass elements, which are free to move in a plane resulting in transverse and longitudinal vibrational modes [22]. The nature of these normal modes depend upon the mass of the string, its length, the tension applied and the end (boundary) conditions. Thus, the motion of transverse waves in a vibrating string can be described using the following equation:

$$\frac{\partial^2 y}{\partial t^2} = \frac{T}{\mu} \frac{\partial^2 y}{\partial x^2} = c^2 \frac{\partial^2 y}{\partial x^2} \quad (2.5)$$

where y is the vertical spatial axis, x is the horizontal spatial axis, t is time, μ is linear density, T is tension, and c is wave velocity. d'Alembert's travelling waves provides a general solution to this equation:

$$y = f_1(ct - x) + f_2(ct + x) \quad (2.6)$$

where $f_1(ct - x)$, and $f_2(ct + x)$ represent waves travelling to the right and left of the string respectively, with the same velocity c . The behaviour of reflections at the ends

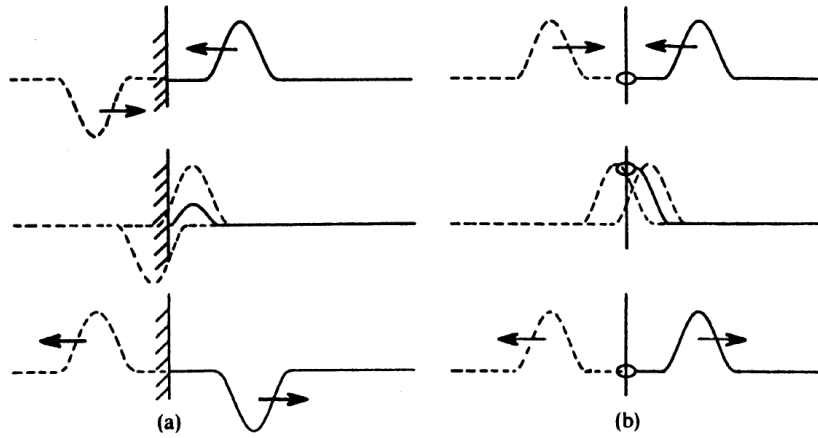


FIGURE 2.3: Reflection of a transverse pulse on a string with: (a) fixed end; and (b) free end. The reflection in (a) is out of phase, unlike the reflection in (b), which is in phase. From [22], p. 38, Fig. 2.4.

of the strings will depend upon the boundary conditions. As seen in Figure 2.3(a), when the end of a string is fixed, the reflection due to an incoming pulse will be out of phase. 2.3(b) shows that the reflection due to an incoming pulse on a free-ended string will be in phase. Standing waves on an ideal vibrating string will occur at frequencies corresponding to a multiple of half wavelengths of the string length [22]. If the string length is L cm, standing waves will occur at frequencies with wavelengths: $\frac{L}{2}$, L , $\frac{3L}{2}$, $2L$, and so on. This is demonstrated in Figure 2.4, which shows standing waves for the first four odd harmonics of a plucked string. Several of the nodal and antinodal points, which correspond to the points of minimum and maximum string displacement respectively for a given vibrational mode, are highlighted for the 3rd harmonic. Plucking the string at either of the nodal points will potentially result in minimal vibration (at frequency = $3f_1$ in the case of the 3rd harmonic), whereas plucking at the antinodal point will potentially result in maximum vibration [22].

2.1.1.6 Periodic and Aperiodic Waveforms

Fourier analysis states that a periodic waveform can be represented as a weighted sum of numerous sinusoidal frequency components [19]. Generally, periodic waveforms convey a strong sensation of pitch, whereas aperiodic waveforms do not. Figure 2.5 displays some periodic waveforms of A_4 (440 Hz) played on a violin, trumpet, flute

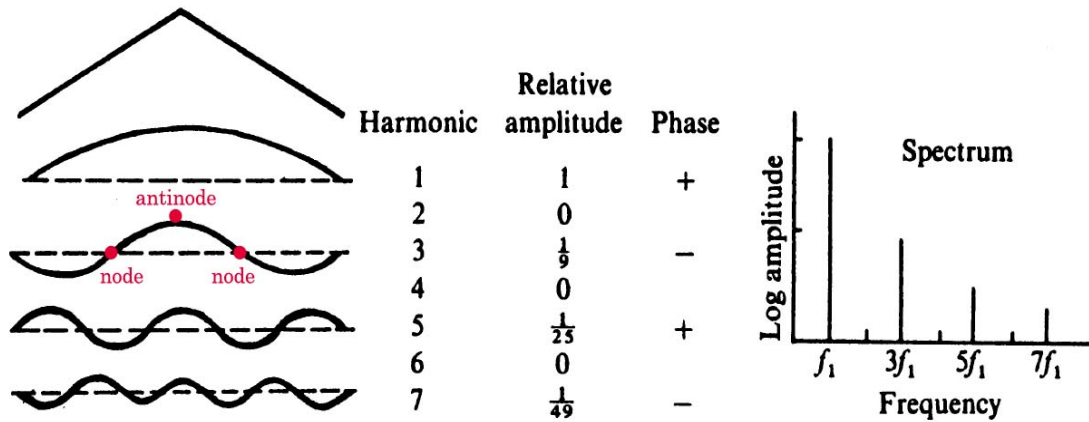


FIGURE 2.4: Frequency analysis of a string plucked at its centre, where the odd-numbered modes of vibration sum to give the initial shape of the plucked string. Adapted from [22], p. 41, Fig. 2.5.

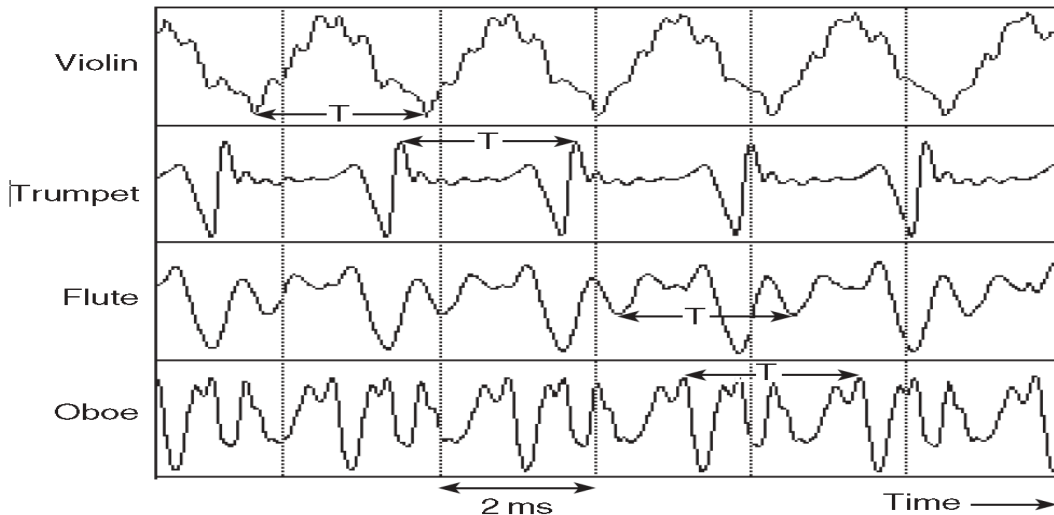


FIGURE 2.5: Periodic waveforms of A_4 (440 Hz) played on a violin, trumpet, flute and oboe, where T indicates one period or cycle of the waveform, which in this case is: $T = \frac{1}{440} = 2.3$ ms. From [19]

and oboe, where T indicates one period or cycle of the waveform, which in this case is: $T = \frac{1}{440} = 2.3$ ms. Individual frequency components of the waveform are known as partials and integer related partials are known as harmonics. Figure 2.4 shows the frequency analysis of a string plucked at its centre, where the odd-numbered modes of vibration (with corresponding odd-numbered harmonic partials shown in the spectrum) sum to give the initial shape of the plucked string.

2.1.2 Metallophones

A metallophone is a musical instrument consisting of tuned metal bars, which are usually struck with a mallet to produce sound [22]. Despite the hand-played nature of the handpan, metallophones are a good starting point to learn about the sound generation mechanism of the handpan as they are also classified as directly struck metallic idiophones. Unlike a membrane or string, which require manual tension to enable vibration, the elastic forces within a solid bar or rod are enough to supply the necessary restoring force to enable vibration [18]. The glockenspiel is a metallophone that consists of several free ended steel bars and is usually played with brass or hard plastic mallets. The mass, shape, and hardness of the mallet can greatly influence the timbre of the glockenspiel. When struck with a hard mallet, this idiophone produces a clear, ringing metallic sound. The glockenspiel bar's fundamental frequency range is normally G_5 (784 Hz) - C_8 (4186 Hz). Thickness of the bar will have an effect on its vibrational behaviour. As an example, frequencies of higher modes in a thick bar are decreased when compared to a thin one [22]. The speed of transverse waves in a bar is frequency dependent, so vibrational mode frequencies are inharmonic and depend upon the boundary conditions, which can be free, clamped, or hinged. Despite the inharmonicity of the glockenspiel's overtones, their role in determining timbre is minor as they decay quickly, and occur in frequency ranges that are less critical for pitch (musical note) discrimination. Figure 2.6 shows the transverse, torsional and longitudinal vibrational modes of a glockenspiel bar.

2.1.3 Cymbals and Gongs

While the metallophone is a good starting point to review the basics of sound generation in struck metallic percussion instruments, the structure of the handpan is much more similar to a plate or shell, like cymbals and gongs. A plate may be considered a two-dimensional bar, which can transmit vibrations as compressional, shear, torsional, or bending waves and can have three different boundary conditions: free, clamped, or hinged. Bending (flexural) waves are most significant for sound radiation in plates [22]. Simple shells may be formed of hollow cylinders, spheres or sections cut from

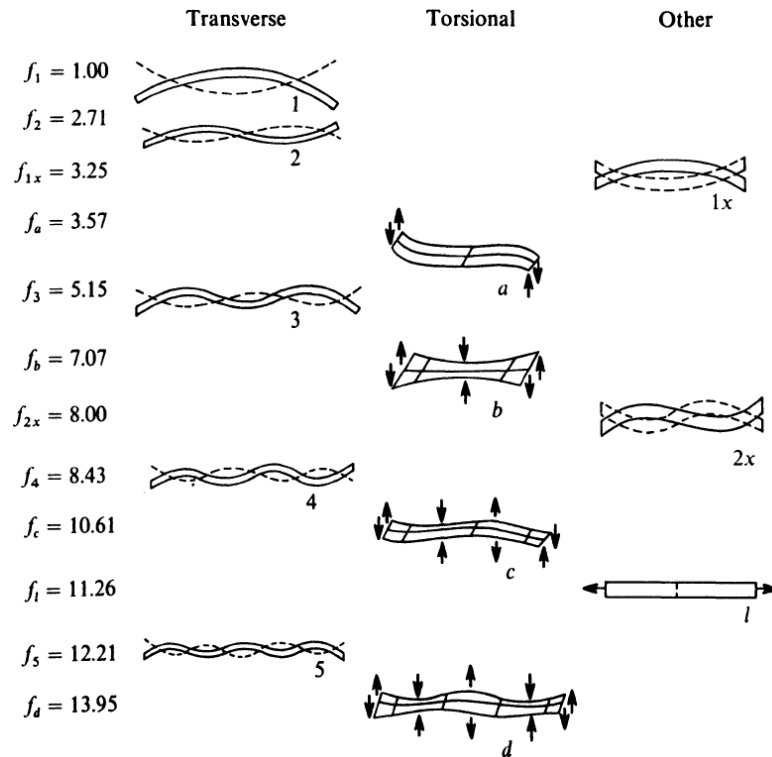


FIGURE 2.6: Vibrational modes of a glockenspiel bar. Relative frequencies for a C_6 bar are given. From [22], p. 626, Fig. 19.1.

these. Generally, vibrational modes of shells involve a combination of longitudinal and transverse motions, where only the transverse vibrations are acoustically relevant [22].

Unlike the glockenspiel, which conveys a strong sensation of pitch when played, the sensation of pitch varies for different types of cymbals [22]. Cymbals are normally made of bronze, and can range from 20 cm to 74 cm in diameter. The low frequency vibrational modes of the cymbal are similar to those of a flat circular plate with free edges, as seen in Figure 2.7. At higher frequencies, vibrational mode identification is not straightforward as they often mix with one another.

The principal modes of vibration and the effect of internal stress in flat and curved plates were investigated by measuring mechanical admittance and performing modal analysis [24]. The research concluded that an increase in frequency is observed when the excitation amplitude is increased for a flat plate under no radial stress.

In another study, at least three prominent features were observed in the cymbal sound [18]:

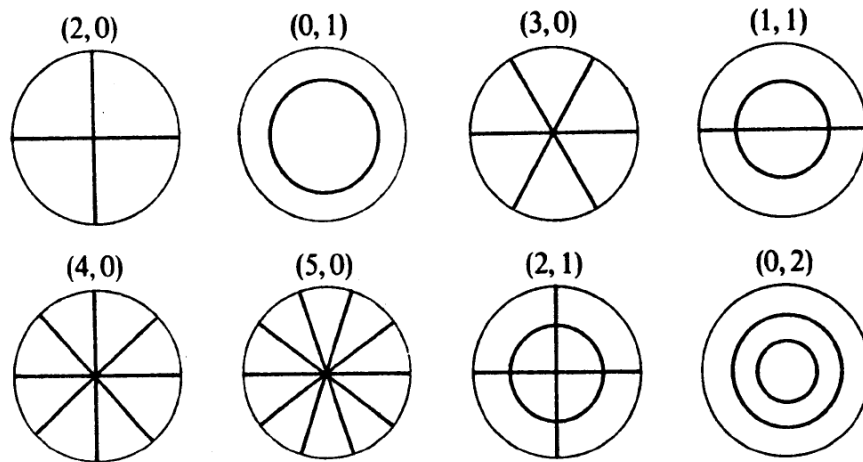


FIGURE 2.7: Vibrational modes of free edged circular plates. The mode number (n, m) gives the number of nodal diameters and circles, respectively. Adapted from [22], p. 79, Fig. 3.8.

1. The transient strike sound.
2. The build-up of peaks around 700 Hz-1 kHz immediately after the transient and during the first 10-20ms.
3. The after-sound in the 3-5 kHz range that dominates the sound around one second after striking.

Gongs are usually cast of bronze with a deep rim and protruding dome [22]. Gongs used in symphony orchestras usually convey some sensation of pitch and range from 0.5-1m in diameter. When struck near the centre with a large mallet the sound builds up and can last for a number of seconds. In a study on the vibrational behaviour of orchestral gongs and cymbals, two major processes occurring in the sound of cymbal-like gongs were identified [25]:

1. Frequency multiplication due to coupling between tensional and shear stress, leading to the transfer of energy from low to high frequency modes after a characteristic time delay.
2. Splitting of major vibrational modes into components having fractional frequency ratios and into chaotic vibrations.

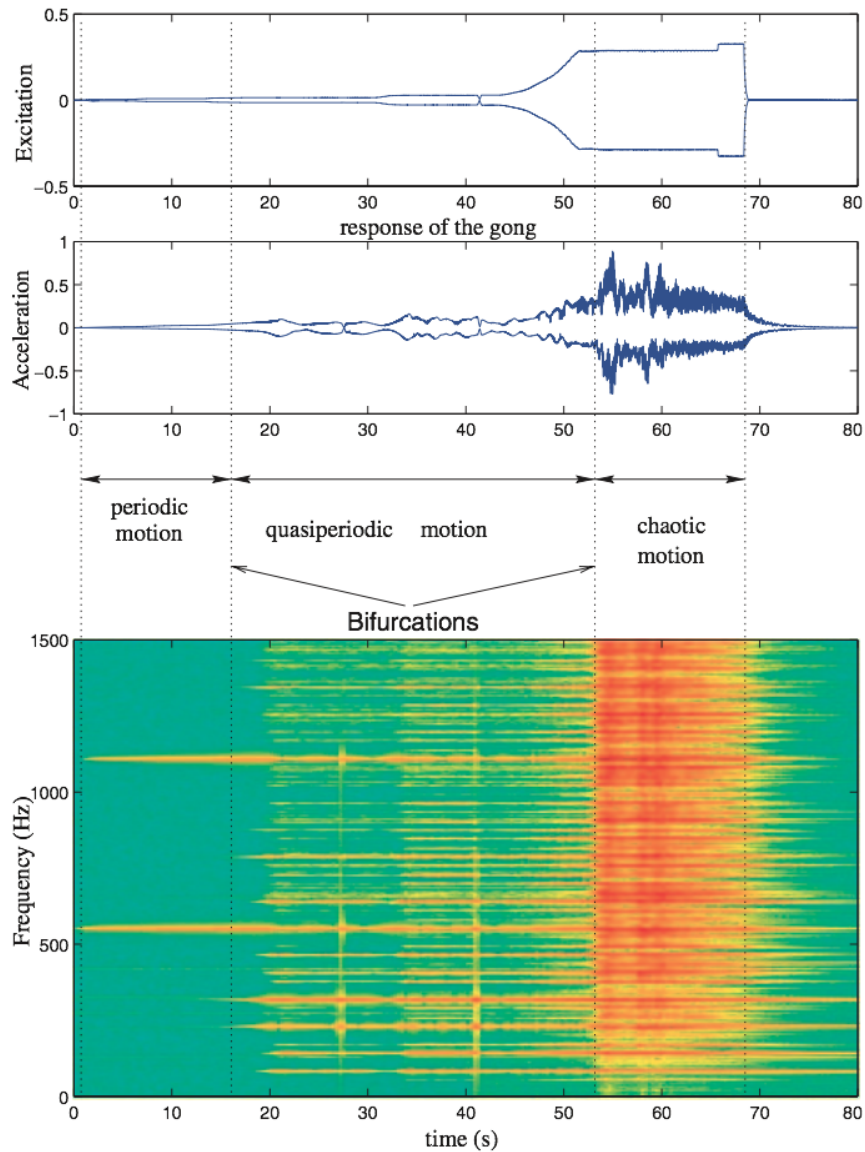


FIGURE 2.8: Harmonic excitation of a gong with increasing force amplitude. From [26]

The process that leads to chaotic vibrations in the gong was investigated by harmonic excitation with increasing force amplitude [26]. The stages that lead to chaotic behaviour can be seen in Figure 2.8, which shows periodic motion for low force amplitude, quasi-periodic motion for medium force amplitude, and chaotic motion for large force amplitude. This research showed that the energy transfer between modes is a consequence of quadratic non-linearity due to the curvature of the shell.

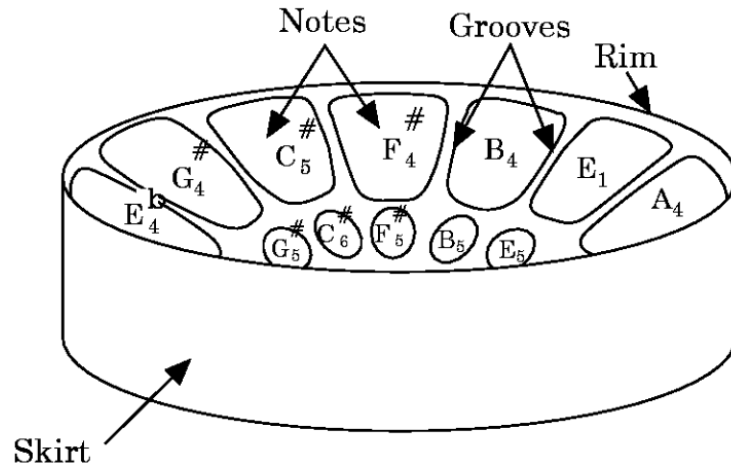


FIGURE 2.9: Sections and note placement of a typical tenor steelpan, showing notes, grooves, rim, and skirt. From [27]

2.1.4 Steelpans

Structurally and spectrally, the steelpan is probably most closely related to the handpan. The first steelpans were made in Trinidad and Tobago using leftover 55-gallon oil drums left by the British navy after the end of World War 2 [22]. Figure 2.9 shows the general sections and note layout of a typical single tenor (lead) steelpan [27]. Steelpans are produced in a variety of musical ranges from the bass steelpan ($G_1(48.9 \text{ Hz}) - G_3(196 \text{ Hz})$) to the single tenor steelpan ($D_4(293 \text{ Hz}) - F_6(1396 \text{ Hz})$), and are usually played with soft rubber-tipped sticks [23]. In Achong's book, "Secrets of the Steelpan" the instrument is described as a shell-like structure, where each note forms a sub-structure of a complex array of shallow shells, each surrounded (bounded) by the stiffer internote sections [23]. Thus, the connection of each note to the rest of the pan face will be characterized by a set of hidden boundary conditions describing the note edges, and by unknown compressive stresses. Steelpan makers usually tune the first overtone to twice the value (octave) of the fundamental frequency, and the second overtone to three (perfect fifth) or four times (double octave) the fundamental on a individual steelpan note. In other words, the first three principal modes of vibration for each steelpan note are tuned to produce a 1:2:3 frequency ratio.

The steelpan tone may be divided into two time domain phases: the impact phase and the free oscillation phase [23]. The impact phase describes the time when the stick remains

in contact with the note, which usually lasts less than a period of the fundamental vibrational mode of the note. The free oscillation phase starts at the moment the stick leaves the pan until the end of the tone. This phase is characterised by a fast rise in amplitude, followed by slow amplitude modulations and decay. The spectra of steelpan are rich in harmonic overtones, which appear to have three physical origins [22]:

1. Radiation from higher modes of vibration of a given note area.
2. Radiation from nearby notes whose frequencies are harmonically related to the struck note.
3. Non-linear motion of the note area.

An analysis of steelpan notes showed localization of the vibrational motions to within elliptical note regions on the pan [27]. When a steelpan note is struck softly, the amplitude structures over time are relatively simple [23]. However, due to the non-linear nature of the steelpan, impacts with increased force will not only proportionally increase the spectral amplitude but will also excite additional spectral components, influencing the perceived timbre [28]. These features are consistent with non-linear mode coupling and interactions [23]. The degree of non-linear mode coupling within a note (via internal resonance) affects the amount of energy transfer between the modes, changing their relative amplitudes. Energy is transferred from low to high modes, but can also be transferred back from high to low modes. Additionally, upwards and downwards pitch glides over the duration of the steelpan tone have been reported [23]. During the initial attack phase of a strongly struck steelpan note, the first mode begins below the set frequency and then rises towards the correct value. This was interpreted as soft spring behaviour of the material which lowers the vibrational frequency due to large amplitude excursions during the transient.

In another study, sand bags were used to dampen the entire steelpan besides the struck note area. Peaks up to the tenth harmonic were still observed in the resulting spectra [22]. Some individual steelpan notes are tuned to operate in sympathetic vibration, with the octave of one note being excited when the lower frequency fundamental is played on a different note [23]. Sympathetic pairs of this type are also known as ‘Marshall-Pairs’,

and in some steelpan are highly dependent on this note-note coupling for tonal quality and structure. Note-note coupling was investigated by placing two velocity transducers on a Marshall-pair of notes and exciting each note, in turn, by stick impact. Despite the coupling of these notes, reciprocity does not apply in the sense that the tonal structures and degree of coupling is quite different depending on which note was struck. Thus, it was concluded that the non-linear coupling that exists between substructures on the instrument is the driving mechanism for sympathetic pairs [23].

As mentioned in Section 2.1.1.5, delivering a strike to the antinodal point of a particular vibrational mode will potentially maximise vibration of this mode [22]. In previous research of the steelpan it was found that vibrational modes of an individual note area can be de-emphasised by stick impacts made along the corresponding nodal lines [23]. Striking at the antinodes (known as “sweetspots”) will emphasise a corresponding vibrational mode. Figure 2.10 shows the sound spectra produced when striking the C \sharp_3 note in different positions of the note area [29]. This demonstrates the influence of strike position on the amplitude and spectral structures of the steelpan sound, as predicted by the theory of normal modes [22]. Comparing 2.10(a), 2.10(b), and 2.10(c) which are spectra produced by normal playing strength at the centre of the note area (marked by a red square), at 90°, and at 180° respectively, it can be seen that the position of the strike has a strong influence on the timbre produced, which is most noticeable in the 100 Hz-400 Hz and 500 Hz-1.4 kHz regions. Additionally, comparing 2.10(a) and 2.10(d), where the latter is the spectrum produced from striking weakly at the centre of the note area, it can be seen that the strength of the strike has an influence on relative amplitudes where most of the content above 400 Hz is attenuated.

The steelpan’s skirt (as seen in Figure 2.9) can also influence the timbre of the instrument. The bass steelpan’s skirt can create an air cavity that can act as a Helmholtz resonator [29]. Figure 2.11 displays a Helmholtz resonator, where S is the area of the cavity opening, L is the length of the cavity neck, and V is the volume of the cavity. The Helmholtz resonance frequency of such a gas container can be calculated by [30]:

$$f_H = \frac{c}{2\pi} \sqrt{\frac{S}{VL}} \quad (2.7)$$

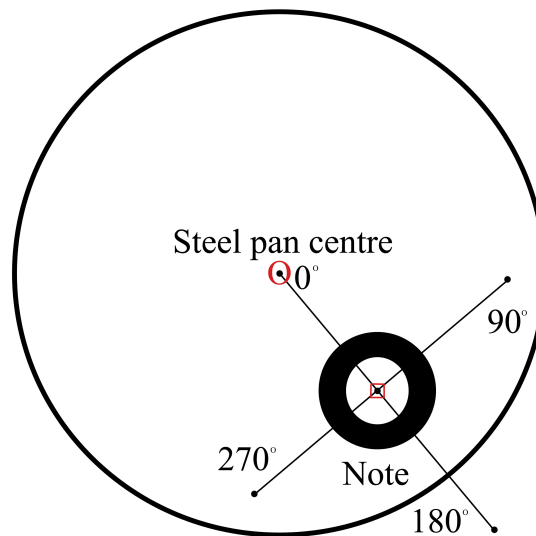
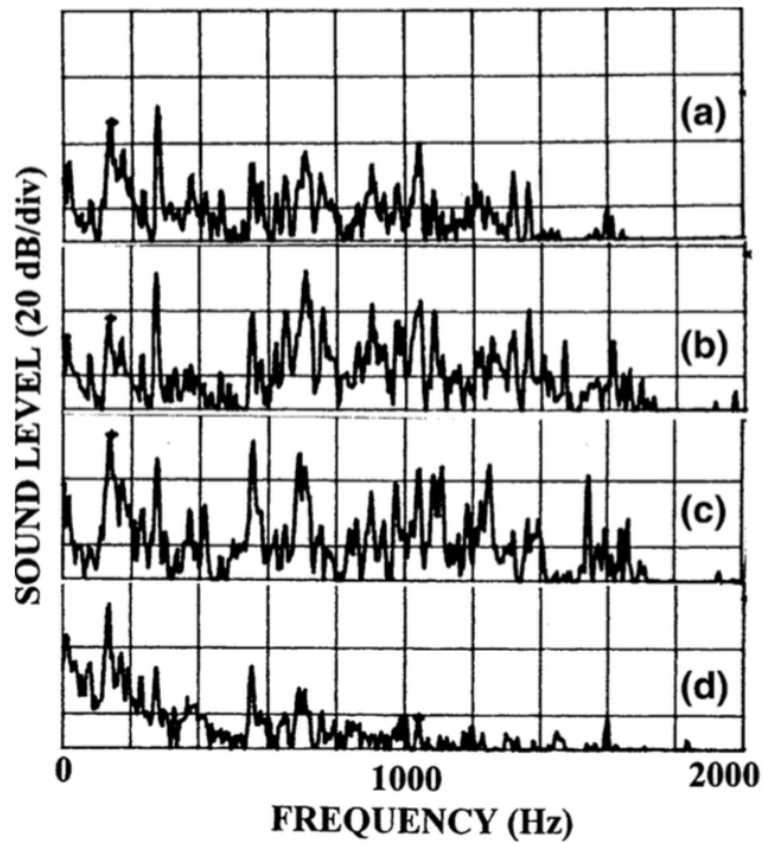


FIGURE 2.10: Sound spectra of the $C\sharp_3$ note in the cello steelpan, viewing the note area as a compass with 0° pointing towards the centre of the pan (marked with a red circle): (a) normal playing strength near the centre of the note area (marked with a red square); (b) striking at 90° ; (c) striking at 180° ; (d) weak strike near the centre of the note area.

From [29]

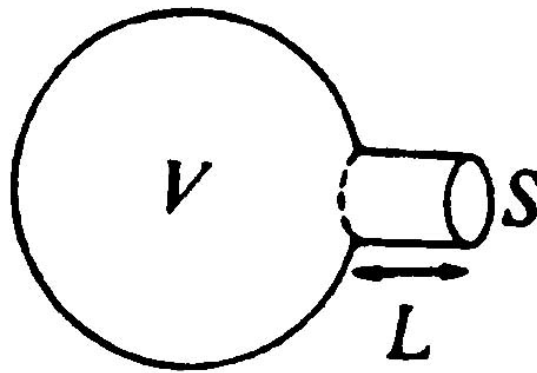


FIGURE 2.11: A Helmholtz resonator, where S is the area of the cavity opening, L is the length of the cavity neck, and V is the volume of the cavity. Adapted from [22], p. 14, Fig. 1.7.

Where c is the velocity of sound in the gas container. It should be noted that Equation 2.7 can only be used to roughly approximate the Helmholtz resonance frequency of gas containers that are similar in shape to the resonator displayed in Figure 2.11. In the case of the steelpan, the air cavity confined by the skirt and pan might be better described as a type of neckless Helmholtz resonator. For a neckless Helmholtz resonator, L can be estimated by using the “end correction” of a flanged tube to determine the effective length of the neck [22]. Thus, the shape of the steelpan cavity, and effective length of the neck should be considered if a more accurate estimation of the steelpan resonance frequency is desired. Interaction between the Helmholtz resonance frequency of the bass steelpan and some of the played notes can cause a split in the lowest frequency peak [29].

2.1.5 Hang

The Hang, developed by Felix Rohner and Sabina Schärer of PANArt Ltd. in Bern, Switzerland in January 2000 [3] is a hand-played instrument made of nitrided steel and is classified as a percussion vessel [20]. The instrument consists of two hemispherical shells, fastened together [14]. For 25 years prior to developing the Hang, PANArt manufactured steelpans and other steel based musical instruments, as well as collaborating with scientists and engineers to research and better understand the complexities of the

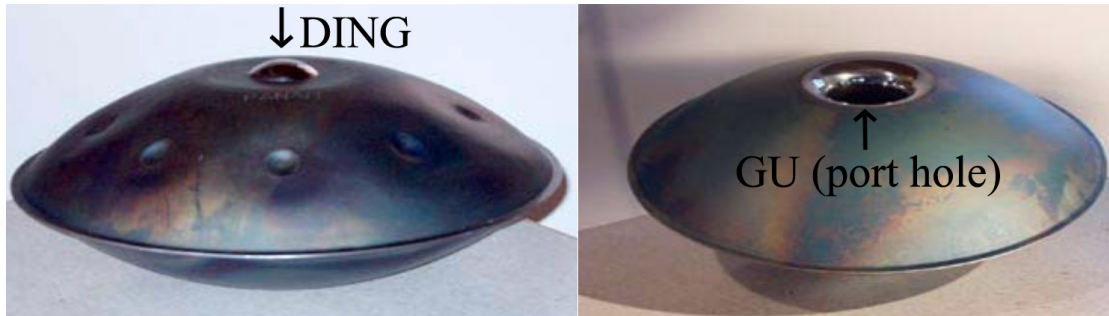


FIGURE 2.12: The Hang. Ding and Gu sides. Adapted from [14]

tuning process. PANArt’s innovation of playing harmonically tuned steel with the hands was the reason for naming their creation as hang, which means “hand” in Bernese dialect.

Figure 2.12 shows both sides of the Hang. PANArt named the central note of the Hang “Ding” (hence the note side being known as the Ding side), and they named the port hole “Gu” (hence the port hole side being known as the Gu side). Similar to steelpan notes, the frequencies produced from the Hang’s principal modes of vibration in each note area have a 1:2:3 ratio [15]. The Hang sound also exhibits a spectral peak at approximately 85 Hz, which is associated with the instrument’s Helmholtz resonance frequency. It is not clear what the area of the cavity opening and effective length of the neck would be in the case of the Hang, due to the inward curvature of the cavity opening. Furthermore, varying the spacing of the player’s knees can influence the tuning of the Helmholtz resonance frequency by effectively changing the acoustical “length” of the neck [14]. Thus, as in the case of the steelpan, Equation 2.7 can only be used to roughly approximate the Helmholtz resonance frequency of the Hang.

Some steelpan and Hang note areas have a similar elliptical shape. One of the most obvious visual differences is the dome (known as “dimple” to handpan enthusiasts) that is present in the centre of each note area. The dome is responsible for creating circular symmetry of the higher vibrational modes around the dome, while minimizing the influence on the lowest three vibrational modes of the note area [28].

Previous studies of the Hang have typically discussed the modes of vibration and sound radiation field when note areas are excited by sinusoidal, hammer, and finger force. Sound intensity measurements and modal analysis were performed on the Hang using

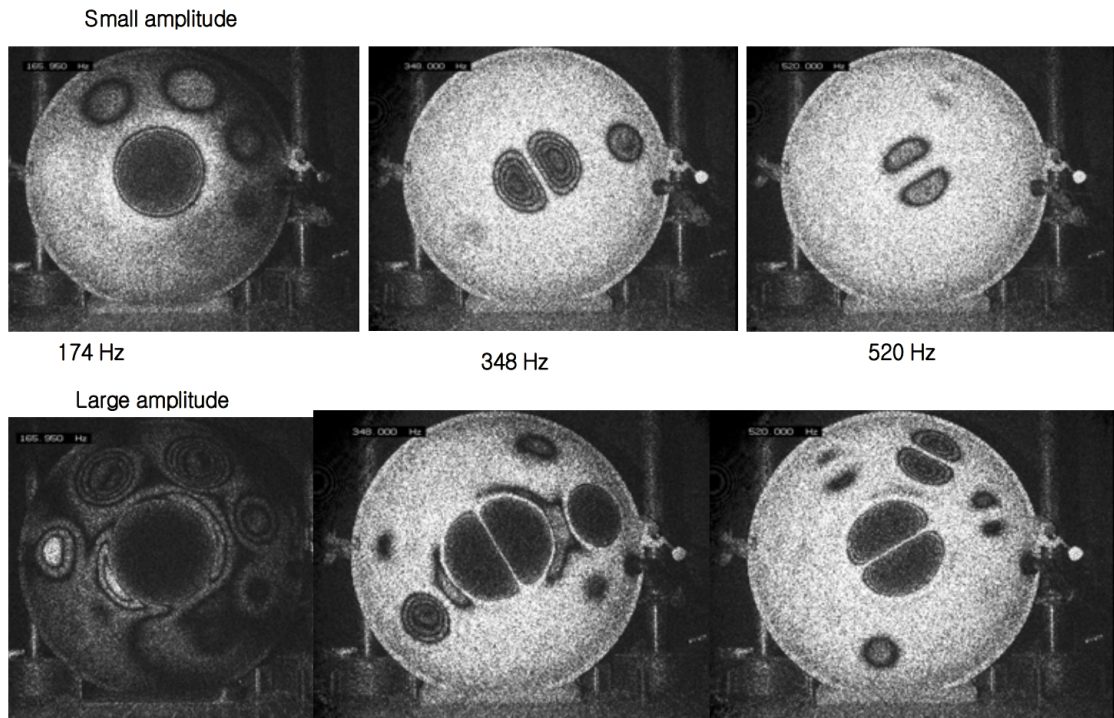


FIGURE 2.13: Interferograms of the Hang driven at low and high amplitude levels at frequencies near the first three vibrational modes of the F_3 Ding: 174 Hz, 348 Hz, and 520 Hz. Increasing the driving amplitude level increases the amount of coupling and number of affected notes. From [14]

a sound intensity probe and an electronic TV holographic interferometer [14]. The interferograms displayed in Figure 2.13 show modal shapes of the Hang's note areas when excited at low and high amplitude levels at the first three vibrational modes of the F_3 Ding. When driving the Hang at 174 Hz, 348 Hz, and 520 Hz the coupling between various notes can be seen. For example, exciting the F_3 Ding at a low amplitude level with a frequency of 348 Hz shows appreciable coupling between the second vibrational mode of the F_3 note and first vibrational mode of the F_4 note. Increasing the amplitude also increases the amount of coupling and number of affected notes. This implies non-linear behaviour, similar to the coupling between a sympathetic pair of steelpan notes, as mentioned in Section 2.1.4. The increase in amount of affected notes can be clearly seen when comparing the low and high amplitude interferograms with an excitation frequency of 348 Hz, where at least three additional notes are affected in the high amplitude case.

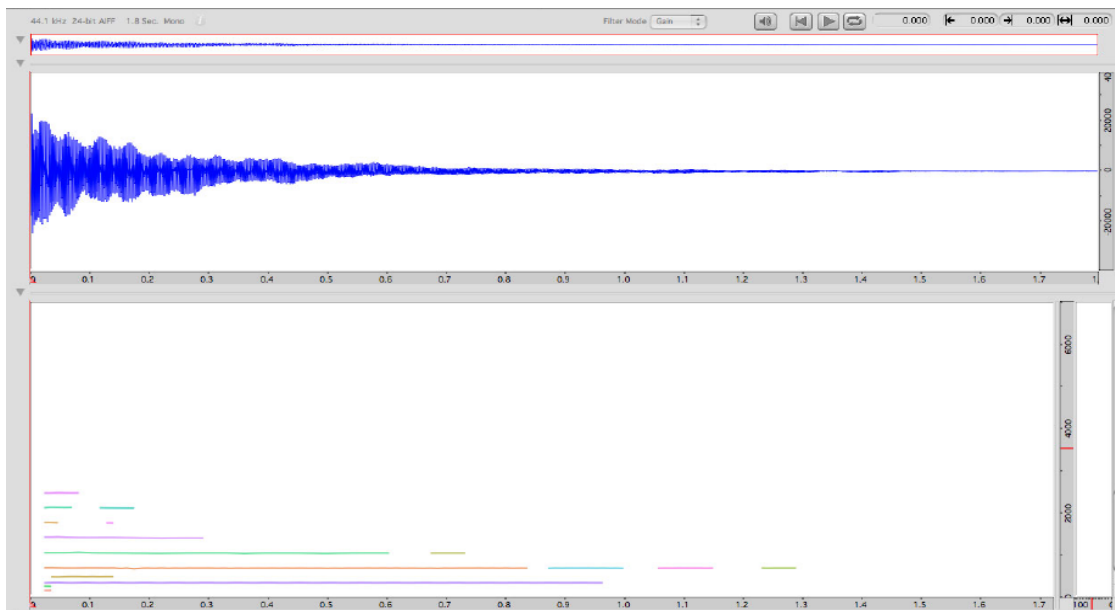
A study by Wessel, Morisson, and Rossing investigated three Hang instruments when excited by sinusoidal force, a variety of hand techniques, and a rubber mallet [15].

Figure 2.14 shows the waveforms and spectrograms of a Hang note played at: (b) soft; and (a) strong levels. Appendix B displays a larger and clearer version of Figure 2.14. A spectrogram (further detail in Section 2.2.1.2) is a time-frequency distribution that specifies magnitude of frequency components over time for a given signal. Comparing 2.14(a) and 2.14(b) clearly shows how an increase in playing strength also increases the amount of detected peaks. Amplitude modulations on individual peaks are also evident (such as for the higher frequency peaks of 2.14(a)). These amplitude modulations are likely a result of beating, due to coupling of note-fields with slightly mismatched tuning of signature vibrational modes, as will be detailed in Section 4.4.

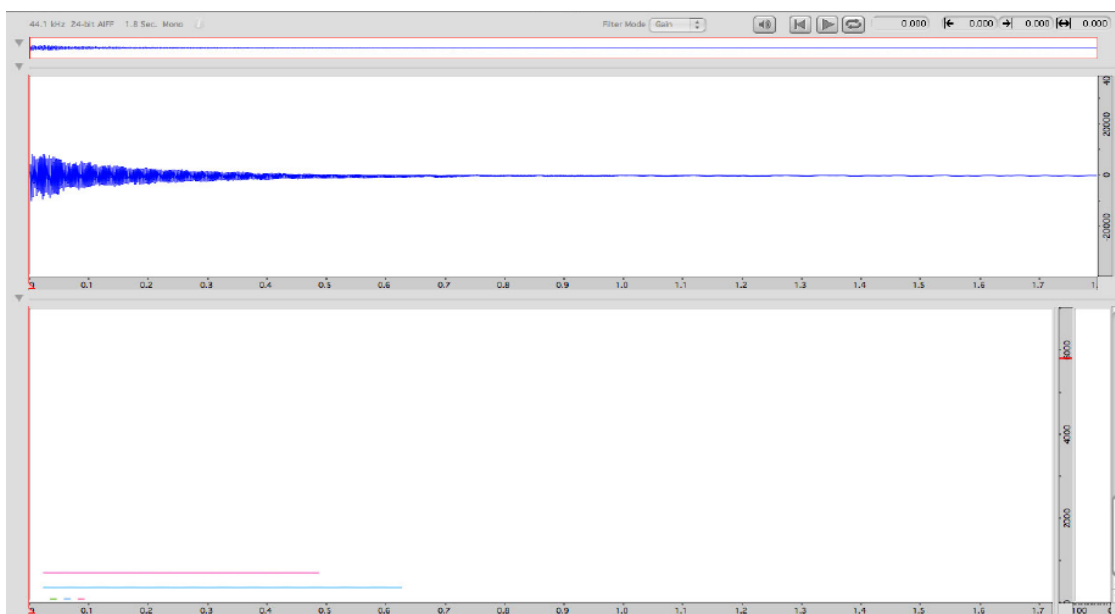
When playing the Hang rapidly, each strike meets the instrument in a different state, which creates a different timbre. Wessel, Morisson, and Rossing demonstrated this by modelling the Hang with resonant filters centred at each of the frequency components using gain and decay values that were extracted from the analysis [15]. Resonant filters, or resonators, amplify frequencies within a narrow bandwidth [31]. The difference in perceived timbre was demonstrated by comparing the free running set of resonant filters with a version of the model where the state of the filters remains constant at each impulse. This synthesis technique is similar to the one developed as part of this thesis work, which is presented in Chapter 5.

2.1.6 Handpan Background

As mentioned in Chapter 1, “handpan” is a term used to describe a group of struck metallic musical instruments, which are similar in shape and sound to the Hang. The term handpan was coined by Kyle Cox and Jim Dusin of Pantheon Steel LLC, who in 2006, produced the first handpan named Halo [7]. The need for a term that describes Hang-like instruments stems from the fact that Hang is a registered trademark [1]. In October 2014, there were approximately 80 handpan makers worldwide [6], however a survey of the online handpan forum, HandPan.org, showed only a relatively small number of them to be considered “top-shelf” or of high quality [32]. An objective standard for classification of handpan quality does not yet exist, however some discussion of this amongst makers and enthusiasts has occurred [13].



(a)



(b)

FIGURE 2.14: Waveform and spectrogram analysis of a Hang note played at soft (b) and strong (a) levels. Comparing (a) and (b) clearly shows how an increase in playing strength also increases the amount of measured peaks. Amplitude modulations on individual peaks are also evident (such as for the higher frequency peaks of (a)). Appendix B displays a larger and clearer version of these figures. Adapted from [15]

Unlike the Hang, not all handpans are made of nitrided steel and no standard exists for handpan making or tuning so each maker creates instruments with different tools, dimensions, shell and note-field architectures. The handpan, as seen in Figure 1.1, typically consists of eight or more note-fields. Despite the seemingly equal areas of all the notes on the diagram, this is not the case in reality. Low register notes usually have larger note-field areas with larger dimples relative to high register notes. The area in between the note-fields is known as the interstitial or internote area.

Different sections of the note-field area are tuned to emphasise the desired modes of vibration. Like the Hang and steelpan, the frequencies produced from the handpan's principal modes of vibration in each note-field have a 1:2:3 ratio, as will be seen in Section 4.2.1. As mentioned in Section 2.1.4, a particular vibrational mode of an individual steelpan note can be emphasised by stick impacts to the antinodal points (known as "sweetspots") of the corresponding vibrational mode. Figure 2.15 shows a typical handpan note-field, nodal lines, and sweetspots. The sweetspot for mode 1, marked as 'D', coincides with the apex of the dimple, and intersection of nodal lines for mode 2, and mode 3. Refer to the interferograms displayed in Figure 2.13, which display nodal lines of the Hang's vibrational modes. Despite the expected de-emphasis of the initial excitation of mode 2, and mode 3 when striking the 'D' sweetspot, the apex is still considered the best impact point for maximum excitation of all the vibrational modes [23]. Additional tones can be emphasised by striking anywhere on the note-field boundary. These tones are known as shoulder tones amongst handpan enthusiasts, and are typically only found (harmonically tuned) in instruments made by more experienced makers. It has been reported that handpans suffer from specific "problematic frequencies" associated with vibration inside the handpan cavity [33]. A vibrational mode on a note-field associated with a wavelength equal in length to the internal diameter of the handpan cavity, would be considered a problematic frequency [34]. It is thought that this cavity phenomenon can significantly influence the sound of an individual note-field in a non complementing manner.

Various playing techniques can be used to play the handpan. The signature handpan sound is a harmonic, sustained sound that results when a rapid and gentle strike using the tip, ball, or side of the finger is delivered to any section of a given note-field area.

Handpan note-field, nodal lines, and sweetspots

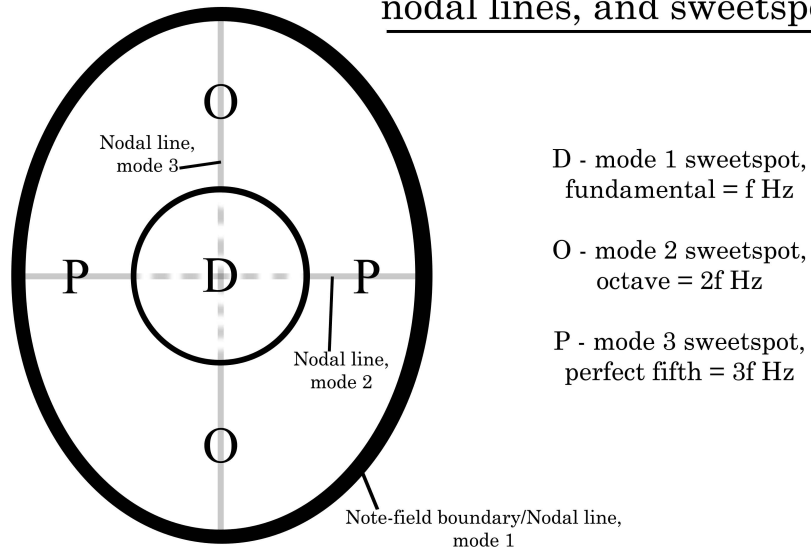


FIGURE 2.15: The typical handpan note-field, nodal lines, and sweetspots. In previous research of the steelpan it was found that vibrational modes of an individual note area can be de-emphasised by stick impacts made along the corresponding nodal lines [23]. Striking at the antinodes (sweetspots) will emphasise a corresponding vibrational mode. The sweetspot for mode 1, marked as 'D', coincides with the apex of the dimple, and intersection of nodal lines for mode 2, and mode 3.

Two of the better known handpan players, Colin Foulke [35] and David Kuckhermann [36], have produced tutorial videos that demonstrate the following techniques and many more [37]:

- **Finger strikes:** A set of rapid and gentle strikes delivered to the note-field.
- **Harmonic isolations:** This technique is done by using a finger to dampen the 'O' sweetspot while delivering finger strikes to the 'P' sweetspot. This emphasises the perfect fifth while significantly de-emphasising the octave. Emphasis of the octave and de-emphasis of the perfect fifth is also possible.
- **Note bending:** When performing harmonic isolations, it is possible to apply pressure with the damping finger to produce a slight pitch bend effect. This technique should be used with caution as it can damage the instrument.

- **Percussive strikes:** Delivering strikes to the interstitial area produces a percussive, non-ringing, transient sound. The timbre of these short-lived percussive sounds will depend upon which note-fields are in close vicinity to the strike location.
- **Helmholtz activation:** The bottom side of the handpan can be played by using the palm of the hand to excite the port hole. This activates the Helmholtz resonance frequency of the handpan. Some handpan makers also tune the lip of the port hole to musically complement the handpan notes.
- **Vertical playing:** Placing the handpan vertically in between the legs makes vertical playing possible. This means that both note-fields and the port hole can be activated simultaneously.

2.1.7 Summary

This section has provided an overview of common acoustic properties and relevant prior research related to the analysis of struck metallic percussion instruments, as well as the history and background of the handpan. The instruments that are most similar to the handpan in terms of physical structure are the steelpan and Hang. The steelpan is described as a shell-like structure, where each note forms a sub-structure of a complex array of shallow shells, each surrounded (bounded) by the stiffer internote sections [23]. The connection of each note to the rest of the pan face is characterized by a set of hidden boundary conditions describing the note edges, and by unknown compressive stresses. An analysis of steelpan notes showed localization of the vibrational motions to within elliptical note regions on the pan [27]. Like the steelpan and Hang, the expected frequencies produced from the handpan's first three principal modes of vibration in each note-field have a 1:2:3 ratio. Vibrational modes of an individual note area can be de-emphasised or emphasised by stick impacts made along the corresponding nodal lines or antinodes (known as "sweetspots") respectively [23].

Several excitation methods have previously been used to investigate the acoustic properties of these instruments such as sinusoidal, hammer, and finger force [15]. Measurement

procedures that involve microphone recordings or velocity transducers have been analysed to determine time-frequency structures of steelpan notes as well as their degree of coupling. Non-linear phenomena such as the increase in amount of coupling and number of affected notes for increased excitation amplitude have a significant influence on the sound radiation and perceived timbre [14]. Some steelpan notes are tuned to operate in sympathetic vibration with other notes (known as sympathetic pairs), and are highly dependent on this note-note coupling for tonal quality and structure [23]. The complex structures, linear and non-linear interactions of the note areas, and their couplings are what make the steelpan, Hang, and hence the handpan complicated instruments to produce, analyse and model.

2.2 Sound Analysis and Synthesis

Spectral analysis techniques can be used to deduce the nature of individual frequency components and their corresponding magnitudes and phase in a given signal. This section details the role of spectral techniques in sound analysis, and presents an overview of relevant musical instrument sound synthesis methods.

2.2.1 Spectral Techniques in Sound Analysis

Sampling of a continuous time signal produces a discrete time sequence. If the signal is sampled every T_s seconds, then the sampling frequency is calculated by: $F_s = \frac{1}{T_s}$. All continuous time signals must be constrained to within a certain bandwidth for discretisation. The sampling theorem states that the sampling frequency should be higher than twice the highest frequency present in the signal to be sampled [38]. So, if F is the highest frequency to be sampled in the signal, then F_s must be greater than $2F$. $\frac{F_s}{2}$ is known as the Nyquist limit. If F is greater than the Nyquist limit, aliasing will occur, which is downward wrapping of frequencies above the Nyquist limit.

Fourier theorem states that any sound can be constructed from elementary sinusoids [39]. The spectrum of a real, continuous time domain signal $x(t)$ is given by application of the

Fourier transform to the signal [38]:

$$X(\omega) \triangleq \int_{-\infty}^{\infty} x(t)e^{-j\omega t} dt \quad (2.8)$$

Where ω is the angular frequency in radians and $X(\omega)$ is the Fourier transform. Digital signals are discrete due to their sampled nature, so the Fourier transform must be adapted accordingly. The Discrete Fourier Transform (DFT) decomposes a discrete, time limited signal into discrete sinusoidal components [38]. The DFT may be defined as:

$$X(\omega_k) \triangleq \sum_{n=0}^{N-1} x(t_n)e^{-j\omega_k t_n}, \quad k = 0, 1, 2, \dots, N - 1 \quad (2.9)$$

Where N is the number of time samples, $x(t_n)$ is the input signal value at time sample n , ω_k is the frequency of the k th bin and $X(\omega_k)$ is the complex valued spectrum. The Fast Fourier Transform (FFT) is an efficient implementation of the DFT. An FFT of length M samples will produce a symmetric spectrum with M frequency bins, although it should be stressed that only $\frac{M}{2} + 1$ frequency bins are available to represent the range of frequencies from 0 Hz through to the Nyquist limit. Sharp discontinuities at the start and end of the discrete, time limited signal, might introduce additional frequency components into the estimated spectrum (this is known as spectral leakage). These discontinuities can cause spectral leakage due to the fact that the DFT assumes it is creating a periodically extended version of the signal. Multiplying the signal by a window function can reduce the effects of spectral leakage, as will be detailed in Section 2.2.1.1.

When performing spectral analysis of signals there is always a compromise between time-domain and frequency-domain resolution. A higher time-domain resolution will result in a poorer frequency-domain resolution and vice-versa. The human hearing system performs a Fourier-like analysis of short audio frames (10 ms-20 ms) resulting in a high quality time and frequency domain resolution [40].

2.2.1.1 Short-Time Fourier Transform

The Short-Time Fourier Transform (STFT) is a time-frequency distribution that specifies magnitude and phase of frequency components over time for a given signal [40]. The

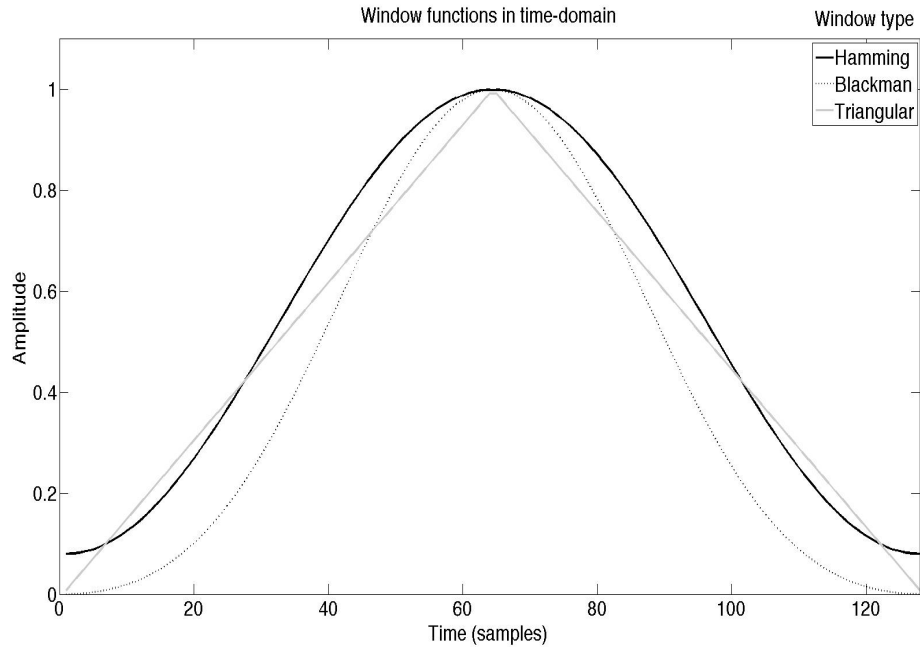


FIGURE 2.16: Window functions in the time-domain: Hamming, Blackman, and triangular.

STFT may be defined as:

$$X_m(\omega) = \sum_{n=-\infty}^{\infty} x(n)w(n - mR)e^{-j\omega n} \quad (2.10)$$

where $x(n)$ is the input signal at time n , $w(n)$ is the window function, R is the hop size in samples (determines amount of overlap between frames), and $X_m(\omega)$ is the transform of the windowed data centred about time mR .

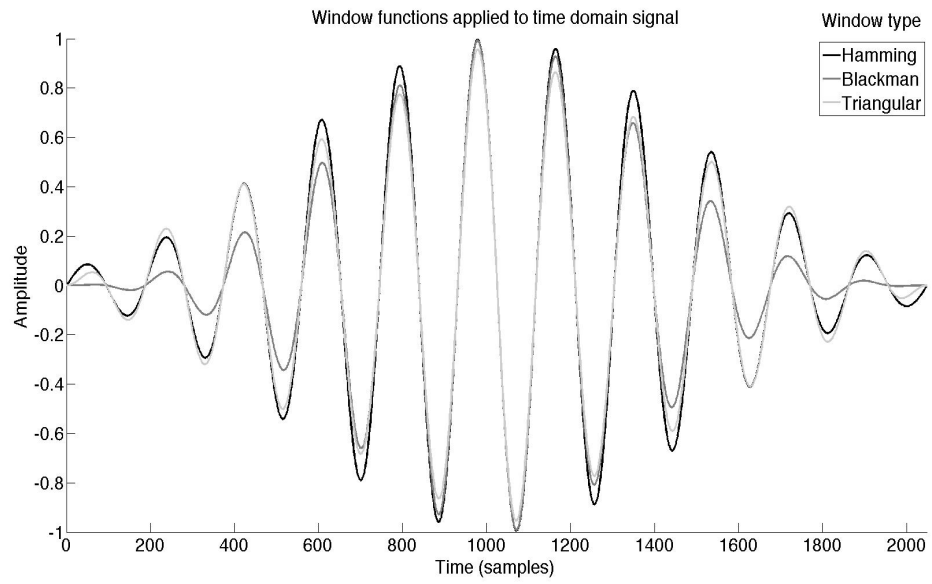
The STFT is calculated by dividing a signal into short frames and performing an FFT on each frame. In order to reduce the effects of spectral leakage, the signal is usually multiplied by a window function. Various window functions can be used for this purpose: triangular, Blackman, Hamming, Kaiser and others. Figure 2.16 displays three types of window functions: Hamming, Blackman, and triangular. The type of window function used will influence the amount of spectral leakage, sideband amplitude, and width of the main lobe [40, 41].

The influence of window type on the estimated spectrum can be demonstrated comparing FFT results for a single sinusoidal signal that has been windowed with different functions. Figure 2.17 displays: (a) time domain; and (b) frequency domain graphs when Hamming, Blackman, and triangular windows (each 2048 samples in length) are applied to a 236.8652 Hz sinusoidal signal, sampled at 44.1 kHz. This frequency value was chosen because it conforms relatively well to the frame length (approximately eleven periods fit into this window). Setting the FFT size to a value that is greater than the frame length (a procedure often referred to as zero padding), increases the apparent frequency resolution of the estimated spectrum, effectively via interpolation, and hence does not actually add additional information. Hence, an FFT size of 16384 was selected. The shape of the estimated spectrum at the peak and its surroundings is different for each window type. Examining Figure 2.17(b), it can be seen that the triangular windowed spectrum produces a relatively wide bandwidth main-lobe with attenuated side lobes when compared to the Hamming windowed spectrum, which produces a narrower main-lobe but less attenuated side-lobes.

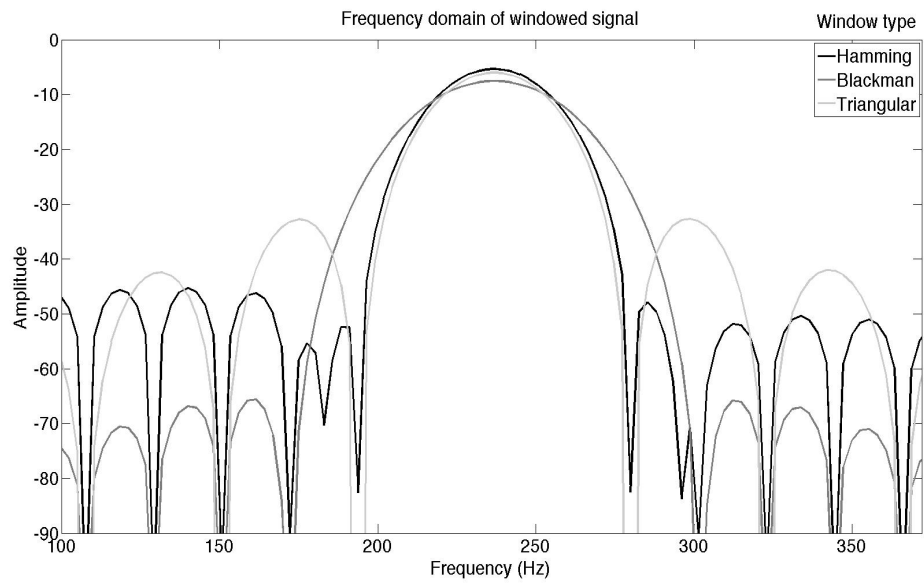
2.2.1.2 Spectrogram

A spectrogram can be defined as an intensity plot of the Short-Time Fourier Transform (STFT) magnitude [40]. Analysis parameters of the spectrogram should be selected according to the nature of the input data and desired qualities of the estimated spectrum. These parameters include: frame length, window type, hop-size and FFT length. The effects of frame length and window type on the estimated spectrum were mentioned in Section 2.2.1.1. The apparent time localisation can be improved to a certain degree by changing the overlap (hop-size) percentage [31]. If the frames do not overlap at all (0% overlap), then a significant portion of the data might be effectively ignored in the analysis [42]. The chosen overlap percentage depends on the window function, and requirements for the analysis. For wide windows (in the time domain), 50% overlap is commonly used, whereas for narrower window functions an overlap of up to 84% might be selected.

Figure 2.18 compares three spectrograms produced from a B₂ handpan note signal. The spectrograms were produced with the following settings: (a) Rectangular window =

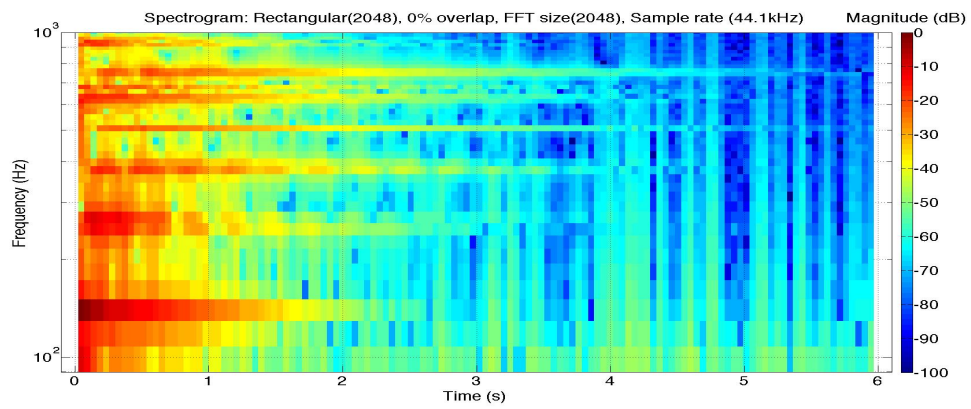


(a)

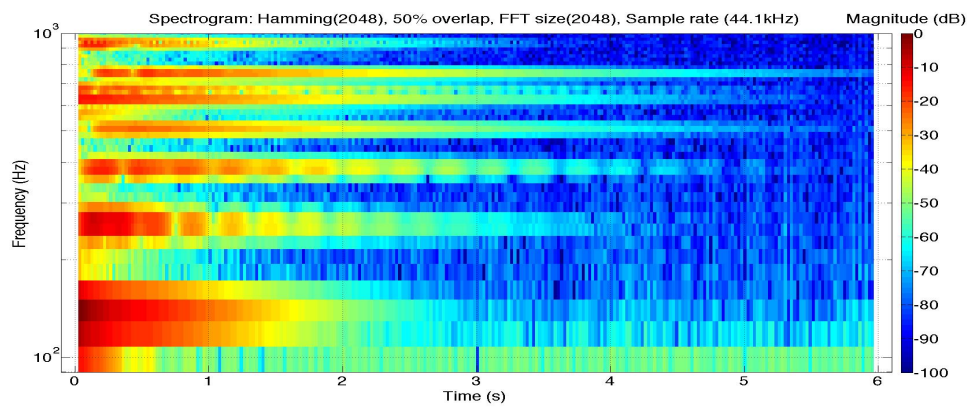


(b)

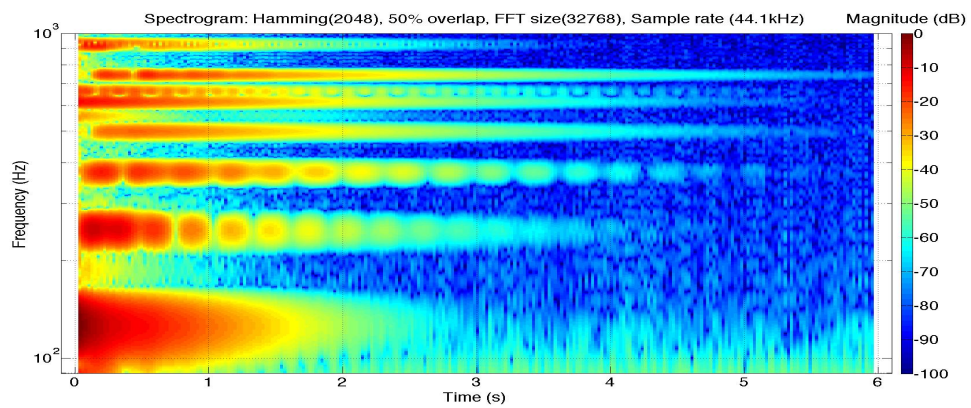
FIGURE 2.17: (a) Time domain; and (b) frequency domain graphs of a 236.8652 Hz signal, 44.1 kHz sample rate, using the following window functions (frame length = 2048, FFT size = 16384): Hamming, Blackman, and triangular.



(a)



(b)



(c)

FIGURE 2.18: Three spectrograms of a B₂ handpan note signal. Spectrogram settings: (a) Rectangular window = 2048, 0% overlap, FFT size = 2048 (no zero padding), sample rate = 44.1 kHz; (b) Hamming window = 2048, 85% overlap, FFT size = 2048 (no zero padding), sample rate = 44.1 kHz; and (c) Hamming window = 2048, 50% overlap, FFT size = 32768 (30720 zero padding), sample rate = 44.1 kHz.

2048, 0% overlap, FFT size = 2048 (no zero padding), sample rate = 44.1 kHz; (b) Hamming window = 2048, 50% overlap, FFT size = 2048 (no zero padding), sample rate = 44.1 kHz; and (c) Hamming window = 2048, 50% overlap, FFT size = 32768 (30720 zero padding), sample rate = 44.1 kHz. Figure 2.18(a) was produced with a rectangular window (this is equivalent to applying no window function) and 0% overlap. This type of window potentially maximises the amount of spectral leakage. Comparison between 2.18(a) and 2.18(b), gives some insight into the adverse effects of spectral leakage and how windowing can minimise this. The spectral leakage is most noticeable in the 0-1 second region where the energy from detected sinusoidal peaks has “leaked” into surrounding frequency bins.

Figure 2.18(b) and 2.18(c) were produced with a Hamming window and 50% overlap value. Comparing 2.18(b) and 2.18(c) shows the apparent improvement (effectively via interpolation) in the spectrograms when zero padding is used. In particular, examining the background noise in the 3-6 second region, and the 0-1 second region at approximately 120 Hz shows the apparent improved frequency resolution and time localisation of 2.18(c).

2.2.1.3 Peak Detection

Detection of peaks in the spectrum of a given sound signal requires implementation of a peak detection method. As mentioned previously in Section 2.2.1, an FFT of size M will produce an estimated spectrum with M frequency bins. The bin width can be calculated by dividing the sample rate value by the frame length. In order to estimate the peak frequency value within a frequency bin, additional computation is required [43]. Parabolic interpolation can be used to fit a parabola through the surrounding samples of a peak to estimate the frequency and magnitude [44]. Other methods of frequency estimation are triangular interpolation and the derivative algorithm. The following equation can be used to perform parabolic interpolation:

$$f_{sinusoid} = B \left(n + \frac{1}{2} \cdot \frac{M_{n-1} - M_{n+1}}{M_{n-1} - 2M_n + M_{n+1}} \right) \quad (2.11)$$

Where B is the bin width, M_n is the magnitude of bin n expressed in decibels, and f_{sinusoid} is the value of the estimated peak frequency. A high resolution method, such as ESPRIT [45, 46] can also be used for detection and estimation of peaks with closely spaced frequencies and their corresponding damping factors. More detail regarding this high resolution method can be found in Section 6.3.1.

2.2.2 Decay Rate Estimation

The unit impulse, impulse response, and convolution are concepts that must be understood properly in order to estimate decay rates of musical instruments or acoustic spaces. The unit impulse signal is defined by [39]:

$$\delta(n) = \begin{cases} 1 & \text{for } n = 0 \\ 0 & \text{for } n \neq 0 \end{cases} \quad (2.12)$$

When a linear, time invariant system (LTI) is excited by an impulse, the resulting output is known as the system's impulse response and can be used to learn about the nature of the system. A system is completely characterised by its impulse response only if it is linear and time-invariant. The output signal of an LTI system can be calculated using convolution if the impulse response and input signal are known. The output of a discrete-time LTI system, $y[n]$, can thus be calculated by:

$$y[n] = \sum_{k=0}^{\infty} x[k] \cdot h[n - k] = x[k] * h[n] \quad (2.13)$$

Where n is the sample number, $x[k]$ is the input or excitation signal, and $h[n]$ is the system's impulse response. The amplitude envelope of an exponentially decaying impulse response should decay in a linear fashion when plotted on a logarithmic scale [39]. Linear regression methods such as the method of least squares or straight line approximation [31] can be used to estimate the decay rates of individual spectral components.

2.2.2.1 Energy Decay Relief

The Energy Decay Curve (EDC) is the total amount of signal energy remaining at any given point in time, and can be used for measuring and defining reverberation times of acoustic spaces [39]. Being an integrated quantity, the EDC decays more smoothly than the amplitude envelope of a signal, which in the context of this thesis means that amplitude modulations appear less prominently, and that the curve decays in a more linear fashion. Therefore, the EDC is more useful for measuring reverberation times than the amplitude envelope. The EDC can be defined as:

$$\text{EDC}(n) \triangleq \int_n^{\infty} x^2(n)dn \quad (2.14)$$

Where $x^2(n)$ is the squared input signal at time sample n . The Energy Decay Relief (EDR) equation generalises the EDC and thus shows the total amount of signal energy remaining at a given point in time per frequency bin. This is particularly useful for analysing the decay curves of individual peaks in the sound of musical instruments. The EDR can be defined as:

$$\text{EDR}(t_n, \omega_k) \triangleq \sum_{m=n}^M |X_m(m, \omega_k)|^2 \quad (2.15)$$

Where $X_m(m, \omega_k)$ denotes frequency bin k of the STFT at time-frame m , M is the total number of time frames, and $\text{EDR}(t_n, \omega_k)$ is the total amount of signal energy remaining at time $t_n = \frac{n \cdot m_L}{F_s}$ (F_s = sample rate, n = frame number, m_L = frame length) in frequency bin k . Figure 2.19 displays a 3D EDR for the B₂ handpan note. Since the EDR is based on the STFT, much like the spectrogram, all of the analysis parameters mentioned in Section 2.2.1.2 should be selected according to the nature of the input data and desired qualities of the estimated spectrum.

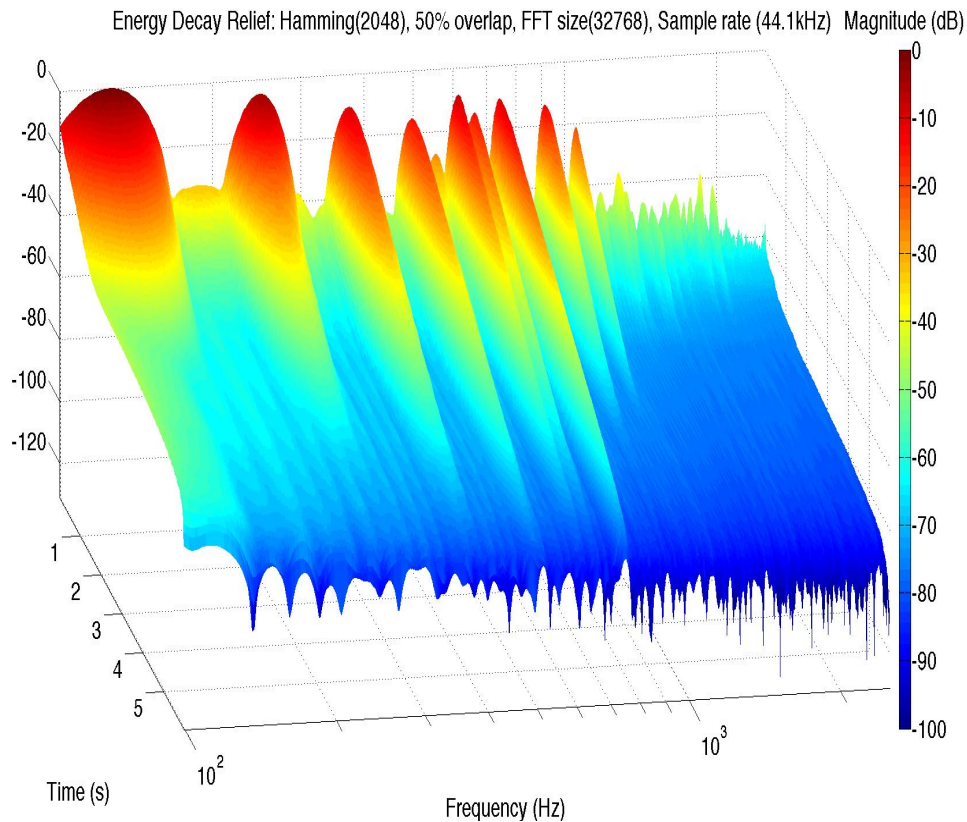


FIGURE 2.19: 3D Energy Decay Relief of a B₂ handpan note signal. Spectrogram settings: Hamming window = 2048, 50% overlap, FFT size = 32768 (30720 zero padding samples), sample rate = 44.1 kHz.

2.2.3 Synthesis of Musical Instrument Sounds

The synthesis of musical instruments is typically performed using one of two techniques: physical modelling methods or abstract synthesis methods [47]. Physical models are derived from mathematical descriptions of acoustic instruments, such as mass-spring models and digital waveguide models [39]. Physical models are known to produce natural sounding synthesis results. Additionally, they require a relatively small amount of control parameters, all of which are physically meaningful such as strike location or blowing pressure. The disadvantage of this synthesis technique is that they usually require a large amount of computations. Abstract synthesis methods, which possess no associated underlying physical interpretation, can be based on an analysis/synthesis approach using the STFT or similar technique for analysis, and the reproduction of sinusoids (sometimes combined with noise-like signals) for synthesis. Examples of

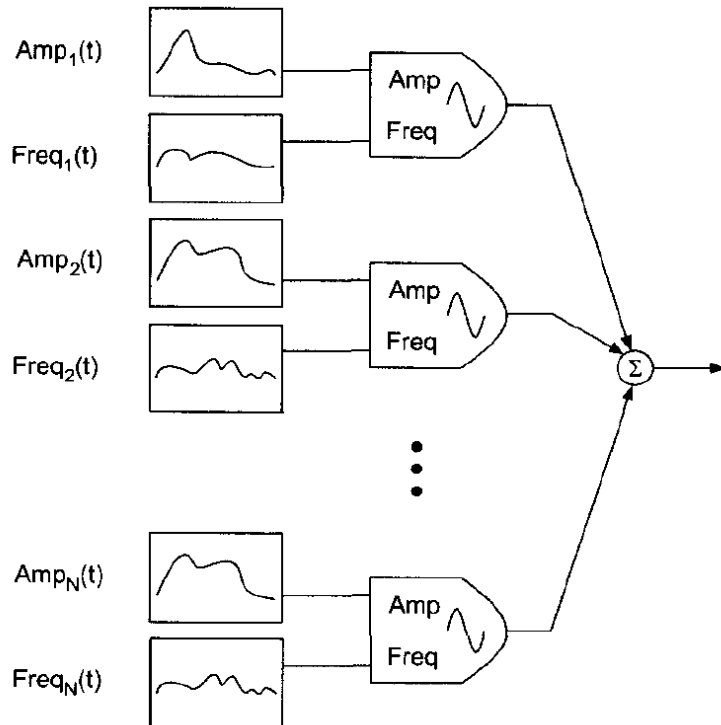


FIGURE 2.20: Additive synthesis block diagram, showing individual control of amplitude and frequency for N sinusoids, summed together to produce the output waveform. From [31]

abstract synthesis methods include additive synthesis, granular synthesis and Frequency Modulation (FM) synthesis [47]. Abstract methods are known to produce synthetic sounding results, with a complex user control system where the inputs are not physically meaningful. Abstract synthesis techniques usually require less computations compared to physical modelling.

2.2.3.1 Additive and Spectral Modelling Synthesis

Additive synthesis is based on the creation of sound by employing and summing a number of oscillators each having independent amplitude and frequency controls [39]. In continuous time, a single sinusoidal oscillator with output $u(t)$ is defined as [47]:

$$u(t) = A \cdot \cos(2\pi f_0 t + \phi) \quad (2.16)$$

Where t is time, A is amplitude, f_0 is frequency, and ϕ is the initial phase of the oscillator. In the case of additive synthesis, the phase is less perceptually relevant due to the uncorrelated nature of the oscillators [19]. Figure 2.20 shows the additive synthesis block diagram, where individual sinusoids with amplitude and frequency values are added together to produce the output signal [31]. In the early 1970s, Moorer developed various analysis programs to support additive synthesis [48]. One of these analysis programs implemented a heterodyne filter to measure the instantaneous amplitude and frequency of individual harmonic sinusoids, however were less successful when used to analyse inharmonic sounds. Additive synthesis in general is computationally expensive, the degree of which depends upon the number of partials required to synthesise a given musical instrument. As an example, the synthesis of an A_1 note on the piano requires approximately 400 sinusoidal partials [39]. Another disadvantage of additive synthesis is that a large number of partials are required to produce any type of noise-like signal [49]. Hence, additive synthesis is most appropriate for modelling of instruments that don't have a significant noise-like component.

Spectral Modelling Synthesis (SMS) assumes the input signal to be composed of deterministic (periodic) and stochastic (noise-like) components [48]. The mathematical representation of the input signal is shown in Equation 2.17, where $s(t)$ is the input signal, t is time, r is the sinusoid number, A_r is the instantaneous amplitude, $\theta_r(t)$ is the instantaneous phase, and $e(t)$ is the noise component.

$$s(t) = \sum_{r=1}^R A_r(t) \cos[\theta_r(t)] + e(t) \quad (2.17)$$

One of the motivations to develop this synthesis method was the poor performance of additive synthesis when modelling noise-like signals [48]. Firstly, the deterministic component is extracted by analysing the input sound to derive a series of magnitude spectra, from which the prominent peaks are detected and organised into frequency trajectories. After this the deterministic component is synthesised using an additive synthesis technique. Then, the stochastic component is calculated by subtracting the magnitude spectrum of the deterministic part from the magnitude spectrum of the input sound and deriving the envelope of the residual signal by a line-segment approximation.

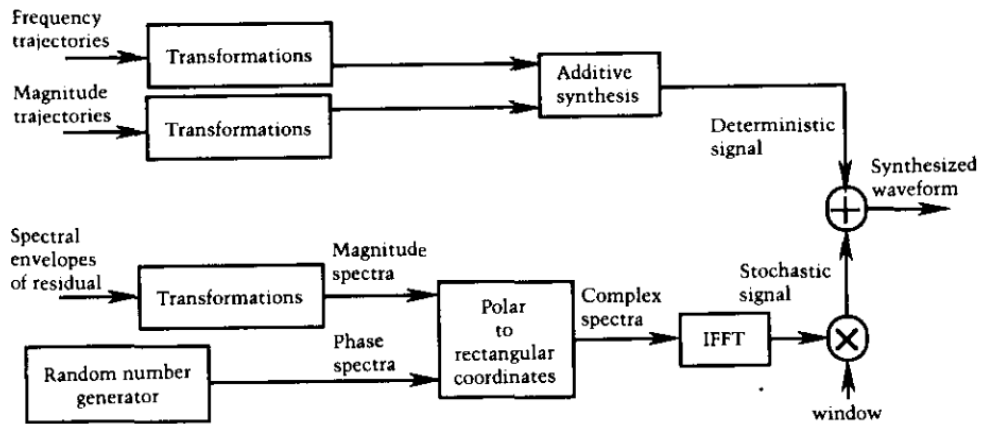


FIGURE 2.21: SMS synthesis block diagram, showing frequency and magnitude trajectories, and spectral envelopes of the residual as inputs. Additive synthesis is used to produce the deterministic signal and inverse-FFT combined with an overlap-add synthesis technique is used to produce the stochastic signal. The deterministic and stochastic signals are then summed to produce the output waveform. From [48]

The stochastic component is then synthesised from the spectral envelopes by using an overlap-add synthesis technique. Figure 2.21 shows the block diagram of the synthesis part of SMS. An advantage of SMS is the reduced computational cost when compared for example to physical models and additive synthesis, however the main disadvantage is the difficulty to capture the complete range of playing conditions for a particular acoustic instrument [50]. An example of SMS is the Vocaloid, a “virtual-singer” synthesiser developed by Yamaha and collaborators. While the sound quality is generally considered excellent, it still requires a significant amount of work to encode a particular singing voice into the synthesiser.

2.2.3.2 Modal Synthesis

Modal synthesis is an application of modal decomposition, which describes a linear system in terms of its modes of vibration [16]. This physical modelling synthesis method is based on the principle that a physical linear system’s response may be decomposed into contributions from individual modes, each of which vibrate at a particular frequency [47]. Modal data can be derived analytically for simple structures or obtained from vibration measurements of a specific physical instrument. Figure 2.22 displays two models of

modal synthesis: (a) decomposition of a linear system's response into contributions from individual modes, each of which vibrate at a particular frequency, and then recombining to produce the synthesised signal [47]; and (b) a more flexible parametric source-filter modal synthesis approach, which includes estimation of resonant filter parameters, but also allows the excitation signal to be arbitrary, and for pseudo-physical rules to be applied [51]. The advantages of modal synthesis is that there are few parameters, which are directly related to the physics of the system, and a synthesis structure that respects the causality of the system. Additionally, it allows extension in the form of replacing the estimated excitation signal with a different excitation model, or arbitrary signal.

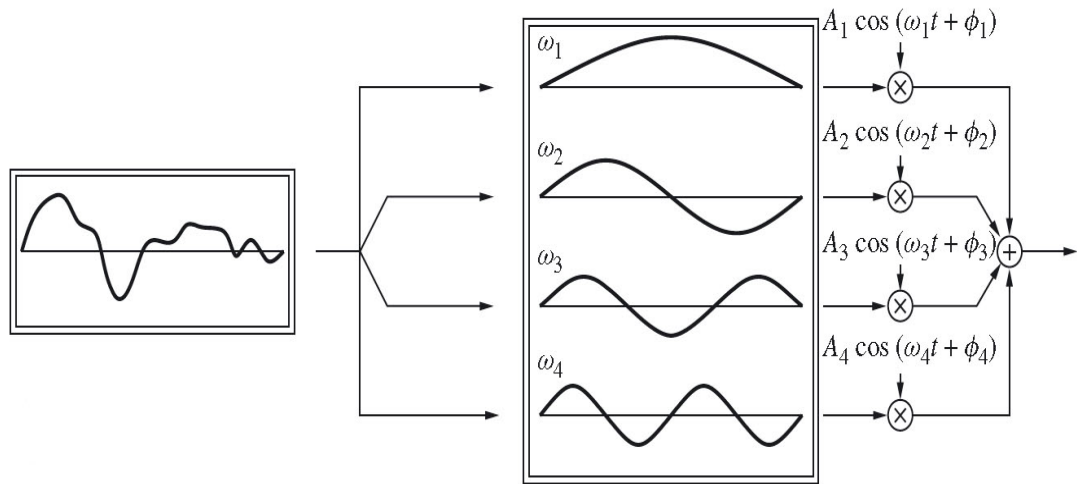
The modal parameters can also be estimated from recorded sounds of the vibrating objects. Fourier analysis and the Energy Decay Relief method can be used to estimate these parameters from a recorded signal [52]. A set of modes (damped sinusoids) is used in modal synthesis for representing the impulse response, $s(n)$, of a linear system:

$$s(n) = \sum_{k=1}^K A_k \cos(\omega_k t + \phi_k) \quad (2.18)$$

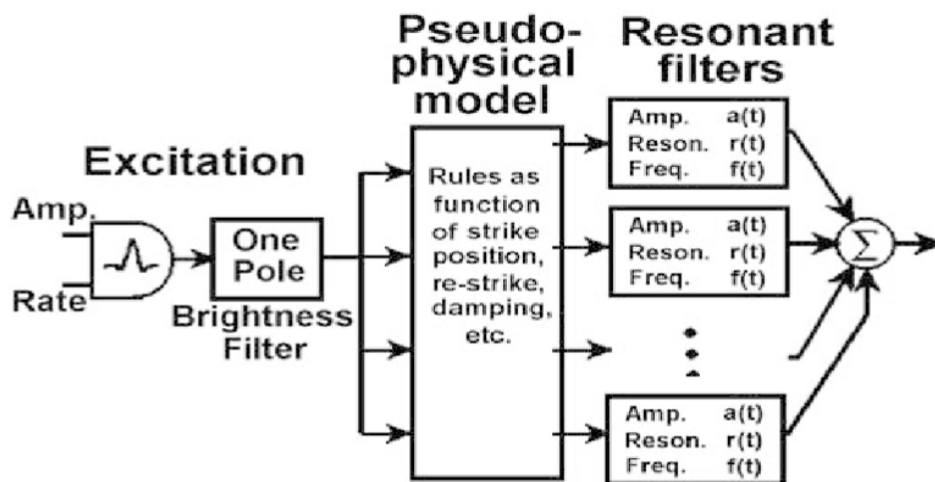
$$A_k = g_k e^{-\lambda_k t} \quad (2.19)$$

where g_k , ϕ_k , λ_k , and ω_k are respectively the gain, phase, decay constant and frequency of the mode k . The set of modes corresponds to the resonances of the vibrating object. The excitation signal in a source-filter model is generally unknown and can be estimated from the recorded sound using inverse filtering techniques [52]. Once vibrational modes have been identified, they can be filtered from the recorded signal by deconvolution, thus extracting a residual signal [51]. This residual would be an appropriate excitation signal in a source-filter modal synthesis model. As described previously in Section 2.2.2, the output of an LTI system, $y[n]$, can be calculated using convolution of the input signal, $x[n]$, with the impulse response of the system, $h[n]$. In the context of modal synthesis, $x[n]$ is the excitation (residual signal), and $h[n]$ is the impulse response of the linear system.

Previous research using modal synthesis techniques have estimated modal parameters such as mode frequencies, dampings, and initial magnitudes from measured impact



(a)



(b)

FIGURE 2.22: Two models of modal synthesis: (a) decomposition of a linear system's response into contributions from individual modes, each of which vibrate at a particular frequency, and then recombining to produce the synthesised signal; and (b) a more flexible parametric source-filter modal synthesis approach, which includes estimation of resonant filter parameters, but also allows the excitation signal to be arbitrary, and for pseudo-physical rules to be applied. Adapted from [47, 51]

sound data [53]. Sound data was gathered for wood, plastic, metal, and porcelain plates, which were excited by impact. A robotic device was used to apply impulses to these objects at a large number of sample points. This technique can be used to construct a virtual sounding instrument, using the measurements from each sample point, however usually results in a large number of measurements and extracted parameters for the modelled object. Modal synthesis can be effective for instruments like the marimba or xylophone, which have a relatively small number of long-ringing vibrational modes [50].

2.2.4 Summary

This section has identified and detailed the key theories and prior research related to the analysis and synthesis of struck metallic percussion instruments. As mentioned in Chapter 1, the Hang is not a type of handpan nor can any handpan be a Hang, however it is sure to say that both belong to the same family of musical instruments, and as such one might expect to see considerable similarity when comparing the results of this project with those obtained from previous Hang related research. The review of spectral techniques in sound analysis showed that Fourier methods can be used to estimate the spectral components of a given sound signal, where the compromise between time-domain and frequency-domain resolution should be considered when selecting the analysis parameters. Additionally, it was shown that spectrograms and EDR plots can be used to extract information related to the magnitudes, frequencies and corresponding decay rates of detected peaks in the measured signals.

The review of musical instrument sound synthesis showed that this is usually performed using one of two techniques: physical modelling methods or abstract synthesis methods [47]. Physical models are known to require a relatively small amount of control parameters, which are usually physically meaningful, and to produce natural sounding synthesis results. Abstract methods are known to produce synthetic sounding results, with a complex user control system where the inputs are not physically meaningful. Abstract synthesis techniques usually require less computations compared to physical modelling. Common methods of musical instrument sound synthesis have been reviewed, such as additive, spectral modelling, and modal synthesis. This showed that additive synthesis is

based on the creation of sound by employing and summing a number of oscillators each having independent amplitude and frequency controls [39]. This synthesis technique is most appropriate for modelling of instruments that don't have a significant noise-like component.

Spectral modelling synthesis, which is an analysis/synthesis based technique, assumes the input signal to be composed of deterministic (periodic) and stochastic (noise-like) components [48]. The deterministic component is extracted from the signal by deriving a series of magnitude spectra, from which the prominent peaks are detected and organised into frequency trajectories. Then, the stochastic component is synthesised by subtracting the magnitude spectrum of the deterministic component from the magnitude spectrum of the input signal. Spectral modelling synthesis is considered to be less computationally expensive compared to additive synthesis and some physical modelling methods. Despite this, it is difficult to capture the complete range of playing conditions for a particular acoustic instrument with spectral modelling synthesis [50].

Modal synthesis is based on the principle that a physical linear system's response may be decomposed into contributions from individual modes, each of which vibrate at a particular frequency [47]. Modal data can be derived analytically for simple structures or obtained from vibration measurements of a specific physical instrument. Upon deriving the modal data, this method can be implemented by convolving the estimated impulse response, and excitation signals. The advantages of modal synthesis is that there are few parameters, which are directly related to the physics of the system, and a synthesis structure that respects the causality of the system. Additionally, it allows extension in the form of replacing the estimated excitation signal with a different excitation model, or arbitrary signal [51].

2.3 Project Objectives

The following set of project objectives, which will enable fulfilment of the project aims, can be defined:

1. Record a set of anechoic handpan recordings.
2. Analyse the recordings to extract signature handpan sound characteristics.
3. Synthesise the handpan sound based on the extracted parameters.
4. Estimate the minimum number of vibrational modes required for synthesis by conducting a subjective listening test.

Chapter 3. Measurement

In order to conduct accurate analysis of the signature handpan sound, a method for the recording of a representative, repeatable, set of samples is required. This requires a basic understanding of the handpan's acoustical properties as well as underlying theories related to room acoustics, recording technologies, and mechanics. For the purposes of this project, the qualities of the measured handpan sound are a function of the following:

- The nature of the excitation (i.e. sinusoidal or mechanical).
- The acoustic characteristics of the source (i.e. the handpan).
- The acoustic characteristics of the environment (i.e. the room used for recording).
- The characteristics of the acoustic transducer (i.e. the frequency response of the microphone).
- The limitations of the digital storage medium (i.e. sample rate and bit depth).

This chapter will cover the design and implementation of a suitable experimental procedure for the measurement of the signature handpan sound, and estimation of note coupling.

3.1 Experimental Procedure

Previous studies of the Hang have typically discussed the modes of vibration, sound radiation fields, and spectra of the instrument. Sinusoidal excitation (by means of a driving coil) was used to produce holographic interferograms in order to visualise several vibrational modes of the note areas [14]. The same excitation method was used to perform sound intensity measurements using a pair of accurately spaced microphones positioned

in a plane 8 cm above the central note [54]. Hammer and finger force excitation were used to investigate the resulting spectra of the Hang [15].

The first aim of this project as stated in Section 1.1 is to design and implement an experimental procedure to record the handpan sound, and estimate note coupling. Implementation of this experimental procedure requires the following:

1. An acoustically neutral recording environment such that the measurements are representative of the sound generated from the handpan, rather than a combination of the handpan and the acoustics of the recording environment.
2. A repeatable excitation mechanism.
3. A frame to securely house the handpan when performing the measurements.
4. A measurement microphone and digital storage medium.
5. A method of note-field “isolation”.

The signature vibrational modes of an individual handpan note are expected to be localised to an elliptical note area, like the localised vibration of steelpan notes [27]. Despite this localisation, note coupling can have an effect on the amplitude and spectral features of the note-field sound, as will be seen in Section 4.4. Therefore, isolating an individual note’s vibration from the surrounding notes is expected to be advantageous. Measurement of an isolated note should be useful in the process of identifying signature vibrational modes and decay rates by reducing the number of measured modes, and beating due to note coupling, in the measured signal. Despite this advantage, the isolation method might also have an undesired effect on the measured note’s signature frequency values and corresponding decay times. This will be further addressed in Section 3.2.

Section 2.1 detailed some of the non-linear phenomenon in metallic percussion instruments like the cymbals, gongs, steelpan, and Hang. Chapter 4 will show that there are also non-linear phenomenon in the handpan sound and note couplings. Such phenomenon must be considered when attempting to accurately model or synthesise the handpan sound.

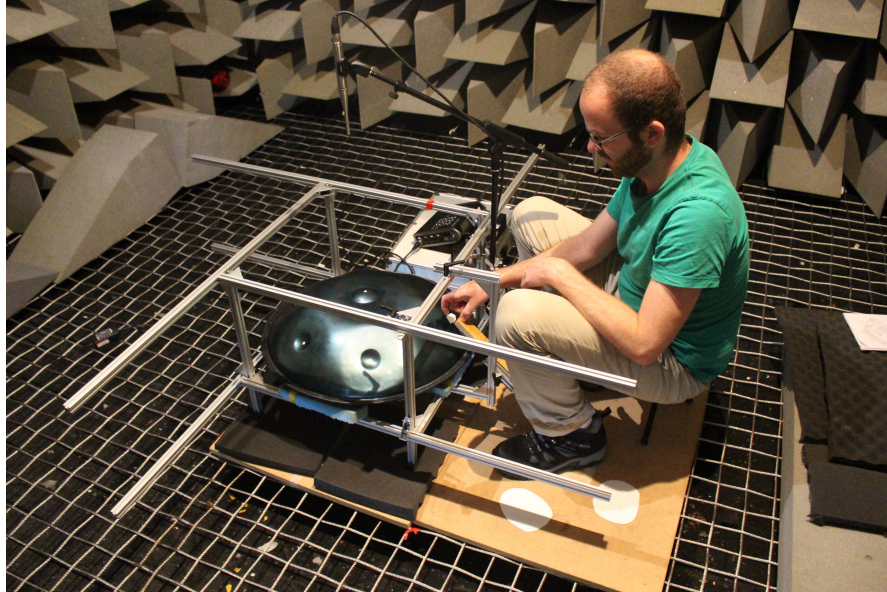


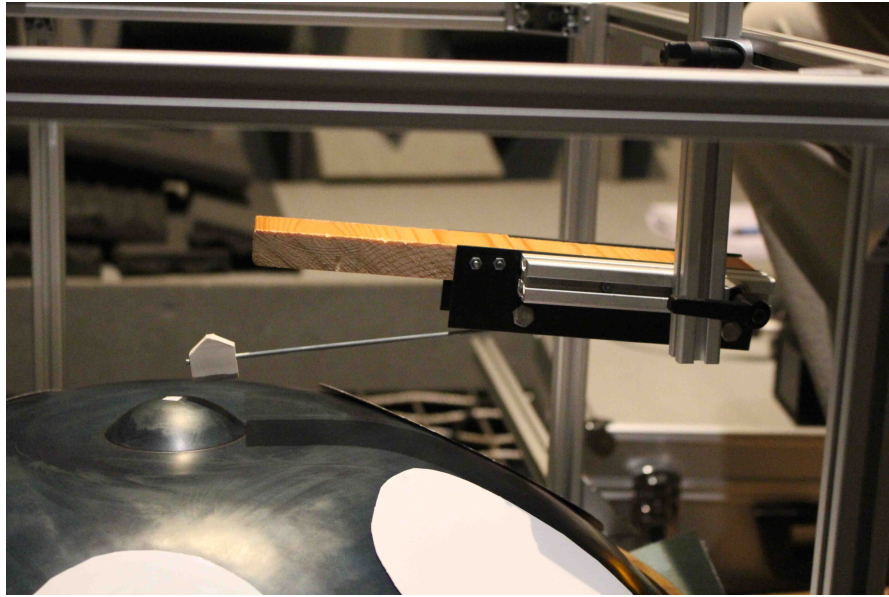
FIGURE 3.1: Recording apparatus set-up for the measurement of the signature handpan sound inside the anechoic chamber, which is a part of the AudioLab, Department of Electronics at the University of York.

3.1.1 Anechoic Chamber

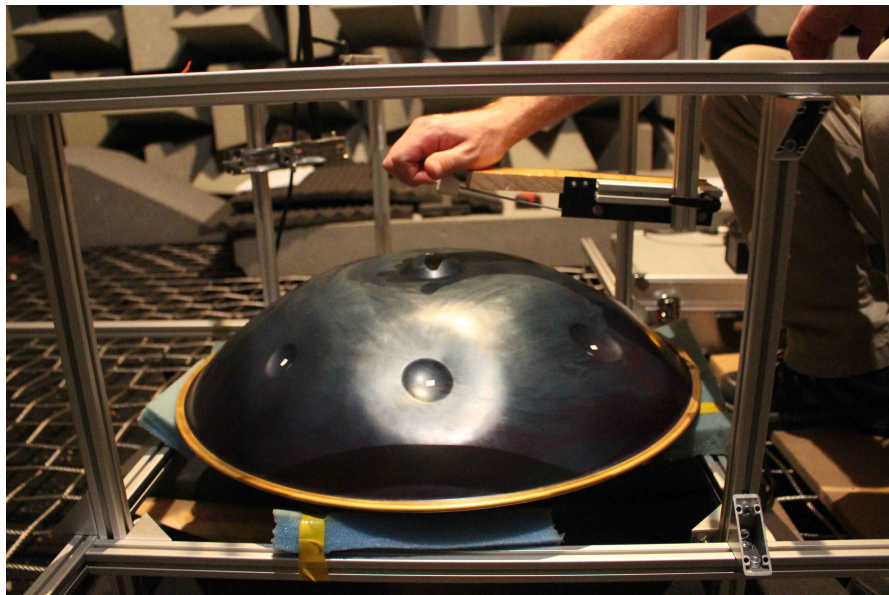
The environment in which the handpan is recorded will have a significant influence on the characteristics of the measured signal, such as timbre (due to standing modes of the room) and decay rates of individual spectral peaks (due to reflections). Additionally, the presence of background noise in a recorded signal can affect the accuracy of the extraction of signature vibrational modes and corresponding decay rates. To minimise the influence of the acoustic environment on the measured handpan sound signal, all recordings were made within an anechoic chamber. An anechoic chamber is a room where all sound reaching its walls is absorbed by large wedges of sound-absorbing material resulting in an effectively reflection free environment [19]. Figure 3.1 shows how the measurement apparatus was set up inside the anechoic chamber.

3.1.2 Note-Field Excitation Method

In order to produce a repeatable excitation simple for use in the recording work, the Note-Field Excitation Mechanism (NFEM), as shown in Figure 3.2, was developed. The



(a)



(b)

FIGURE 3.2: The torsional spring based Note-Field Excitation Mechanism (NFEM) used for this project's experimental procedure: (a) the NFEM in resting position; and (b) the NFEM prior to delivering an impulse to the central note-field of the handpan.

NFEM is formed of a torsional spring (2.7 mm wire diameter, 30 mm body length) fixed at one end and attached to a rounded rubber tip at the other. The NFEM is used by pulling the rubber tipped end of the spring back to a fixed wood block (seen in Figure 3.2) and then releasing to generate a strike. The NFEM was designed to produce repeatable strikes to an individual note, provided the NFEM is securely attached to the handpan frame in a stationary position. The degree of repeatability is assessed in Section 4.1. This method of excitation was preferred over sinusoidal or finger force as it allows variable excitation position with repeatable strikes for a single strike position, which are similar in nature to the finger strikes described in Section 2.1.6.

Due to time and budget considerations, no method was employed to directly measure contact time of the rubber tip with the instrument, and velocity of the NFEM when used to strike a note. These measurements would have been useful in determining the repeatability of strikes delivered to different notes, and strike positions. Previous studies of the steelpan used an electrodynamic vibrator to sinusoidally excite notes and estimate note couplings with velocity transducers [23]. This excitation method might have been more suitable to estimate handpan note couplings than the excitation and measurement system chosen for this project, as the NFEM was not designed to be able to avoid non-linear behaviour in the handpan. Several degrees of NFEM strike force (such as: soft, medium, and strong), would be useful to estimate when non-linear phenomena occurs. Section 6.3.1 will detail possible future improvements to the NFEM and measurement system.

The NFEM's success at producing repeatable strikes will be assessed in Section 4.1 by comparing the measured waveforms produced due to successive strikes. As will be detailed in Section 3.2, the NFEM strike's repeatability can only be determined when it is in a fixed position and attached securely to the handpan frame. Figure 3.2 shows close-up images of: (a) the NFEM in resting position; and (b) the NFEM prior to delivering an impulse to the central note-field of a handpan. A video demonstration of the NFEM can be found in the accompanying DVD¹.

¹Can be found in the following directory on the DVD: **EyalMSc/Video/anechoic_handpan.mov**.

3.1.3 Handpan Frame

The handpan frame, as seen in Figure 3.1, was constructed from extruded aluminium rods, and was designed to support the handpan, NFEM, and microphone securely when making measurements. This requires the frame to be strong enough to provide support whilst at the same time minimising the influence of the frame itself on the measurements. It was noted from previous research on the Hang that varying the spacing of the player's knees can influence the tuning of the Helmholtz resonance frequency [14]. The size of the frame was adjusted to provide support as close to the rim of the handpan as possible. Another consideration for the design of the frame was the placement of the microphone relative to the frame and instrument. As can be seen in Figure 3.3, the frame's size was adjusted so that there were no obstructions between the microphone and each of the note-fields. The reflections from the aluminium rods themselves should have a negligible effect on the measurements due to their small dimensions [19] (2 cm for each side) when compared to wavelengths of the expected relevant signature frequencies in the handpan sound. Reflections from incident sound on an object, known as scattering, becomes significant when the object is equal to or larger than two thirds of the incident wavelength. Equation 3.1 can be used to estimate the incident wavelength, λ_{inc} for which scattering might become significant for an object of length, L_{sc} :

$$\lambda_{inc} \leq L_{sc} \cdot \frac{3}{2} \quad (3.1)$$

The length of a single side of the aluminum rod (2 cm) can be used as an approximate value for L_{sc} , in order to calculate: $\lambda_{inc} \leq 0.02 \cdot \frac{3}{2} = 0.03$ cm. Thus, the frequency, f_{sc} , at which scattering will potentially become significant using the handpan frame can be estimated by:

$$f_{sc} \geq \frac{c_{air}}{\lambda_{inc}} \quad (3.2)$$

Where c_{air} is the approximate speed of sound in air at 20°C [19]. In the case of the aluminum rods used in the design of the handpan frame: $f_{sc} \geq \frac{344}{0.03} = 11.47$ kHz. This

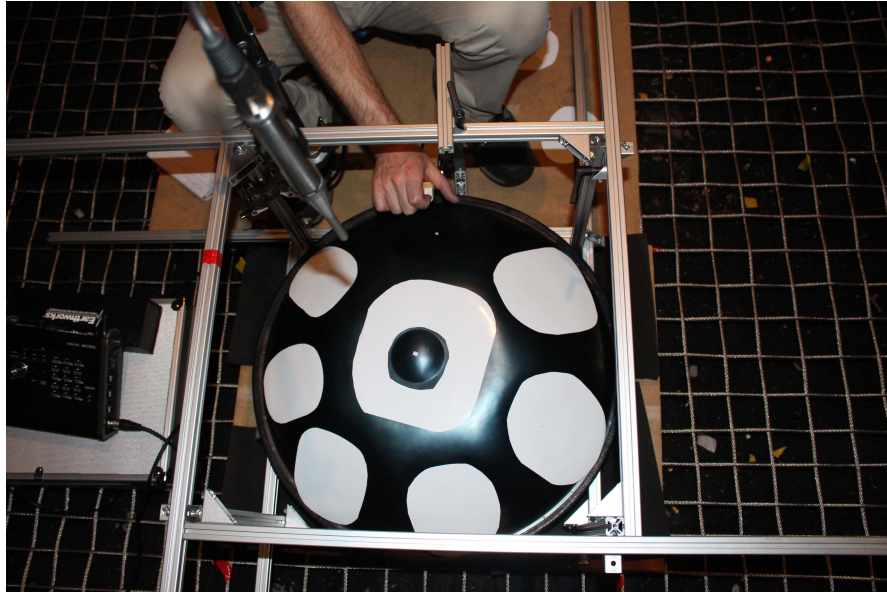


FIGURE 3.3: Top view of the handpan inside the frame with no obstructions between the microphone and each of the note-fields.

shows that the estimated lowest frequency to be affected by scattering from the aluminium rod is 11.47 kHz, which is much higher than the frequency range of expected signature vibrational modes.

3.1.4 Measurement System

Measurement microphones are acoustic transducers that exhibit a (mostly) flat frequency response across all frequencies within the human hearing range. The microphone used for this project was the Earthworks M30 omnidirectional measurement microphone. The frequency response of the M30 is flat across the whole audible frequency range and is shown in Figure 3.4. The neutral frequency response of this microphone type is suitable for the transparent capture of a given sound source. Figure 3.1 and Figure 3.3 show the placement of the M30 microphone relative to the handpan. The M30 was positioned 50 cm above the central note of the handpan, pointing directly at the dimple, for all recordings produced for this project. All recorded audio signals were produced with 44.1 kHz sample rate and 24 bit audio. These allow artefact free capture and reproduction of audio up to 22.5 kHz and a dynamic range of 144 dB.

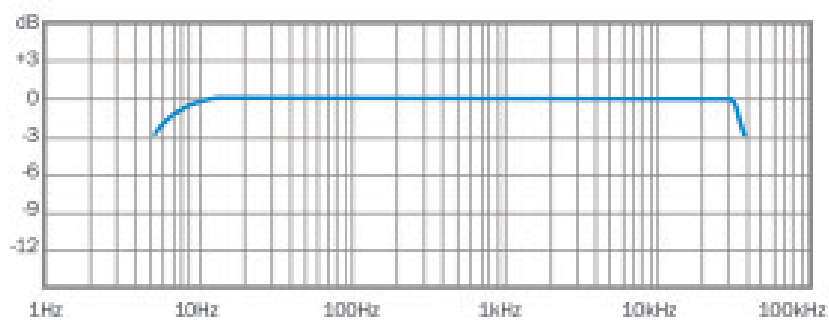


FIGURE 3.4: Frequency response of the Earthworks M30 measurement microphone, showing a flat response over the entire audible frequency range (20 Hz-20 kHz). From [55]

3.2 Measuring the Signature Handpan Sound

As mentioned previously in Chapter 2, the handpan is classified as a directly struck idiophone [20, 21]. Each shell-shaped note-field is coupled to surrounding note-fields on the shell shaped body of the instrument through the internote area. Similar to the strong coupling of Marshall-pair notes in the steelpan mentioned in Section 2.1.4, some of the handpan’s note-pairs are expected to exhibit a greater degree of coupling than others.

When a note-field is struck in the ‘D’ sweetspot, the first three vibrational modes are expected to produce three unique spectral peaks with a 1:2:3 frequency ratio, much like the Hang and steelpan [22]. Delivering strikes to different sections of the note-field are expected to emphasise one of these vibrational modes, however due to coupling and non-linear behaviour, modes of surrounding note-fields might also be excited. Thus the following questions arise:

1. What is the signature sound of an isolated handpan note-field? This refers to the sound produced from an individual note-field without coupling to surrounding note-fields.
2. What degree of similarity will the resulting sound signals exhibit, provided identical excitation and initial conditions?

As seen in Section 2.1.4, a previous study of the steelpan used sand bags to dampen vibration, and minimise radiation from surrounding notes. Some steelpan makers use

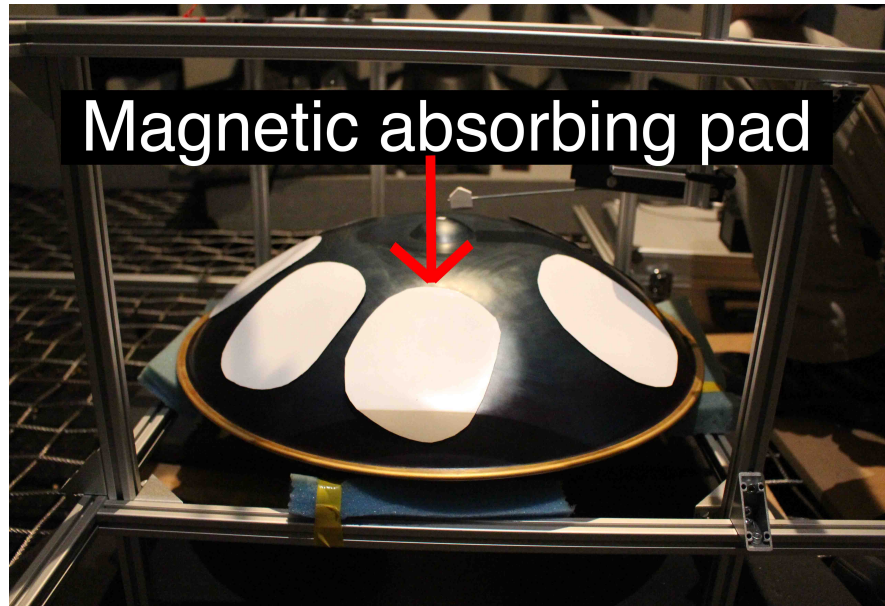


FIGURE 3.5: The magnetic absorbing pads used in the damped configuration.

magnets to achieve a similar effect as note coupling can interfere with the tuning process [56]. In order to determine the signature sound of an isolated handpan note-field, and to estimate the coupling of surrounding notes, each note-field sound was measured in two configurations:

- Damped: Magnetic absorbing pads were placed to cover all note-fields other than the one currently being recorded, in order to suppress their vibration. The magnetic absorbing pad is shown in Figure 3.5 and the damped configuration is shown in Figure 3.3.
- Undamped: No magnetic absorbing pads were used to dampen surrounding note-fields. This configuration is shown in Figure 3.1.

The isolation method using magnetic absorbing pads is not expected to have a significant influence on the frequencies of signature vibrational modes of the targeted note, due to expected localisation of these vibrations to the elliptical note area, as has been observed previously with steelpan notes [23]. Measurement of a note in the damped configuration should therefore ease the process of estimating vibrational mode frequencies and corresponding decay rates. Despite this, placing the magnetic absorbing pads on the shell-like

structure of the handpan is expected to decrease the measured note's decay time, as they also dampen vibration of surrounding notes, and the shell-like structure.

The measurement procedure for an individual handpan note-field was implemented in the following sequence: securely place the handpan inside the frame, position the microphone and NFEM appropriately, adjust recording levels to avoid clipping, deliver a strike to the note-field allowing the sound to decay to an inaudible level, place magnetic absorbing pads on all surrounding note-fields and deliver an additional strike. Eight strikes were delivered to each note-field in each configuration. The note-field sound was allowed to decay for ten seconds prior to delivering the next strike. Once the handpan and microphone were positioned securely, they were not moved until all notes of the handpan were recorded.

The NFEM and handpan frame were designed to be used in such a way that the NFEM should produce repeatable strikes to an individual note in the damped or undamped configuration provided the NFEM is securely attached to the frame and is left in a stationary position. The velocity at which the NFEM's rubber tip meets the targeted note will differ from note to note, as the NFEM's position on the frame required adjustment in order to target different notes of a given handpan. This means that strike repeatability using the NFEM can only possibly be valid for an individual note, with the NFEM in a fixed position.

Figure 3.6 displays the time domain waveforms of an F#₃ note-field in the undamped and damped configurations when struck at the 'D' sweetspot, which shows the shorter decay time of the damped signal. Table 3.1 provides a key of measurements taken for all four instruments investigated in this project. Additionally, measurements for Instrument 3 and Instrument 4 were made both prior to, and following, tuning by an established handpan maker. Appendix C displays an image that lists the musical note names and corresponding fundamental frequencies (e.g. A₄ = 440 Hz).

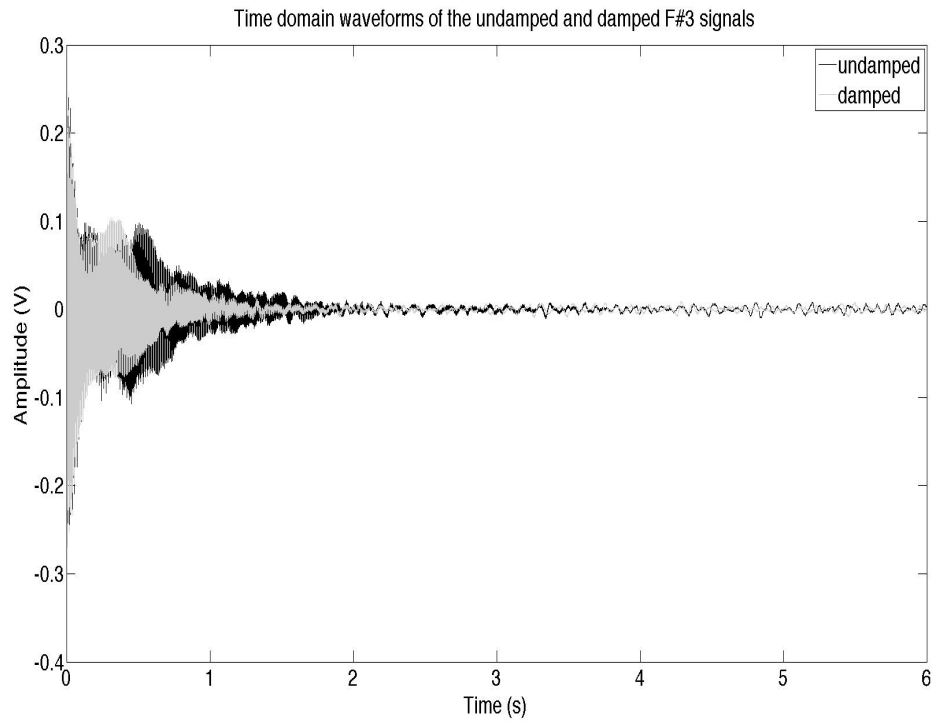


FIGURE 3.6: Time domain waveforms of the undamped and damped F#₃ signals, struck at the ‘D’ sweetspot.

Instrument 1	Instrument 2	Instrument 3	Instrument 4
B ₂	C ₃	D ₃	G ₃
F# ₃	G ₃	A ₃	C ₄
A ₃	Ab ₃	A# ₃	D ₄
B ₃	B ₃	D ₄	E ₄
C# ₄	C ₄	E ₄	F ₄
D ₄	D ₄	F ₄	G ₄
E ₄	Eb ₄	G ₄	A ₄
F# ₄	G ₄	A ₄	B ₄
-	-	-	C ₅

TABLE 3.1: A key of measurements taken for all four instruments investigated in this project. All note-fields were measured in both undamped and damped configurations.

3.3 Summary

This chapter has covered the design and implementation of an experimental procedure for the measurement of the signature handpan sound, and estimation of note coupling. Previous studies of the steelpan employed rubber-tipped standard pan sticks to excite

notes and record the sound in order to estimate modes of vibration [23]. The rubber-tipped NFEM was used to produce repeatable strikes to an individual note, provided the NFEM was securely attached to the handpan frame in a stationary position. The handpan frame was designed to support the handpan, NFEM, and microphone securely, whilst minimising the influence of the frame itself on the measurements. Magnetic absorbing pads were used to dampen vibration, and minimise radiation from surrounding note-fields. This experimental procedure should be useful in estimating the signature handpan sound, and the degree of note coupling. A measurement microphone was used to record a set of samples, inside an acoustically neutral environment (the anechoic chamber), for all notes of all four instruments in Table 3.1, in both undamped and damped configurations. In Chapter 4, these measurements will be analysed using the Fourier methods detailed in Chapter 2, in order to estimate signature vibrational modes and decay rates of handpan notes, and the degree of note-coupling.

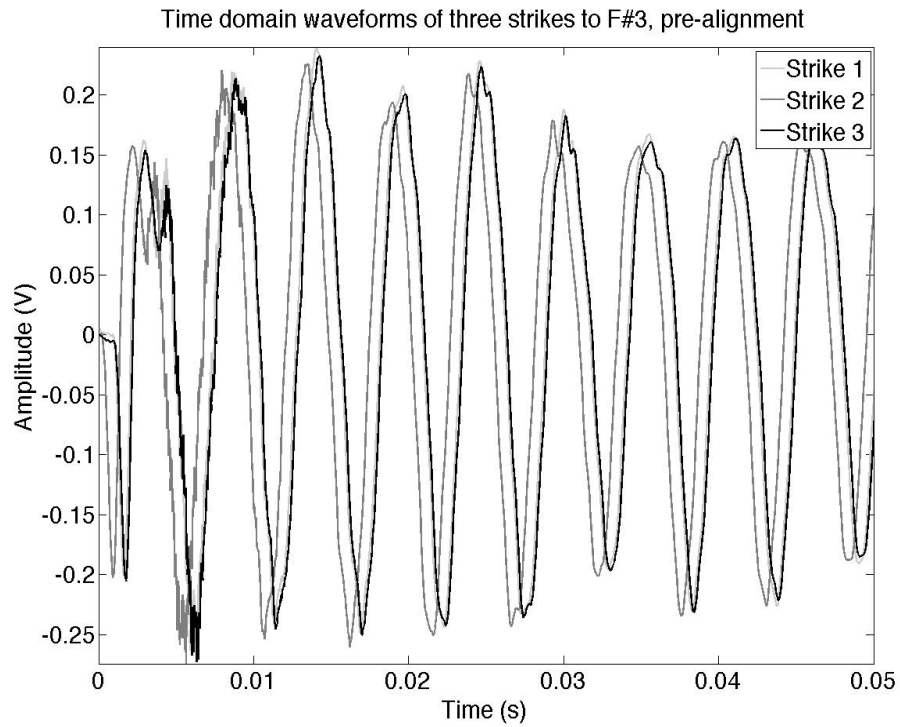
Chapter 4. Analysis

This chapter presents an analysis of the results from the experimental procedure outlined in Chapter 3. Fourier analysis methods were preferred over high resolution methods due to the extensive use of these techniques in the related steplan and Hang literature [15, 23], the author's proficiency with these methods, the project time limitations, and the uncertainty whether high resolution accuracy is required for the purpose of identifying the signature handpan sound. The success of the NFEM at producing repeatable strikes is assessed through comparison of the waveforms and frequency spectra produced by three successive strikes to a fixed position of a single note-field. In addition, Energy Decay Relief (EDR) plots of recorded handpan notes are analysed in order to extract the frequencies and decay rates of signature vibrational modes. In the context of this project, a signature mode is defined as one of a number of highest magnitude detected peaks in the spectrum of the handpan sound. The decay curve associated with modes that exhibit beating phenomena is then considered in order to obtain a measure of the beating rate for individual signature modes. Following this, the significance of strike position on an individual note-field is estimated by analysing EDR plots of three different strike positions on an individual note-field to extract and compare initial magnitudes and decay times. Finally, spectrograms, EDR plots, and frequency spectra of measurements made in damped and undamped configurations are displayed and analysed. All of the MATLAB code used to produce the results displayed in this Chapter and Chapter 5 can be found on the data DVD¹.

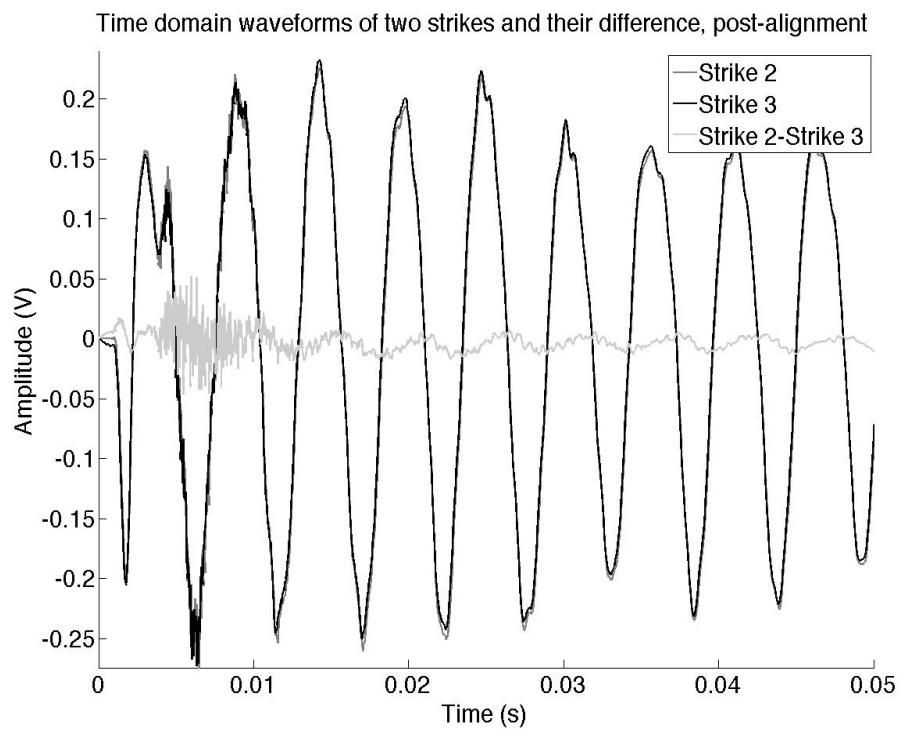
4.1 Excitation Repeatability

In order to compare multiple handpan recordings, the repeatability of the NFEM strike must be confirmed. To achieve this, the undamped F#₃ note-field signal, which belongs to Instrument 1 in Table 3.1 was analysed. As can be seen in Figure 4.1(a), which displays

¹Can be found in the following directory on the DVD: **EyalMSc/Code/**.



(a)



(b)

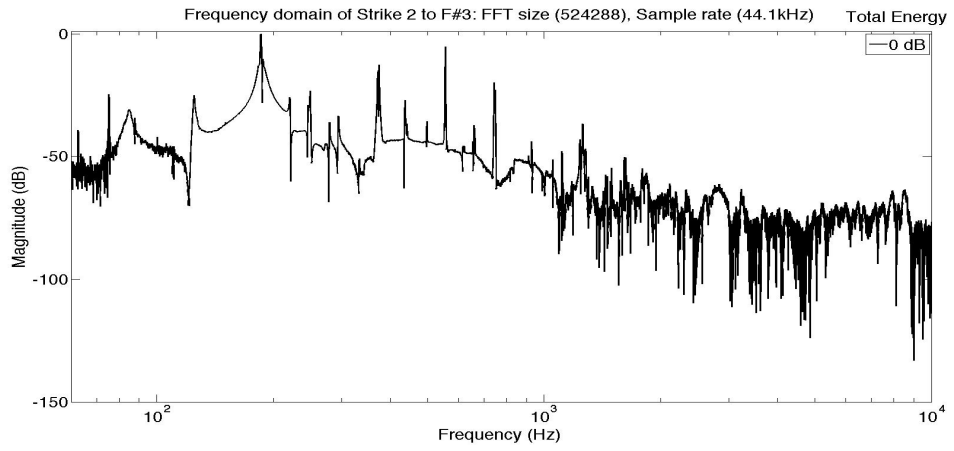
FIGURE 4.1: Alignment of successive strikes delivered to the 'D' sweetspot of the undamped F#₃ note-field: (a) pre-alignment; and (b) post-alignment.

time domain waveforms of three successive strikes delivered to the ‘D’ sweetspot of the undamped F#₃ note-field, the signals are not aligned. The alignment method involved identification of the sample value of the single largest peak from the three time domain signals. Each signal was then aligned by determining the time sample location of the peak value and adding a corresponding amount of leading zero valued samples. Figure 4.1(b) displays the post-alignment Strike 2 and Strike 3 signals as well as the difference between them. Although not used for signal alignment, a correlation based approach provided an additional indication of the degree of strike repeatability. The discrete cross-correlation of two real-valued signals, $x[n]$ and $y[n]$ is defined as:

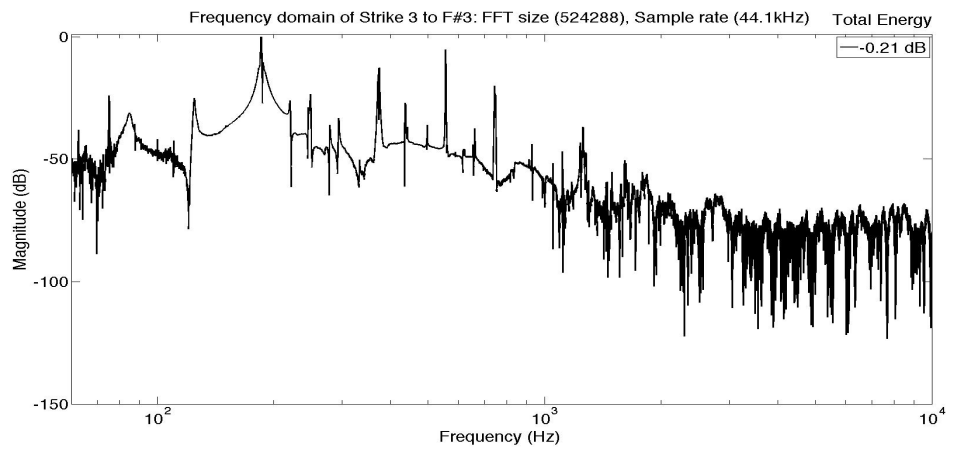
$$x[n] \star y[n] = \sum_{m=-\infty}^{\infty} x[n] \cdot y[m + n] \quad (4.1)$$

Autocorrelation of a real-valued signal is the cross-correlation of the signal with itself. For signals which are very similar, a strong peak will be present at the corresponding sample lag value. This lag value can then be used for signal alignment. If the signals are identical both in length and individual sample values, the strong peak will be located at sample lag zero. Appendix D displays autocorrelation results for Strike 1, and cross correlation results for Strike 1 and Strike 2, which show the high degree of similarity between Strike 1 and Strike 2.

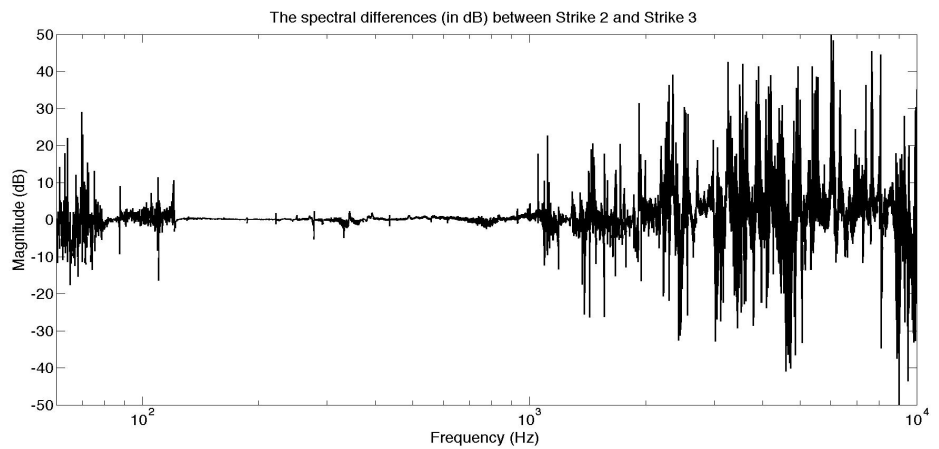
Figure 4.2 displays spectra of: (a) Strike 2; (b) Strike 3; and (c) the difference signal (Strike 2 - Strike 3) to the ‘D’ sweetspot of an undamped F#₃ note. Comparing the spectra of the two strikes displayed in this figure shows a high degree of similarity within the 120 Hz-1000 Hz range. Examining 4.2(c) shows an absence of significant peaks in this frequency range, which also suggests a high degree of similarity. The total amount of energy for each strike signal was calculated by summing the squared signals [57] and converting to decibel values, which were normalized to the highest energy value out of the three strikes (Strike 2 in Figure 4.1(a)). Equation 4.2 displays calculation of the normalized total energy value in decibels for a single strike, where $y(n)$ is the value of the time domain signal at sample n , N is the total number of samples, $y_{e_{sum}}^{max}$ is the highest total energy value out of all three strikes, and $y_{e_{sum}}$ is the normalized total energy value



(a)



(b)



(c)

FIGURE 4.2: Spectra of: (a) Strike 2; (b) Strike 3; and (c) the difference signal (Strike 2 - Strike 3) to the 'D' sweetspot of an undamped $F\#_3$ note. FFT size = 524288, sample rate = 44.1 kHz. Time domain waveforms of Strike 2 and Strike 3 are displayed in Figure 4.1(a).

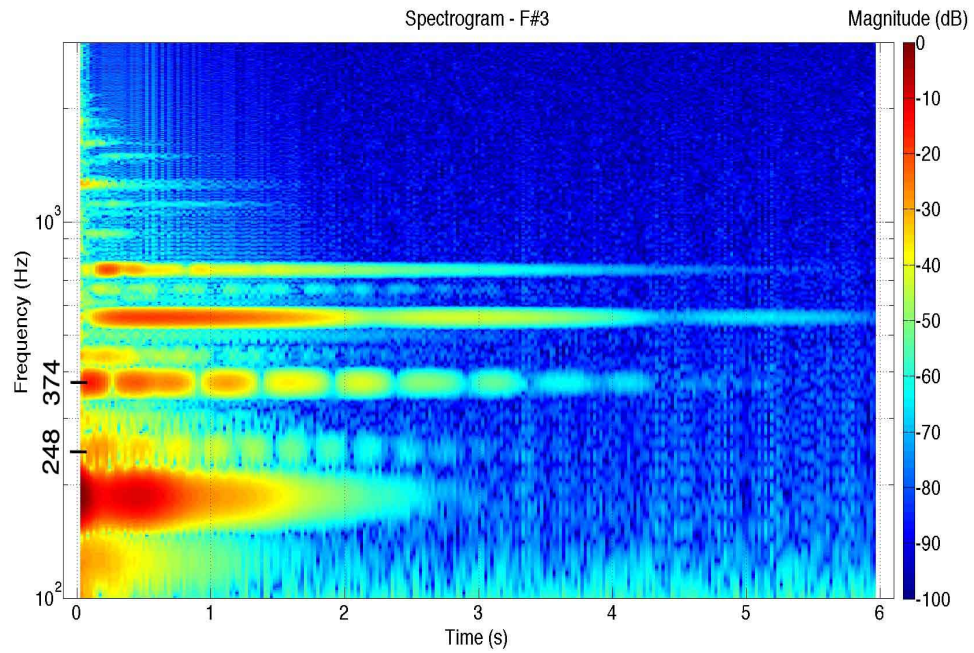
for a single strike in decibels.

$$y_{e_{sum}} = 10 \log_{10} \frac{\sum_1^N y^2(n)}{y_{e_{sum}}^{max}} \quad (4.2)$$

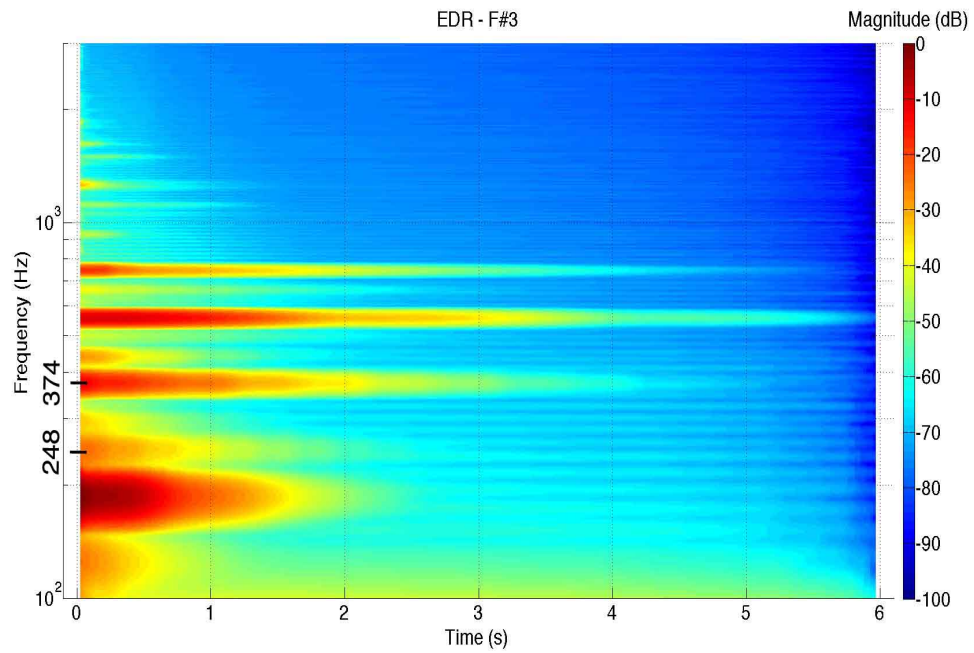
The just noticeable difference in sound level is typically quoted at 1 dB [19]. The total energy values calculated for all three strikes displayed in Figure 4.1(a) are: -0.25 dB, 0 dB, and -0.21 dB. These are all within 1 dB of each other, which leads to the conclusion that successive strikes delivered to an individual note-field in a single strike position using the NFEM are sufficiently similar for the purposes of this project.

4.2 Signature Handpan Sound

As seen in Section 2.2.2.1, the Energy Decay Relief decays more smoothly than the amplitude envelope of a signal. Since the EDR is an integrative quantity, amplitude modulations appear less prominently than in the amplitude envelope, and curves of peaks decay in a more linear fashion. Thus, this method allows the easier identification of signature mode frequencies and decay rates. Figure 4.3 displays: (a) spectrogram; and (b) EDR plot of a measured signal produced by striking the ‘D’ sweetspot of the undamped F#₃ note-field using the NFEM. Previous research of the steelpan and Hang have shown a 1:2:3 frequency value ratio associated with the first three signature modes of notes on these instruments [15, 23]. The parameters of the STFT used for analysis of the measured handpan signals were selected to produce a suitable frequency bin size for resolving between signature modes of the instruments investigated in this project. The spectrogram in 4.3(a) was produced using a 2048 Hamming window, with 50% overlap and FFT size of 32768. Calculation of the bin width is achieved by dividing the sample rate by the frame length: $\frac{44100}{2048} = 21.5$ Hz. Each frame duration is approximately 46 ms in length, compared to the 4-6 second audible duration of some signature vibrational modes. Thus, this frame duration was considered sufficient for resolving relevant changes in the signal, and estimating decay times of signature vibrational modes.



(a)



(b)

FIGURE 4.3: (a) Spectrogram; and (b) EDR plot of a measured signal produced by striking the ‘D’ sweetspot of the undamped F#₃ note-field using the NFEM. Analysis settings: Hamming window = 2048, 50% overlap, FFT size = 32768, sample rate = 44.1 kHz. Highlighted on the frequency axis are the 248 Hz and 374 Hz frequency peaks.

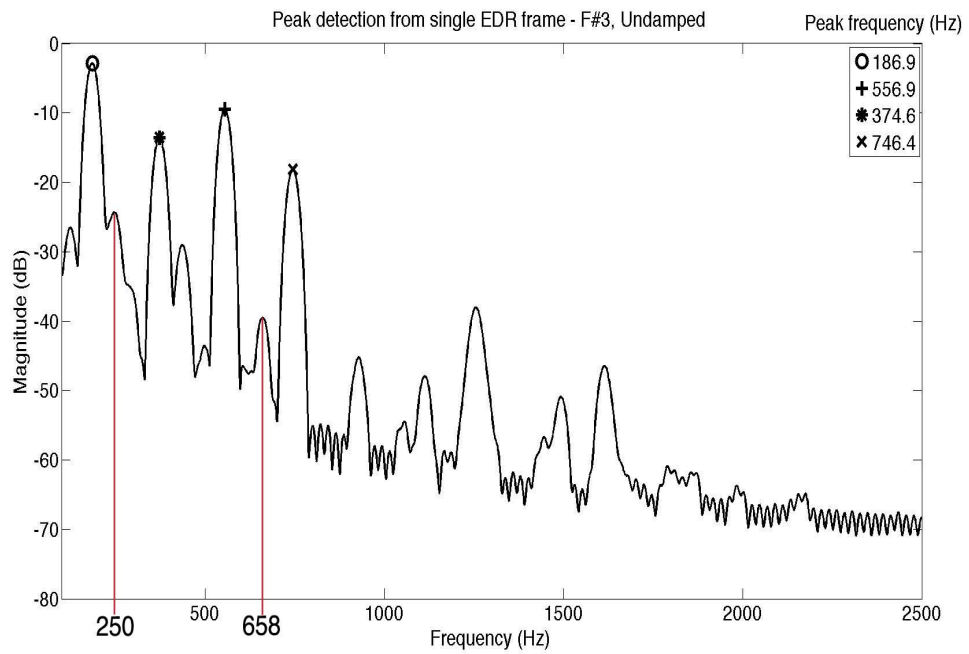
Comparing (a) and (b) in Figure 4.3 shows that the majority of the beating phenomena do not appear as prominently in the EDR plot. This is most evident in the 248 Hz and 374 Hz frequency peaks. 374 Hz is approximately an $F\#_4$, whereas 248 Hz is approximately a B_3 . Amongst the expected signature modes of Instrument 1, the $F\#_4$ is present as the octave of the $F\#_3$ note-field, and the fundamental of the $F\#_4$ note-field. These notes are thought to behave as a sympathetic pair (or Marshall-pair as mentioned in Section 2.1.4). The B_3 is present as the octave of the B_2 note-field, and the fundamental of the B_3 note-field, which also are thought to form another sympathetic pair of notes.

4.2.1 Signature Vibrational Modes

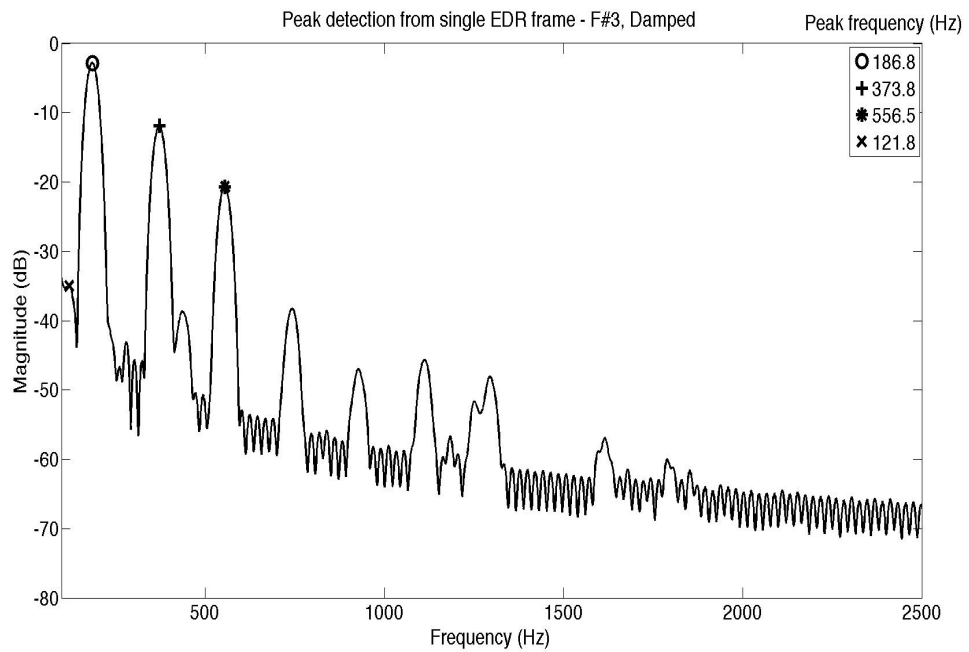
For each recorded handpan note, a single EDR analysis frame was used to extract the frequency values of signature vibrational modes. This frame was chosen as the first to follow the transient onset of the recorded note (approximately 4-10 ms), in order to avoid erroneous frequency selection due to the broadband nature of the note onset. Figure 4.4 shows an example EDR analysis frame highlighting the four highest detected peaks (in order of descending magnitude from top to bottom) and corresponding estimated frequency values for: (a) undamped $F\#_3$; and (b) damped $F\#_3$, struck in the 'D' sweetspot.

In an attempt to improve the accuracy of the identified frequency values associated with each peak, the parabolic interpolation method identified by Equation 2.11 was used. Despite using this method, no significant improvement in frequency value estimation was observed as the STFT analysis frame was already heavily zero padded. This zero padding decreases the bin width from 21.5 Hz to 1.3 Hz, effectively by means of interpolation.

Comparing (a) and (b) in Figure 4.4, it is clear that the three strongest detected peaks have an approximate 1:2:3 frequency ratio, even though their relative magnitude is different for both cases. In 4.4(a), the fourth largest magnitude detected peak's frequency value is 746 Hz, which is an $F\#_5$. In the damped case, this frequency peak value contains significantly lower energy compared to the highest magnitude detected peaks. For the undamped handpan signal, this suggests non-linear behaviour in the coupling interaction between the $F\#_3$ and $F\#_4$ note. The presence of some of the peaks in 4.4(a), such as



(a)



(b)

FIGURE 4.4: Peak detection using a single EDR analysis frame highlighting the four highest detected peaks (in order of descending magnitude from top to bottom) and corresponding estimated frequency values for: (a) undamped F#₃; and (b) damped F#₃, struck in the 'D' sweetspot.

the 250 Hz (approximately B₃), and 658 Hz (approximately E₃) peaks is likely due to coupling of the F#₃ with surrounding note fields on Instrument 1. This suggestion is strengthened by noticing the absence of these peaks in 4.4(b). The highest expected frequency value for the first three vibrational modes of Instrument 1 is approximately 1108 Hz, which is a C#₆ (this is the perfect fifth of the F#₄ note). Therefore, it is not clear whether the peaks above 1108 Hz, which are present in 4.4(a) and 4.4(b) are due to non-linear behaviour of the F#₃ note area or additional note coupling.

Note-field	Pk.1 mag. (dB), frequency (Hz), frequency ratio	Pk.2 mag. (dB), frequency (Hz), frequency ratio	Pk.3 mag. (dB), frequency (Hz), frequency ratio	Pk.4 mag. (dB), frequency (Hz), frequency ratio
D ₃	-1.79 152.1 1	-8.32 297.7 1.96	-21 592.3 3.89	-23.9 443.6 2.92
A ₃	-2.13 226.3 1	-2.46 444.6 1.96	-9.43 664.3 2.93	-27.1 151.2 0.67
A# ₃	-2.56 234.8 1	-22.6 697.7 2.98	-25 463.3 1.98	-33.1 152 0.65
D ₄	-0.845 591.8 1.99	-2.67 297.1 1	-18 884.1 2.97	-31.3 152.4 0.51
E ₄	-2.08 334.6 1	-3.82 664.1 1.98	-15.5 993.4 2.97	-22.4 234.6 0.7
F ₄	-1.71 700.6 1.99	-2.24 352 1	-18.8 1053 2.99	-22.5 397.8 1.13
G ₄	-2 395.5 1	-11.5 788.3 1.99	-13.3 1175 2.97	-29 349.3 0.88
A ₄	-2.44 444.1 1	-6.12 884.3 1.99	-12 1325 2.98	-27.9 490.5 1.1

TABLE 4.1: Highest magnitude peaks, corresponding frequency values, and frequency ratios (relative to the fundamental frequency) of all eight undamped note-fields of Instrument 3 (pre-tuned), when struck in the ‘D’ sweetspot. Peaks are sorted in order of descending magnitude from left to right.

Table 4.1 shows the four highest magnitude detected peaks for all eight undamped note-fields of Instrument 3 (prior to tuning by an established handpan maker as mentioned in

Section 3.2) when struck in the ‘D’ sweetspot, and their corresponding frequency values and ratios. These peaks are sorted in order of descending magnitude from left to right, in order to ease identification of the three highest magnitude signature peaks. Four peaks have been detected and displayed in the table in order to show that like the steelpan and Hang, the first three signature vibrational modes of individual handpan notes are tuned to produce a 1:2:3 frequency value ratio. For seven out of eight note-fields, the three highest magnitude peaks detected have an approximate 1:2:3 frequency value ratio. The third highest magnitude peak of the undamped D_3 note-field is approximately four times the value (i.e. the double octave) of the fundamental frequency, which produces an approximate 1:2:4 frequency ratio. The perfect fifth vibrational mode for the D_3 note-field was detected as the fourth highest magnitude peak. The presence of the double octave peak seems to suggest a strong coupling between the D_3 and D_4 note-fields, which act as a sympathetic pair. This emphasises the D_5 frequency (c. 592 Hz), which is the octave of the D_4 note-field. This suggestion is strengthened by examining the three highest magnitude peaks detected from the damped D_3 signal: 152.2 Hz, 298.1 Hz, and 449.2 Hz which have a frequency ratio of approximately 1:2:3. Additional comparisons between undamped and damped signals will be displayed in Section 4.3, and Section 4.4. Tables of the highest magnitude detected peaks of all note-fields for the remaining three handpans investigated in this project are presented in Appendix E.

Mismatches in identified peak frequency values between different note-fields are evident when examining Table 4.1. For example, the octave of the D_3 is 297.7 Hz, however the fundamental of the D_4 is 297.1 Hz. It is not clear whether these mismatches are due to tuning limitations of the instrument, inharmonicities due to non-linear behaviour, or accuracy limitation inherent in the analysis. A potential explanation might be attributed to pitch glide effects of the struck note, similar to those reported for the steelpan in Section 2.1.4.

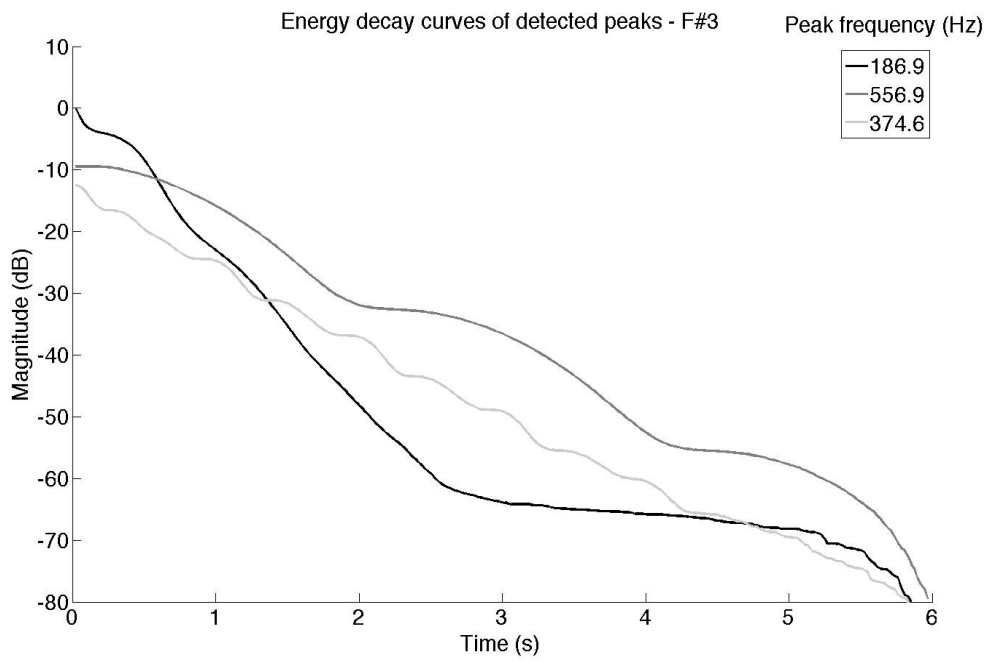
It is worth noting that magnitudes identified in this project were not considered part of the signature handpan sound, as the velocity of the stick was not measured or kept consistent between individual notes, so inevitably, individual handpan notes were excited with different strike strength, even though repeatability for a single strike location was shown in Section 4.1. Despite this, the magnitude values identified here were used as

part of the modal synthesis method for synthesising the handpan sound, which is detailed in Chapter 5.

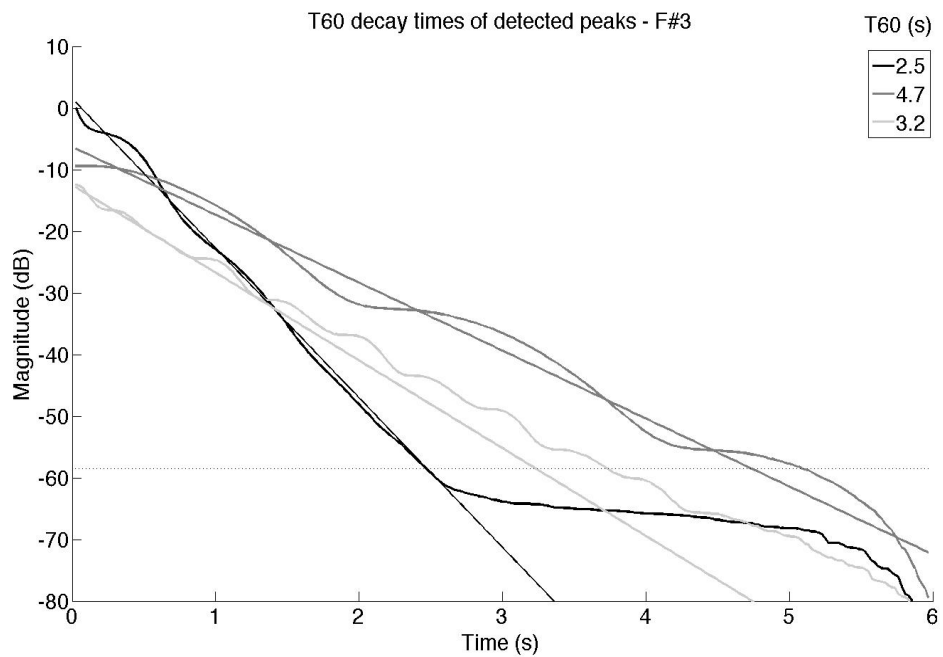
4.2.2 Decay Rates

Upon detection of the signature vibrational modes it is desirable to estimate their corresponding T60 decay times. In the context of this project, the T60 decay time is defined as the amount of time it takes for a signature mode to decay by 60 dB from its initial magnitude value. The highest magnitude detected signature mode for an individual note-field measurement was used to determine the -60 dB threshold. To implement this, Matlab's `polyfit` function was used to calculate the coefficients of a second degree polynomial that best fits a section of the corresponding decay curve (using a least-squares method [58]). In order to select the appropriate section for calculation of the polynomial, the gradient of the selected frequency bin over time was calculated. Where this gradient approaches zero represents the point where the decay curve reaches the noise floor, and this can be seen as a suitable end point for best-fit calculation.

Figure 4.5 displays the Energy Decay Curves (EDCs) of the detected vibrational modes identified in Figure 4.4, from a strike to the 'D' sweetspot of the undamped F#₃ signal: (a) EDCs and corresponding estimated frequency values; and (b) EDCs, estimated straight line fits and calculated T60 decay times. The T60 decay times were determined by calculating the second degree polynomial for each mode, and identifying the -60 dB point on that polynomial. The straight line fit reliability was not consistent for all detected peaks of all note-field measurements. The most accurate fits were produced for detected peaks that exhibited a mostly linear decay (such as the 186.9 Hz peak in Figure 4.4 between 1 s - 2.6 s). The behaviour of the 186.9 Hz curve at 2.6 s might be indicative of the combined behaviour of two modes (one fast and one slow) with similar frequency. Examining the 186.9 Hz peak in Figure 4.3 shows that the energy of this peak is prominent only up until approximately 3 s. Thus, the 186.9 Hz curve seems to reach the noise floor at approximately 2.6 s in Figure 4.5. The estimated point where the decay curve reaches the noise floor was not as accurate for peaks that exhibited somewhat



(a)



(b)

FIGURE 4.5: (a) Energy Decay Curves (EDCs) of the detected vibrational modes identified in Figure 4.4, from striking the ‘D’ sweetspot of the undamped $F\#_3$ signal, showing corresponding estimated frequency values; and (b) estimated straight line fits and calculated T60 decay times. The -60 dB threshold is shown as a black horizontal dashed line.

noisy decay curves (such as the 374.6 Hz peak in Figure 4.4), which also resulted in less accurate corresponding straight line fits.

Tables of all the estimated T60 decay times for note-fields of all four handpans is displayed in Appendix F. Table 4.2 displays the mean T60 decay times, standard deviations, and minimum and maximum values of the three highest magnitude peaks for undamped individual instruments, note groups, and all instruments. Only three highest magnitude detected peaks were used to calculate these results, as opposed to four, due to the low degree of reliability of the T60 estimates for many of the fourth highest magnitude detected peaks. The three note groups are: low (B₂-B₃), mid (C₄-E₄), and high (F₄-C₅). Generally, the mean T60 values decrease for higher register note groups. Despite this, the longest measured T60 value (5.9 s) is from the mid note group. Instrument 1 and Instrument 2 have very similar results for all parameters, possibly due to the fact that they are both from the same handpan maker. The similarity of results for these instruments suggests that the method used to estimate T60 decay times has managed to identify decay characteristics of instruments from the same maker, despite the variable reliability of estimated T60 decay times. Instrument 3 and Instrument 4 have relatively short mean T60 values, which could be due to several reasons. Firstly, they contain more higher register notes compared to Instrument 1 and Instrument 2. Secondly, these mean T60 values were calculated from measurements made prior to the retuning of Instrument 3 and Instrument 4 by an established handpan maker. This will be further addressed in Section 4.4.2.

Instrument/note group	Mean T60 (s)	Standard deviation	Min (s)	Max (s)
Instrument 1	3.3	1.1	1.7	5.9
Instrument 2	3.3	1.2	1.6	5.9
Instrument 3	2.8	0.7	1.4	4.0
Instrument 4	2.1	0.5	0.9	3.4
Low (B ₂ -B ₃)	3.2	0.9	1.6	5.1
Mid (C ₄ -E ₄)	3.0	1.2	1.2	5.9
High (F ₄ -C ₅)	2.5	0.9	0.9	4.2
All instruments	2.9	1.0	0.9	5.9

TABLE 4.2: Mean T60 decay times, standard deviations, and minimum and maximum values of the three highest magnitude modes for undamped individual instruments, note groups, and all instruments. Strikes were delivered to the ‘D’ sweetspot.

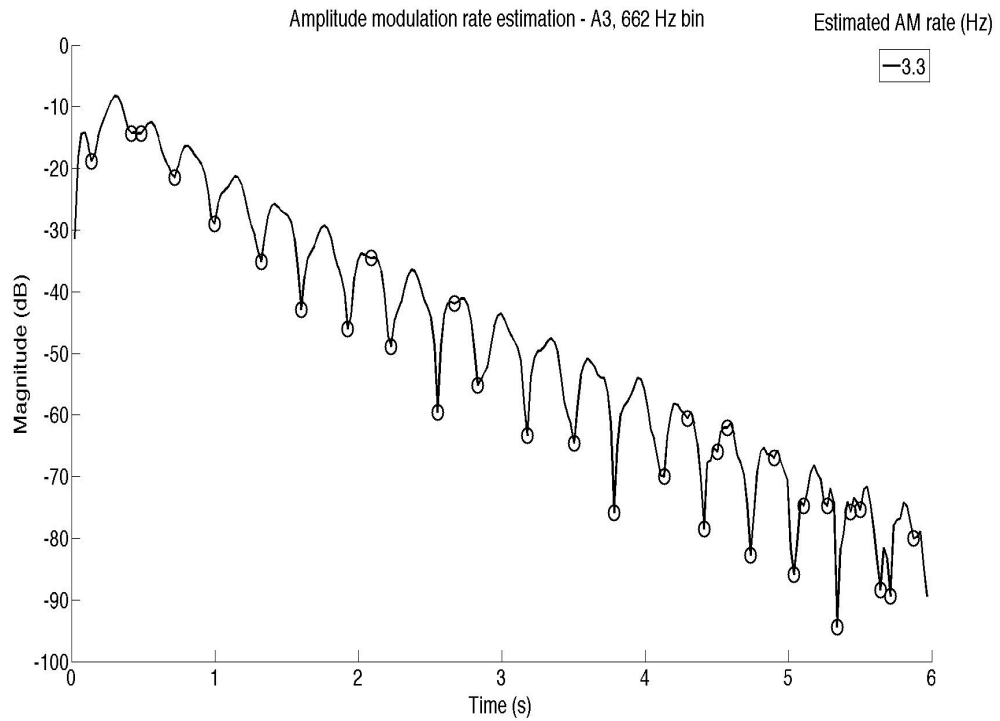


FIGURE 4.6: The 662 Hz peak’s amplitude envelope from a spectrogram of the undamped A₃ note-field signal (struck in the ‘D’ sweetspot), with local minima marked with circles.

4.2.3 Beating

Several of the signature vibrational modes detected in the handpan signal displayed in Figure 4.3 exhibit beating. This beating, which is likely due to coupling of note-fields with slightly mismatched tuning of signature vibrational modes, manifests as visible amplitude modulations in the spectrogram of the signal. Further analysis of measurements that support this hypothesis are presented in Section 4.4. In order to calculate the beating rate, an algorithm was developed that finds the local minima in the magnitude envelope of a signature mode and calculates the average sample distance between the minima. The rate is then calculated by taking the inverse of the average sample distance.

Figure 4.6 shows the amplitude envelope of the 662 Hz peak from a spectrogram of the undamped A₃ note-field signal (struck in the ‘D’ sweetspot), with local minima marked with circles. The beating rate calculated for this signature mode was 3.3 Hz.

Table 4.3 displays the estimated beating rates for several vibrational modes of undamped Instrument 1. The amplitude envelopes of these modes are displayed in Appendix G.

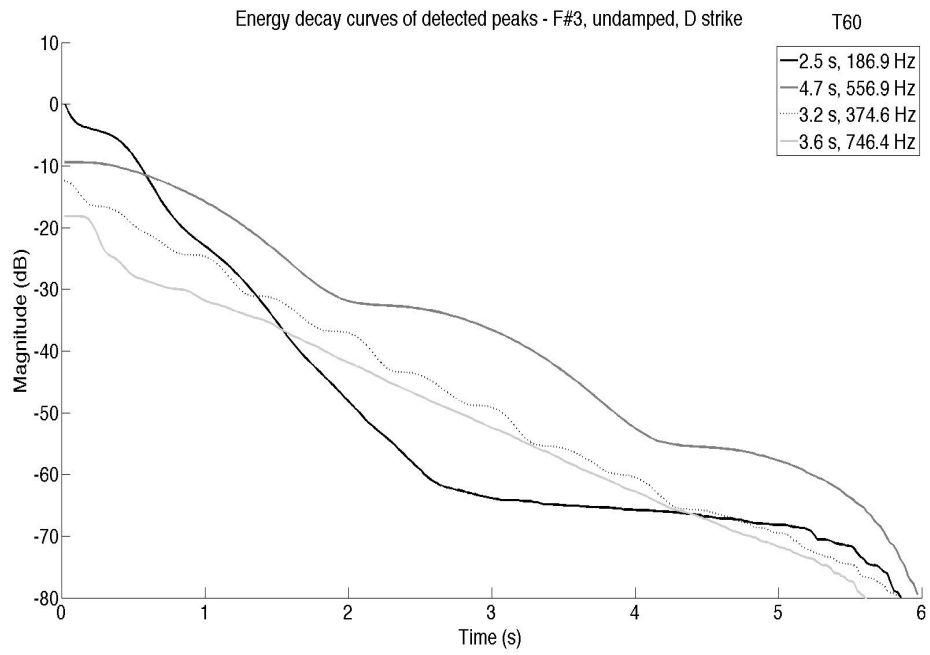
Note-field	Peak frequency (Hz)	Estimated beating rate (Hz)
A ₃	662	3.3
A ₃	438	8.6
B ₃	248	3.9
F# ₃	373	3.1
F# ₄	374	3.3

TABLE 4.3: Estimated beating rates for several vibrational modes from undamped Instrument 1. Strikes were delivered to the ‘D’ sweetspot.

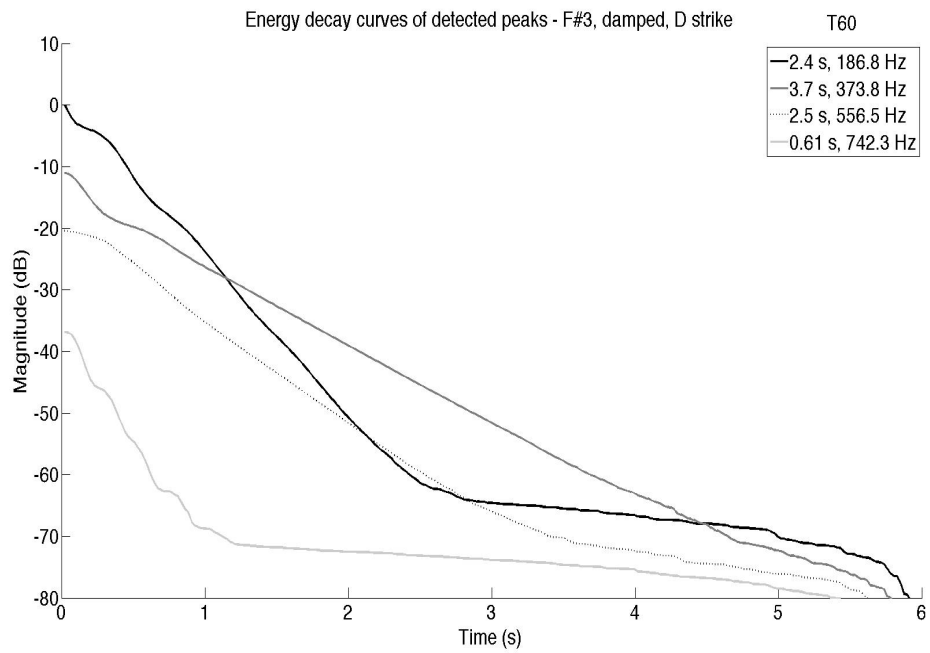
4.3 Note-Field Strike Position

As mentioned in Section 2.1.6, strikes delivered to the ‘D’ sweetspot (as seen in Figure 2.15) are expected to emphasise the fundamental frequency of the note-field. Strikes delivered to the sweetspots labelled ‘O’, and ‘P’ are expected to emphasise the octave and perfect fifth frequencies respectively. Comparing EDCs of the highest magnitude detected peaks from different strike positions in both undamped and damped configurations provides insight into the influence of strike position for an individual note-field. It should be noted that the NFEM was not designed to produce repeatable strikes to different note-field positions, rather only a single position in both undamped and damped configurations. Thus, setting the highest value initial magnitude of a given EDC plot to 0 dB assisted in comparing the relative initial magnitudes of vibrational modes in different strike positions.

Figure 4.7 displays EDCs of four highest magnitude detected peaks in the measured signal of the F#₃ when struck in the ‘D’ sweetspot: (a) undamped; and (b) damped. The results displayed in Table 4.1 showed mismatches in identified peak frequency value between different note-fields. There are also mismatches of identified peak frequency values displayed in this section between the damped and undamped measurements, as well as between undamped measurements made for different strike positions. Similar to the mismatches identified in Table 4.1, it is not clear whether these mismatches are due



(a)



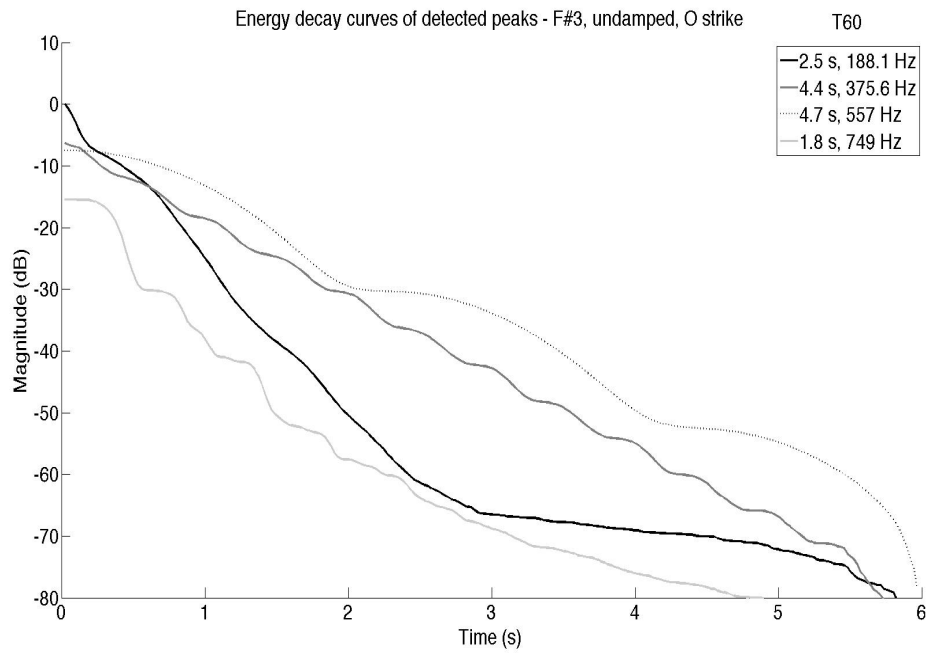
(b)

FIGURE 4.7: Energy Decay Curves of four highest magnitude detected peaks in the measured signal of the F#₃ when struck in the ‘D’ sweetspot: (a) undamped; and (b) damped.

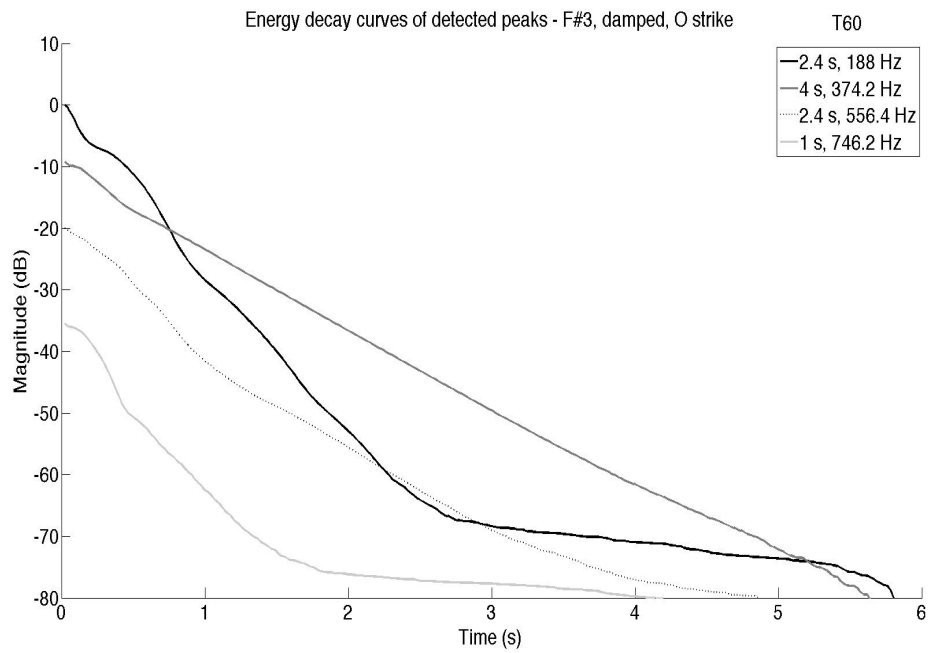
to tuning limitations of the instrument, inharmonicities due to non-linear behaviour, or accuracy limitation inherent in the analysis.

The fundamental frequency (186.9 Hz) peak in 4.7(a) has the highest initial magnitude, followed by the perfect fifth (556.9 Hz), octave (374.6 Hz), and double octave (746.4 Hz). Except for the 746 Hz peak, all curves in 4.7(b) decay more linearly than in 4.7(a). Additionally, the beating phenomena appears to be much less prominent, as can be seen for the curve of the 556.9 Hz peak. The curve of the 374.6 Hz peak appears to be quite noisy in the undamped measurement so the corresponding T60 decay time estimate is not as reliable in this case. Even though the T60 decay time estimate for the 742.3 Hz curve in 4.7(b) is not extremely reliable due to noise, its clear by visually comparing to the 746.4 Hz curve in 4.7(a) that the initial magnitude and T60 decay time have significantly decreased in the damped case. A more in depth comparison of undamped and damped measurements will be displayed in Section 4.4.

Figure 4.8 displays EDCs of four highest magnitude detected peaks in the measured signal of the $F\#_3$ when struck in the 'O' sweetspot: (a) undamped; and (b) damped. The fundamental frequency (188.1 Hz) peak in 4.8(a) has the highest initial magnitude, followed by the octave (375.6 Hz), perfect fifth (557 Hz), and double octave (749 Hz). Comparing the octave decay curve in 4.8(a) to 4.7(a), shows that the initial magnitude has increased by approximately 5 dB. Additionally, the octave curve in 4.8(a) appears to exhibit a regular beating, and is less noisy compared to 4.7(a). The beating phenomena and noisy characteristics of the octave decay curve are less prominent in the damped measurements displayed in 4.7(b) and 4.8(b), which makes the T60 decay time estimates more reliable for these measurements than the undamped measurements. The T60 decay time for the octave curve has increased by approximately 0.3 s in 4.8(b) when compared to 4.7(b). It is worth recalling that the global -60 dB threshold was determined by the highest magnitude detected peak's initial magnitude. Therefore, this increase in decay time might be due to the slight increase in the initial magnitude value (approximately 2 dB) of the octave mode, or non-linear vibration of the note when struck in the 'O' sweetspot.

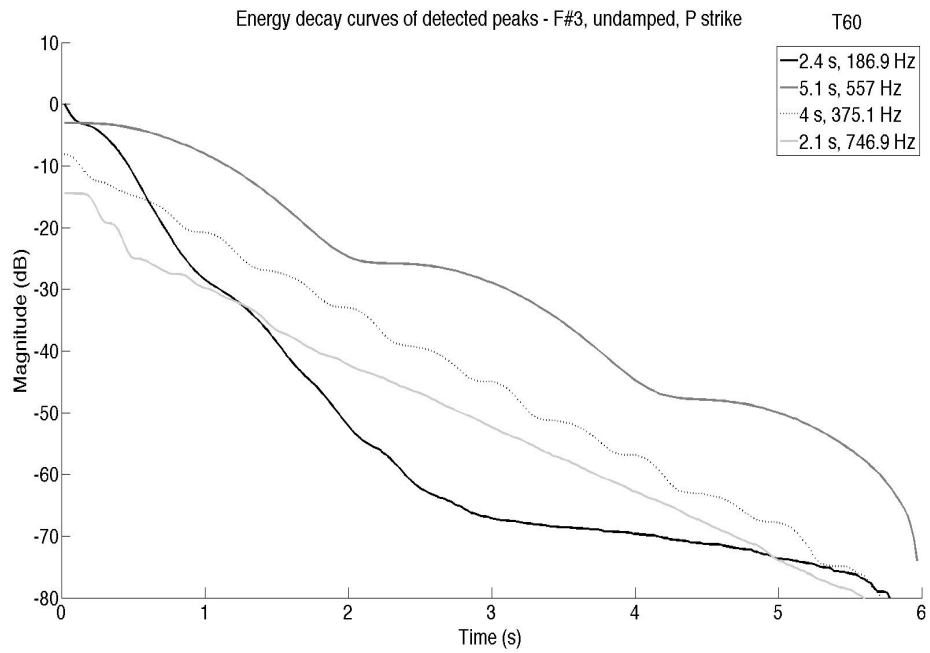


(a)

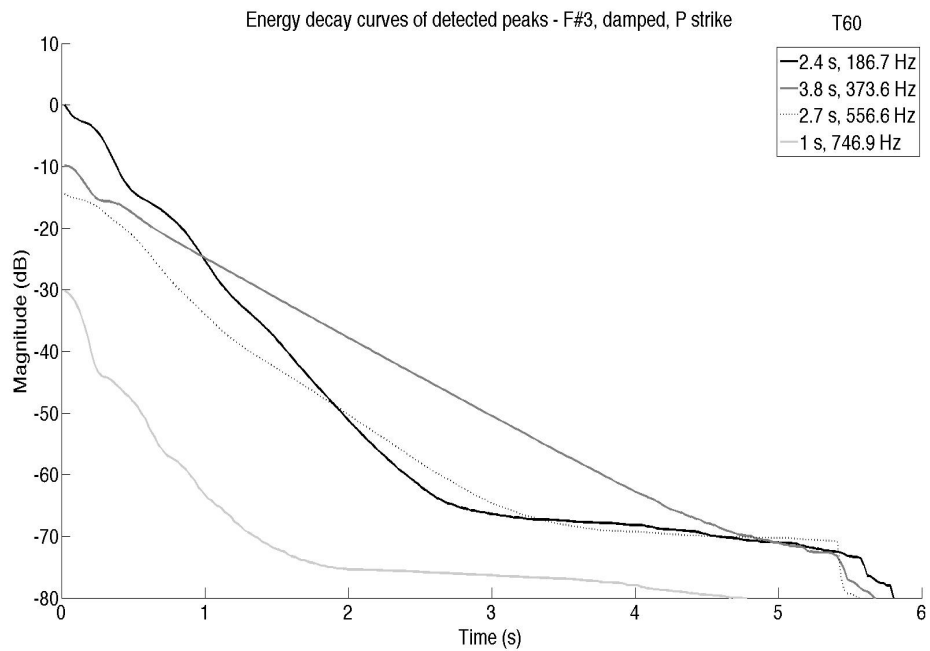


(b)

FIGURE 4.8: Energy Decay Curves of four highest magnitude detected peaks in the measured signal of the F#₃ when struck in the ‘O’ sweetspot: (a) undamped; and (b) damped.



(a)



(b)

FIGURE 4.9: Energy Decay Curves of four highest magnitude detected peaks in the measured signal of the F#₃ when struck in the ‘P’ sweetspot: (a) undamped; and (b) damped.

Figure 4.9 displays EDCs of four highest magnitude detected peaks in the measured signal of the F#₃ when struck in the ‘P’ sweetspot: (a) undamped; and (b) damped. The fundamental frequency (186.9 Hz) peak in 4.9(a) has the highest initial magnitude, followed by the perfect fifth (557 Hz), octave (375.1 Hz), and double octave (746.9 Hz). Comparing the perfect fifth decay curve in 4.9(a) to 4.7(a), shows that the initial magnitude has increased by approximately 7 dB. The estimated T60 decay time of the damped perfect fifth mode displayed in 4.9(b) has increased by approximately 0.3 s, when compared to 4.7(b).

Interestingly, the decay curves of the fundamental vibrational mode (approximately 186.9 Hz) for all strike positions, in both undamped and damped configurations are very similar. This can be seen by comparing the estimated T60 decay times, and visually inspecting the curves of this mode. The regular slow beating rate of the perfect fifth curve (approximately 557 Hz) also appears to be very similar for all three undamped strike positions. Additionally, the order of highest magnitude detected peaks was consistent for all damped measurements of the F#₃ note-field (fundamental, octave, perfect fifth, and double octave) regardless of strike position, unlike the undamped measurements, where the strike position influenced the order of highest magnitude detected peaks.

The initial magnitudes and T60 decay times of the damped double octave decay curves are significantly lower than the corresponding undamped double octave decay curves. This suggests a strong coupling to the F#₄ note-field, which emphasises the 746.9 Hz peak. Despite this, the decay curve of the undamped double octave mode when striking the ‘O’ sweetspot displayed in 4.8(a), looks quite different to the double octave curves in 4.7(a) and 4.9(a). It is not clear why the double octave curve in 4.8(a) does not decay in a very linear fashion, and is also quite noisy compared to the results of the other undamped strike positions.

This analysis seems to confirm that strike position has a significant influence on the timbre of a handpan note-field, though it is worth recalling that the repeatability of the NFEM strike was only confirmed for a single strike position, and that the reliability of the estimated T60 decay times is not consistent for all decay curves of vibrational modes. Curves that exhibited a mostly linear decay produced the most reliable T60 decay time

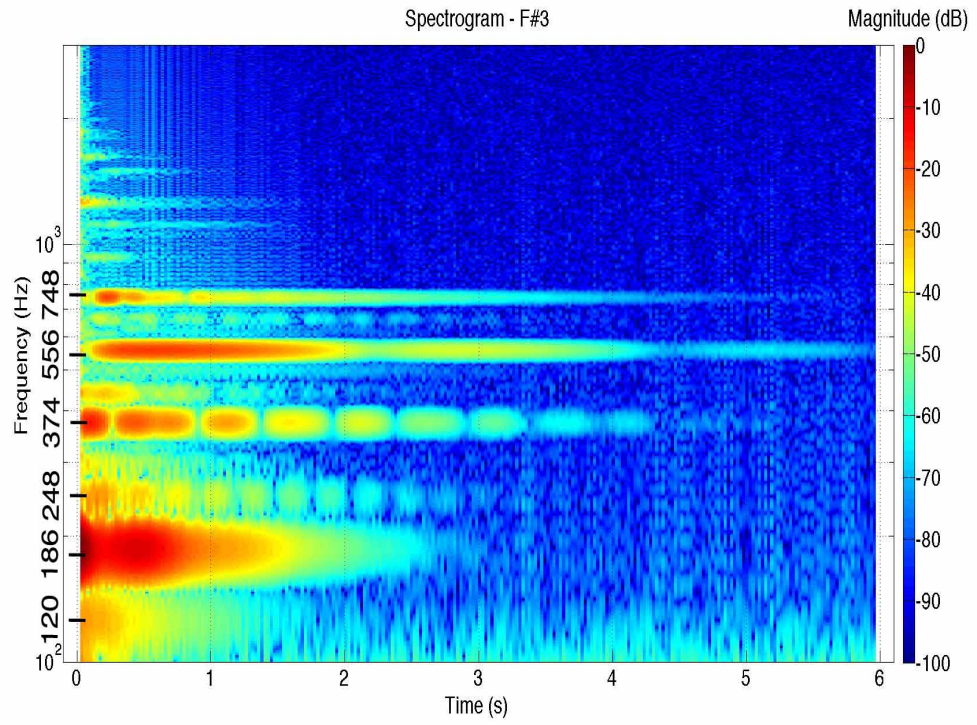
estimates. Potential improvements to the NFEM and T60 decay time estimation will be proposed in Section 6.3 as part of the future work to build upon this project.

4.4 Undamped and Damped Measurements

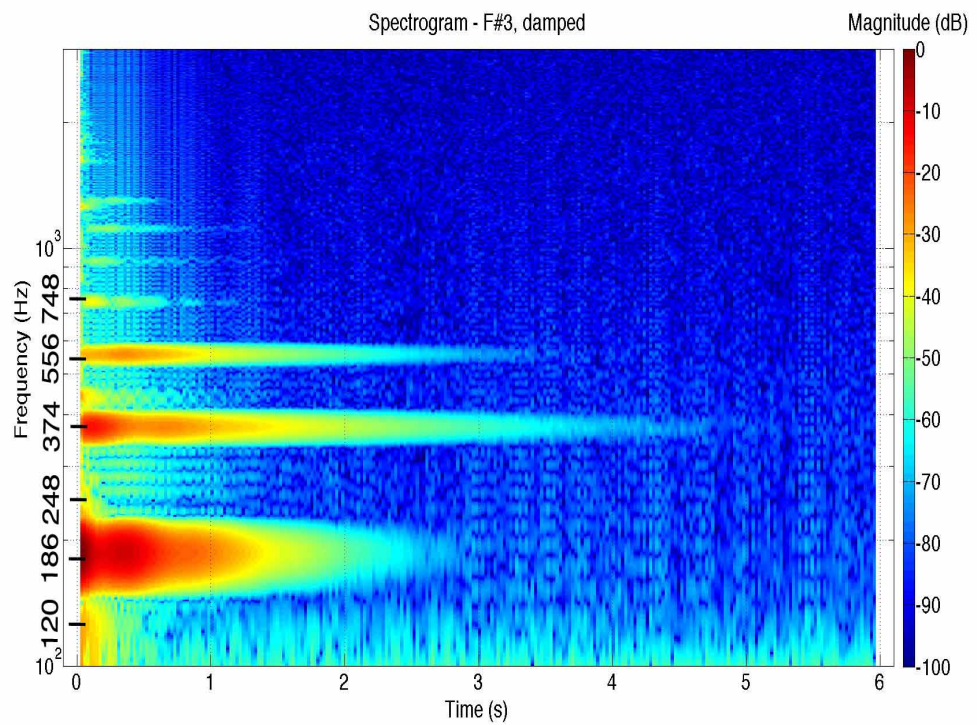
The high degree of strike repeatability to an individual note-field allows for a useful analysis and comparison of signals produced in the undamped and damped configurations. The comparison provides insight regarding the signature vibrational modes of an individual handpan note, degree of note coupling, the effect that tuning has on the spectrum, and the differing timbral characteristics of note-fields between instruments.

Figure 4.10 displays spectrograms of the signals produced from strikes delivered to the $F\#_3$ note-field at the ‘D’ sweetspot, in both configurations: (a) undamped; and (b) damped. Spectrograms are used for this comparison rather than EDR plots in order to clearly show the beating characteristics of the individual vibrational modes. The same STFT analysis parameters detailed in Section 4.2 were selected. The 374 Hz peak’s beating depth is drastically reduced in the damped spectrogram. This strengthens the hypothesis that some of the signature beating phenomena are due to coupling of notes with a slight mismatch in tuning of signature modes. Beating refers to an acoustic effect, which can be demonstrated by summing two oscillators with driving frequencies that have an absolute difference of under approximately 12.5 Hz [19]. The resultant waveform will exhibit an amplitude modulation (beating) rate equal to the absolute difference in frequency between both oscillators. This will be further addressed in Section 5.1.3, which details the method used to reproduce this beating effect in the synthesised handpan sound.

The decay times of some signature modes are significantly reduced in the damped spectrogram, such as for the 556 Hz and 748 Hz frequency components. The onsets of these modes in Figure 4.10(a) occur slightly later in time than the onsets of the 186 Hz and 374 Hz modes.



(a)



(b)

FIGURE 4.10: Spectrograms of measured signals when striking the F#₃ note-field at the 'D' sweetspot, in both configurations: (a) undamped; and (b) damped.

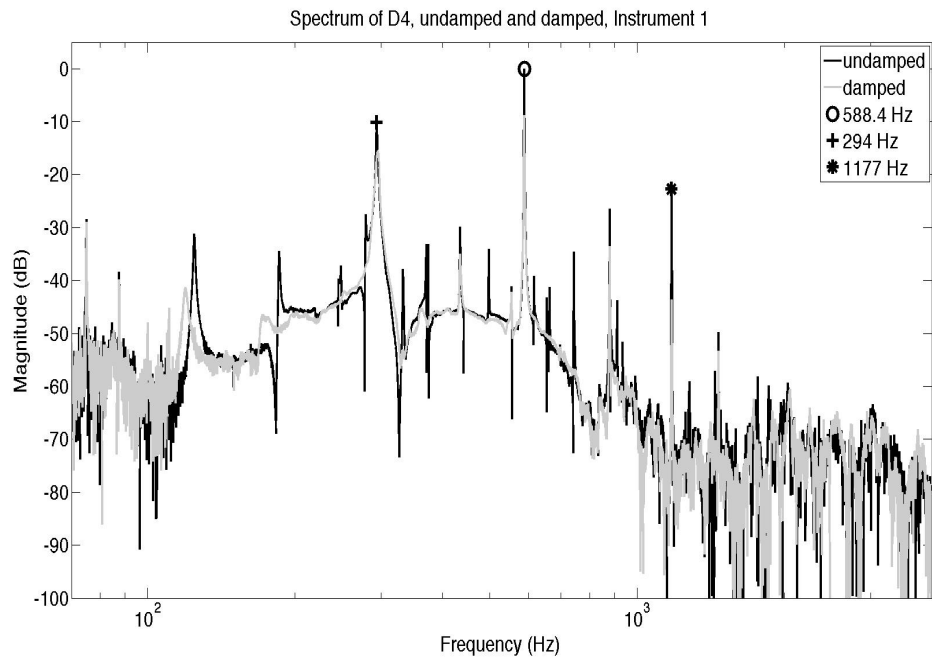
Approximate peak frequency (Hz)	Approximate onset time, undamped (ms)	Approximate onset time, damped (ms)
186	23	23
374	92	92
556	510	372
748	209	92

TABLE 4.4: Approximate onset times for relevant signature modes from the undamped and damped measurements of the F#₃ note-field, struck in the ‘D’ sweetspot.

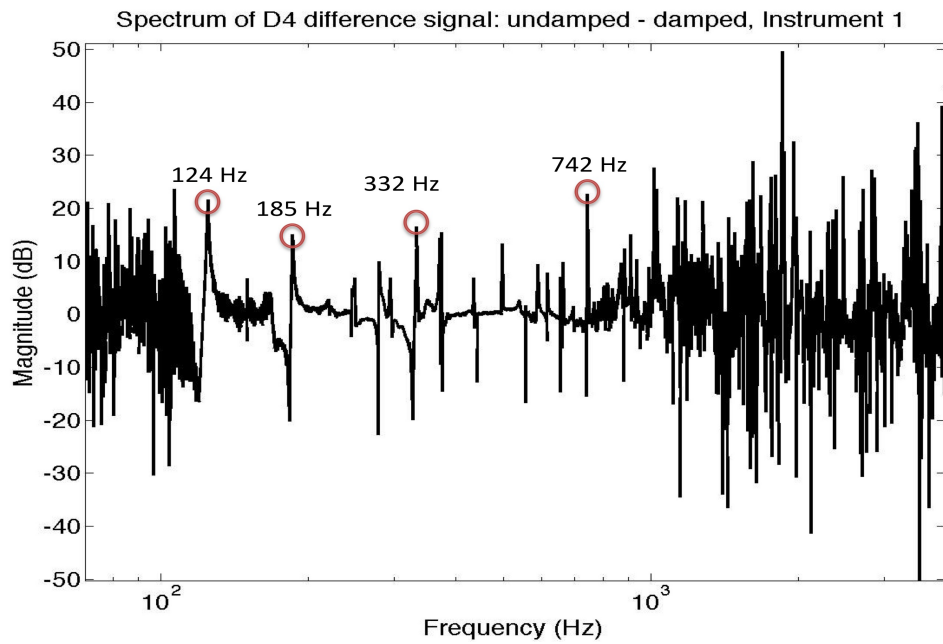
Table 4.4 displays the approximate onset times for relevant signature modes from the undamped and damped measurements of the F#₃ note-field, struck in the ‘D’ sweetspot. As mentioned previously in Section 4.2, the frame length used for Fourier analysis of the handpan measurements was 46 ms. With an overlap of 50% this produces an apparent time resolution of 23 ms. Therefore, the onset times in Table 4.4 are accurate within ±23 ms of the displayed values. The onset times for the undamped and damped 186 Hz peak in Table 4.4 are approximately equal. This means that the peak magnitude value in the spectrogram for the 186 Hz peak for both undamped and damped measurements is reached within the first 23 ms. The peak value for the 374 Hz peak for both undamped and damped measurements is reached approximately 92 ms after the strike. The results displayed in Table 4.4 seem to be consistent with the observations made in Section 2.1.3 for cymbals and gongs, where there is a transfer of energy from low to high vibrational modes. Despite this, another process seems to be occurring in the vibration of the F#₃ note-field or coupling to surrounding notes that causes the 556 Hz peak to reach its maximum value much later than the 748 Hz peak. Finally, many of the relatively short lived peaks present in 4.10(a) are nearly non-existent in 4.10(b) such as the 120 Hz, 248 Hz, and many other peaks in the 1 kHz-2 kHz region. This seems to suggest that note-field coupling can potentially have a significant influence on the overall signature sound of the handpan when an individual note-field is struck.

4.4.1 Multiple Instruments

All four handpans investigated in this project contain eight or nine note-fields. The musical scale of each instrument is different, as is the degree of coupling between the



(a)



(b)

FIGURE 4.11: Spectra of: (a) the undamped and damped D_4 note-field signals for Instrument 1; and (b) the D_4 difference signal, undamped-damped, Instrument 1. Strikes were delivered to the ‘D’ sweetspot.

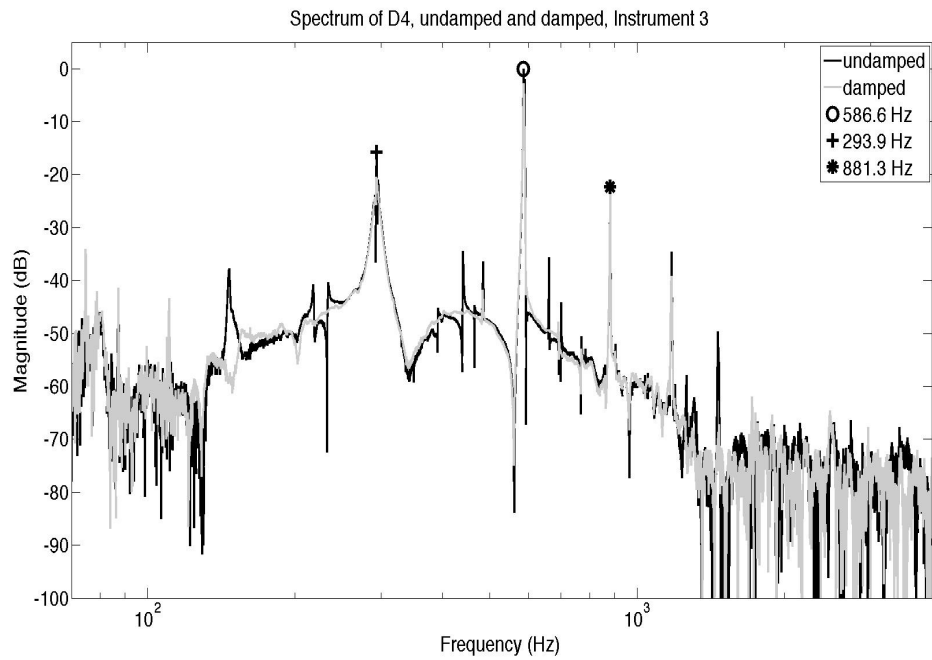
note-fields. Therefore, the spectra of a measured signal for a given note is expected to contain additional peaks, which don't necessarily originate from the struck elliptical note region. The frequency values of these peaks and their prominence in the measured signal will depend upon the notes that are present in the specific handpan, and their degree of coupling to the struck note.

Figure 4.11 displays: (a) the undamped and damped D_4 note-field signals for Instrument 1; and (b) the D_4 difference signal: undamped-damped, when struck at the 'D' sweetspot. If the undamped and damped signals were identical, their difference signal would result in a 0dB value for every frequency bin. It should be noted that the highest similarity degree was expected for the frequency range of the first three signature vibrational modes, which in the case of the D_4 is approximately 294 Hz-880 Hz. Examining 4.11(a), it is clear that numerous peaks in the undamped note-field spectrum are not present in their corresponding damped spectrum. This is confirmed in 4.11(b), which shows the highest degree of similarity in the 115 Hz-1 kHz region. Despite the high degree of similarity in this region, clear differences are noticeable such as the peak at 124 Hz. This peak's presence in the undamped signal is thought to be due to coupling between the D_4 and B_2 note-fields. This coupling is likely due to close proximity between the note-fields, as the B_2 is the central note-field in Instrument 1.

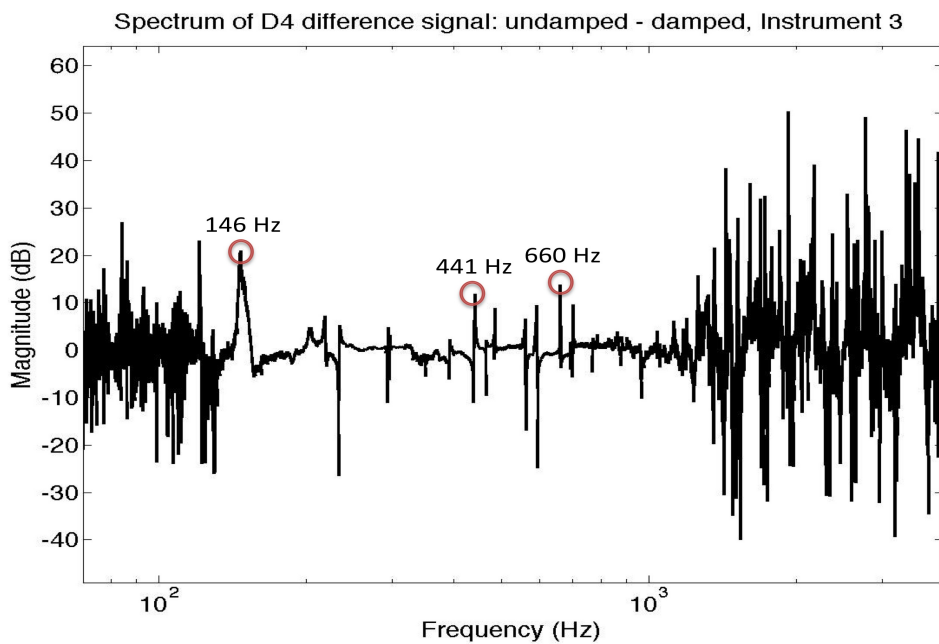
Frequency (Hz)	Estimated note	Magnitude difference (dB)
124.7	B_2	+21
185.9	$F\#_3$	+15
332.9	E_4	+16
374.1	$F\#_4$	+15
497.8	B_4	+13
742.6	$F\#_5$	+22

TABLE 4.5: Six identified peaks in the undamped spectrum (above +10 dB in the 115 Hz-1 kHz region), which are not present in the corresponding damped spectrum for the D_4 note-field of Instrument 1 struck at the 'D' sweetspot, as seen in 4.11(b).

Table 4.5 displays six of the identified peaks in the undamped spectrum (above +10 dB in the 115 Hz-1 kHz region), which are not present in the corresponding damped spectrum for the D_4 note-field of Instrument 1, when struck at the 'D' sweetspot. All of



(a)



(b)

FIGURE 4.12: Spectra of: (a) the undamped and damped D_4 note-field signals for Instrument 3; and (b) the D_4 difference signal, undamped-damped, Instrument 3. Strikes were delivered to the 'D' sweetspot.

these peaks are one of the 1:2:3 frequency ratio signature vibrational modes present on Instrument 1 as seen in Table 3.1.

Figure 4.12 displays: (a) the undamped and damped D_4 note-field signals for Instrument 3; and (b) the D_4 difference signal: undamped-damped, when struck in the ‘D’ sweetspot. Examining 4.12(a), it is clear that some peaks in the undamped note-field spectrum are not present in their corresponding damped spectrum. This is confirmed in 4.12(b), which shows the highest degree of similarity in the 130 Hz-1.2 kHz region. The 146 Hz peak’s presence in the undamped signal is thought to be due to coupling between the D_4 and D_3 note-fields, the latter having a fundamental frequency of 146.8 Hz. The degree of coupling between these notes is likely increased by their close proximity, as the D_3 is the central note-field in Instrument 3.

Comparing the difference signals for Instrument 1 in Figure 4.11(b) and Instrument 3 in Figure 4.12(b) shows the undamped and damped spectrum of the D_4 note-field to be more similar for Instrument 3. This is seen by the fewer amount of peaks with a magnitude over 10 dB in the 130 Hz-1.2 kHz region. Additionally, comparing both these figures to Figure 4.2(c), supports the conclusion that the NFEM produces sufficiently similar strikes to the note-fields. This was deduced by comparing the 120 Hz-1000 Hz range for all three figures, and noticing the absence of peaks in 4.2(c).

Frequency (Hz)	Estimated note	Magnitude difference (dB)
146.6	D_3	+20
441.3	A_4	+11
660.7	E_5	+13

TABLE 4.6: Three identified peaks in the undamped spectrum (above +10 dB, in the 130 Hz-1.2 kHz region), which are not present in the corresponding damped spectrum for the D_4 note-field of Instrument 3 struck in ‘D’ sweetspot, as seen in 4.12(b).

Table 4.6 displays three of the identified peaks in the undamped spectrum (above +10 dB, in the 130 Hz-1.2 kHz region), which are not present in the corresponding damped spectrum for the D_4 note-field of Instrument 3 struck in the ‘D’ sweetspot. All of these peaks are one of the 1:2:3 frequency ratio signature vibrational modes present on Instrument 3 as seen in Table 3.1.

Comparing the number of peaks displayed in Table 4.5 and Table 4.6, suggests that the degree of note coupling is greater in the undamped signals of Instrument 1 than Instrument 3. The spectra of the D₄ note-fields for the remaining two handpans are displayed in Appendix H. To provide an additional estimate of the degree of note coupling, the sum of the squared undamped and damped signals were converted to decibel values, using Equation 4.2. Examining Table 4.7, which displays the total energy

Instrument	Undamped D ₄ signal, total energy	Damped D ₄ signal, total energy
1	0 dB	-10 dB
2	-1.1 dB	0 dB
3	0 dB	-5.7 dB
4	0 dB	-4.3 dB

TABLE 4.7: Total energy values in decibel for all D₄ signals, struck in the ‘D’ sweetspot.

values in decibels for all four D₄ signals struck in the ‘D’ sweetspot, the variation between the undamped and damped results can be seen. The damped total signal energy for Instrument 1 was estimated at -10 dB when compared to the corresponding undamped value. This suggests a strong coupling between the D₄ and at least one surrounding note-field on Instrument 1. Interestingly, the undamped total signal energy for Instrument 2 was estimated at -1.1 dB when compared to the damped value. This suggests no significant coupling between the D₄ and surrounding note-fields on Instrument 2.

4.4.2 Pre-tuned and Post-tuned Instrument

Instrument 3 and Instrument 4 were recorded both prior to, and following, tuning by an established handpan maker. Figure 4.13 displays spectra of the undamped A₄ note-field signals of Instrument 4 struck in the ‘D’ sweetspot, pre and post-tuning. Examining this figure, it is clear that most of the signature vibrational modes in the pre-tuned spectrum have slightly higher frequency values. Furthermore, three peaks in the 1.5 kHz-3 kHz region of the post-tuned spectrum have significant magnitude whereas in the pre-tuned spectrum they are hardly distinguishable from surrounding noise components. Figure 4.14 displays spectra of the damped A₄ handpan note-field signals struck in the ‘D’

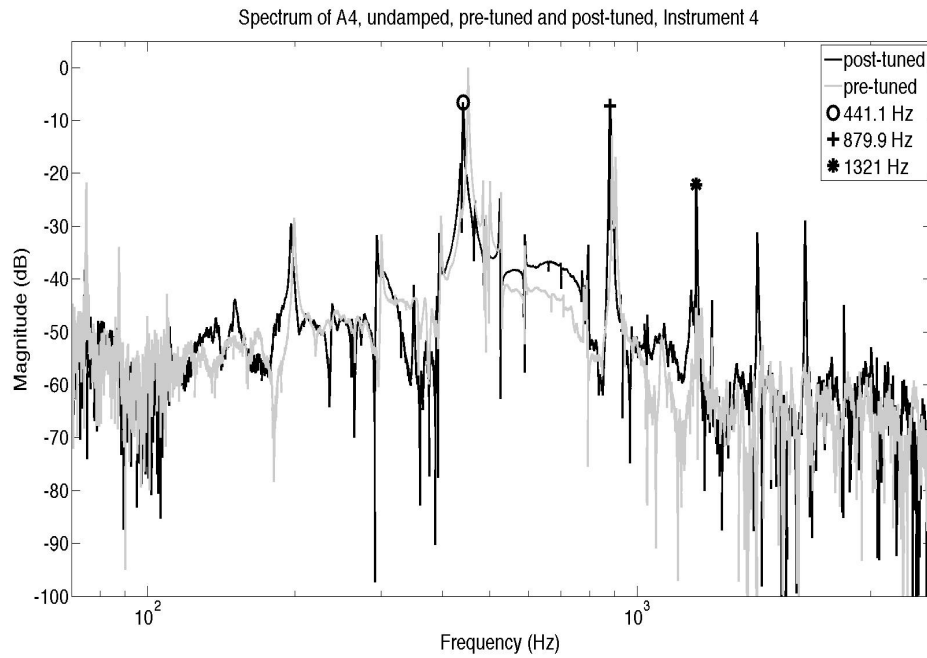


FIGURE 4.13: Spectra of the undamped A₄ handpan note-field signals of Instrument 4 struck in the ‘D’ sweetspot, pre and post-tuning.

sweetspot, pre and post-tuning. Much like the undamped signals, the pre-tuned damped signature modes have slightly higher frequency values than their corresponding pre-tuned signature modes.

Comparing the undamped and damped spectra shows that there are several detected peaks in the undamped spectrum, which are not present in the damped spectrum (such as in the 200 Hz-400 Hz and 500 Hz-600 Hz regions). Furthermore, the reduced magnitude of the three peaks in the 1.5 kHz-3 kHz region in the damped spectrum suggests a significant coupling to surrounding note-fields. The average T60 values for Instrument 3 and Instrument 4 were 2.8 s, and 2.1 s respectively, as seen in Table 4.2. Interestingly, these average T60 values did not change after the tuning process, despite the change in T60 values for individual vibrational modes when compared to the pre-tuned measurements as can be seen in Appendix F.

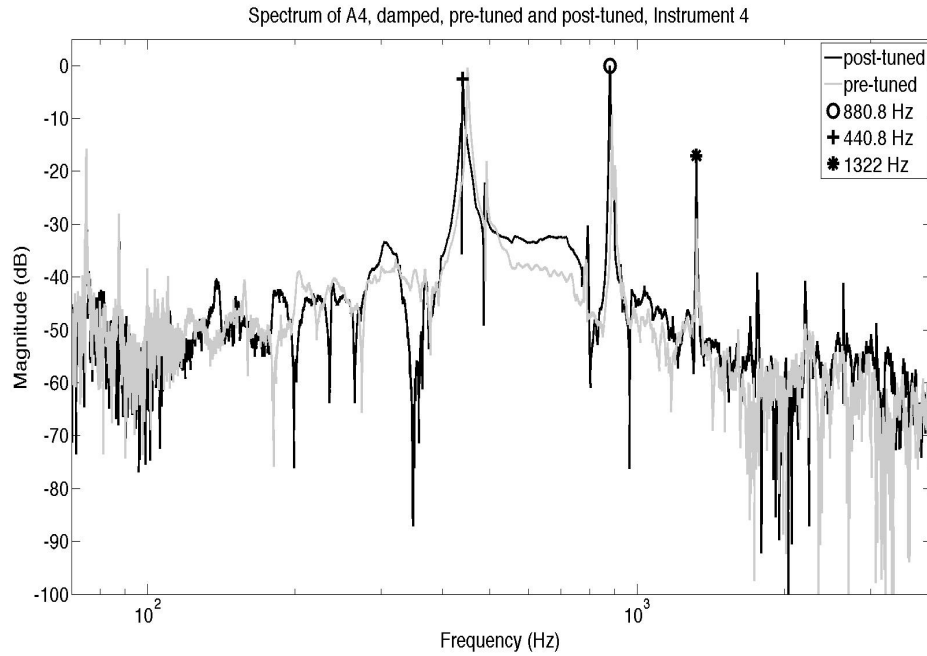


FIGURE 4.14: Spectra of the damped A₄ handpan note-field signals of Instrument 4 struck in the ‘D’ sweetspot, pre and post-tuning.

4.5 Summary

This chapter has presented an analysis of the measured handpan signals. Fourier methods and spectral techniques were employed to produce the analysis results. Initially, the repeatability of NFEM strikes to a single position were confirmed to be sufficient for the purposes of this thesis, by analysing the spectra of consecutive strikes, and showing that the total amount of energy in the signal of these strikes to be within a ± 1 dB range. Then the analysis resulted in the identification of signature vibrational modes, corresponding decay rates, and beating rates. These showed that like the Hang and steelpan, the first three principal modes of vibration for most handpan note have a 1:2:3 frequency ratio. The high degree of similarity for T60 decay time results for Instrument 1 and Instrument 2 displayed in Table 4.2, suggest that the method used to estimate T60 decay times has managed to identify decay characteristics of instruments from the same maker, despite the variable reliability of estimated T60 decay times. The influence of strike position on timbral quality of an individual note-field was demonstrated by showing that the relative magnitudes and decay times of the signature vibrational modes were affected

by strike position in both undamped and damped configurations. Comparisons of the undamped and damped measurements have strengthened the hypothesis that beating, evident as amplitude modulations in the spectrograms, are due to coupling of note-fields with slightly mismatched tuning of signature vibrational modes. It was also shown that fewer distinct peaks are present in the spectra of damped signals when compared to undamped signals, and that surrounding note-fields can have a significant influence on the overall handpan sound, the degree of which might depend upon the nature of coupling between the note-fields of an individual instrument.

Chapter 5. Synthesis and Listening Test

Following the analysis of the handpan recordings and extraction of signature mode frequencies and corresponding decay rates, a method for the synthesis of the handpan sound can be designed. The modal synthesis approach will make use of a set of exponentially decaying sinusoids, each corresponding to the frequency of the detected signature vibrational mode, initial magnitude, and estimated decay time. This chapter first presents an explanation of the synthesis method used, followed by results from a listening test conducted in order to assess the quality of the synthesised handpan sounds. The listening test is designed to do this by comparing the similarity of synthesised sounds formed using different numbers of signature vibrational modes to reference recorded signals. This should go some way towards answering a question central to this research by estimating the minimum number of vibrational modes required for synthesis of the handpan sound, as stated in project aim 3, in Section 1.1.

5.1 Modal Synthesis of the Handpan Sound

The synthesis approach taken here is similar to a source-filter form of modal synthesis, using the estimated mode frequencies, magnitudes, and decay rates calculated in Chapter 4 to estimate the impulse response of an individual handpan note. The estimated impulse response is calculated as a linear summation of individual mode responses. It should be noted that operations such as summation and linear convolution can be modelled using an appropriate filter [31]. Thus, the linear summation of mode responses and convolution with an excitation signal is equivalent to a source-filter form of modal synthesis, which is based on running a signal through a set of modal resonators.

For the purposes of this project, the waveform of the handpan sound is comprised of two stages: attack and decay. The attack is associated with a transient, broadband onset whilst the decay is associated with a mostly sinusoidal, exponential decay. Considering the

definitions of impulse response and convolution detailed in Section 2.2.2, and assuming that the handpan can be treated as an LTI system, the decay stage of the handpan sound is approximately equivalent to the impulse response, $h[n]$ in Equation 2.13, whereas the attack stage is characterised by the nature of the excitation signal, $x[n]$ in Equation 2.13. Thus, the recorded signature handpan signal can be estimated by the following equation:

$$y_{conv}[n] = h_{allr}[n] * x_{ex}[n] \quad (5.1)$$

where $h_{allr}[n]$ is the estimated impulse response signal calculated as a linear summation of individual mode responses of a given handpan note-field, $x_{ex}[n]$ is the excitation signal, and $y_{conv}[n]$ is the output modal synthesis signal. An experimental method of estimating the excitation signal, $x_{ex}[n]$, was implemented by employing magnetic absorbing pads to dampen handpan notes, and cavity resonance vibration. This is identical to the damped configuration, with an additional magnet positioned to entirely cover the port hole of the handpan. Thus, the measured signal when striking the internote area of the handpan using the NFEM can be used as an experimental excitation signal in the modal synthesis model. Further discussion of the excitation signal and its suitability for this synthesis model is presented in Section 5.1.2.

Upon estimation and generation of the impulse response and excitation signals, they are then convolved to produce the estimated synthesised output signal, $y_{conv}[n]$, as shown in Equation 5.1. Treating the handpan as an LTI system is necessary to implement this modal synthesis approach, however it was established in Section 4.4 that non-linear phenomenon are an integral part of the handpan sound, such as note coupling in undamped measurements, which lead to beating, and the transfer of energy from low to high vibrational modes.

A method has been implemented to introduce a basic correction factor for note coupling, which leads to beating. This beating manifests as amplitude modulations on some vibrational modes, as seen previously in Figure 4.10. The need for this correction factor is likely due to the relatively large bin width of 21.5 Hz (as stated in Section 4.2)

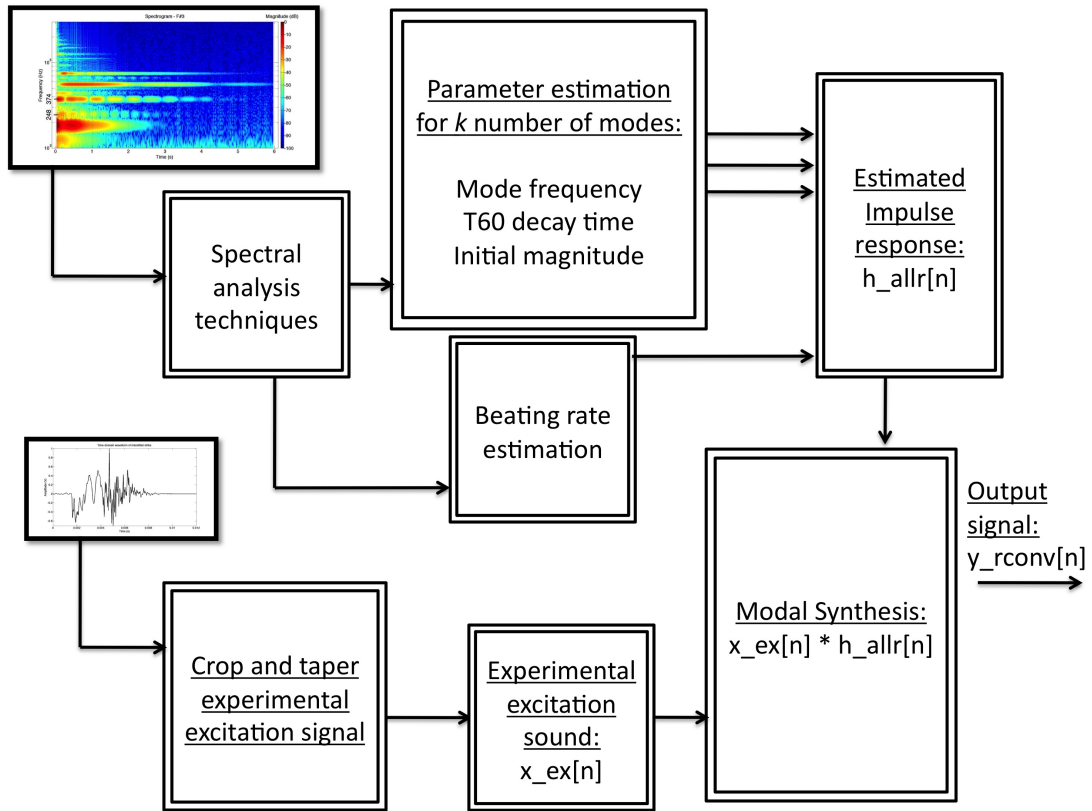


FIGURE 5.1: Block diagram of the modal synthesis model implemented for this project. The signature handpan sound is analysed to estimate mode frequency, T60 decay time, and initial magnitude parameters for k vibrational modes. The number k is selected by the user prior to analysis. The beating rate of a signature mode is also estimated. The k vibrational modes oscillators are summed together along with the beating correction oscillator to produce the estimated impulse response $h_{allr}[n]$. The experimental excitation signal, $x_{ex}[n]$, is convolved with the impulse response to produce the modal synthesis output signal $y_{rconv}[n]$.

produced by the selected analysis parameters. This bin width value is comparable to audible beat rates (± 12.5 Hz difference [19]), which might explain why closely spaced beating frequencies were not consistently and independently resolved in the analysis results. This method will be further detailed in Section 5.1.3. The block diagram of the modal synthesis model implemented in this Section is displayed in Figure 5.1.

5.1.1 Estimation of the Impulse Response

The signature mode frequencies, magnitudes, and corresponding decay rates identified in Section 4.2 can be used to estimate the impulse response signal of the handpan

sound in the form of a simple linear summation. The simplified approach used here assumes linearity of the system, in the sense that there is no energy transfer between frequency bins, and that the decay of energy in each bin can be characterised by a simple exponential decay. The frequencies of detected modes were used to set the oscillators used for synthesis:

$$\phi[n] = 2\pi \cdot f_{sin} \cdot t[n] \quad (5.2)$$

Equation 5.2 describes the creation of the phase vector $\phi[n]$, where f_{sin} is the frequency of the signature mode, and $t[n]$ is the time value at sample number n (sample rate = 44.1 kHz).

$$A = EDR_{max} \cdot 10^{\frac{A_{dB}}{20}} \quad (5.3)$$

A in Equation 5.3 is the initial magnitude used for synthesis, EDR_{max} is the maximum value of the EDR, and A_{dB} is the initial magnitude (in decibels) of the second degree polynomial described in Section 4.2.2. It should be noted that the initial magnitude values were calculated using EDR plots of the original measured note-field signals. Thus, a more accurate estimation of the impulse response signal could have been derived by deconvolving the estimated excitation signal and the measured signal [51]. Estimating the initial magnitudes of detected peaks from EDR plots of this resulting signal would have provided a more accurate estimation of the initial magnitudes for the estimated impulse response in the synthesis model. This was only considered after completing the subjective listening tests detailed in Section 5.2, and therefore was not included within the modal synthesis model. Additional detail regarding this potentially more accurate method of estimating the impulse response signal and initial magnitudes of detected peaks is presented in Section 6.3.1.

$$h_{sin}[n] = A \cdot \sin(\phi[n]) \quad (5.4)$$

$$\tau = \frac{T60}{\log_{10}(1 \cdot 10^{-3})} \quad (5.5)$$

$h_{sin}[n]$ in Equation 5.4 is the sinusoidal vector, initialised with peak magnitude A . Equation 5.5 details the calculation of the exponential decay time constant τ , where T60 is the estimated T60 decay time for the signature mode.

$$h_r[n] = h_{sin}[n] \cdot e^{\frac{t[n]}{\tau}} \quad (5.6)$$

$$h_{allr}[n] = h_{r1}[n] + h_{r2}[n] + \dots + h_{rk}[n] \quad (5.7)$$

Equation 5.6 describes the generation of the synthesised signature mode vector $h_r[n]$. Upon creation of all signature mode vectors for a given measurement, they were summed together to produce the overall estimated impulse response signal, $h_{allr}[n]$, as seen in Equation 5.7, where k is the total number of desired signature vibrational modes.

Figure 5.2 displays the decay curves of detected peaks, estimated straight line fits, and calculated T60 decay times for: (a) the original signal; and (b) the estimated impulse response signal, for the undamped A_3 handpan signal struck in the ‘D’ sweetspot. The A_3 note-field is one of the notes on Instrument 1, as can be seen in Table 3.1. This synthesised signal was created using three detected signature modes. Firstly, it should be noted that the curves of the 664.5 Hz and 913.9 Hz peaks do not decay in a very linear fashion. This reduces the reliability of their straight line fits and estimated T60 decay times, unlike the straight line fit and T60 decay time of the 223.2 Hz peak, which appears to be more reliable. A few differences can be observed when comparing 5.2(a) and 5.2(b). First, it is clear that there is no beating in the synthesised signal on any of the signature modes. Second, the noise floor in the original signal is visible within a magnitude range of 80 dB (noticeable on the 223.2 Hz curve at approximately 3 s), whereas this is not the case for the synthesised signal. Finally, the estimated T60 values for the three highest magnitude peaks in the original signal are: 2.7 s, 4.1 s, and 2.5 s, whilst the T60 values for the synthesised signals are: 2.7 s, 3.9 s, and 1.9 s. Despite the identical T60 decay time of 2.7 s for the 223 Hz curve in both 5.2(a) and 5.2(b), the remaining modes T60 decay times exhibit a lower degree of similarity. The reason for this was identified as

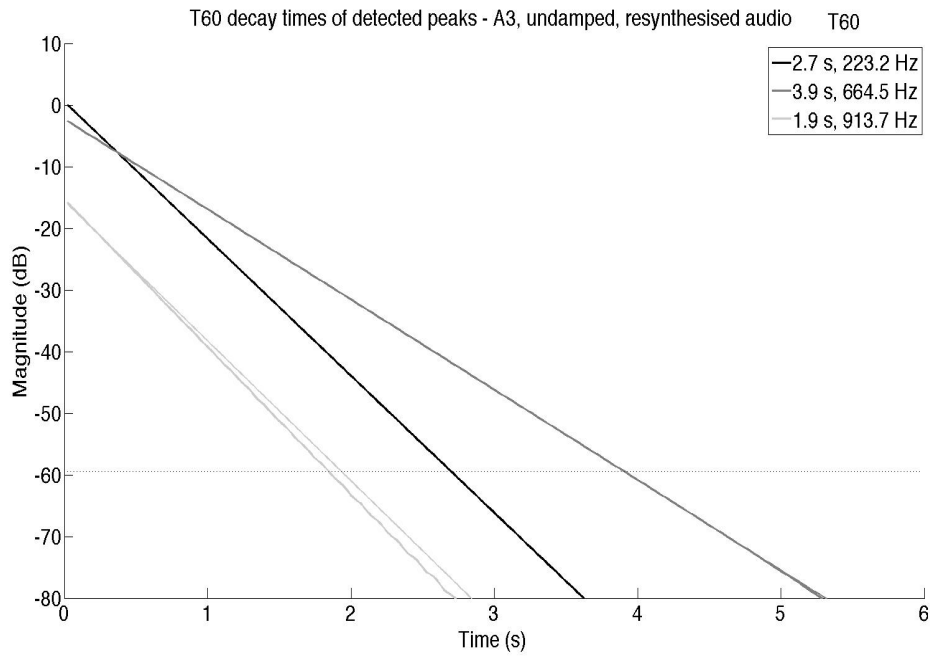
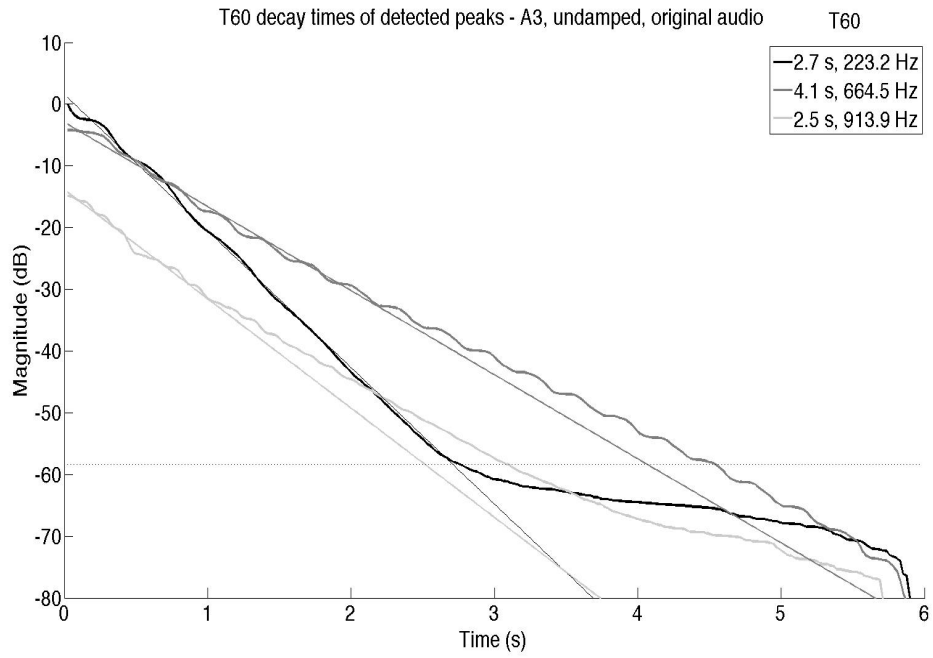


FIGURE 5.2: Decay curves of detected peaks, estimated straight line fits, and calculated T60 decay times for: (a) the original signal; and (b) the estimated impulse response signal, for the undamped A₃ handpan signal struck in the ‘D’ sweetspot.

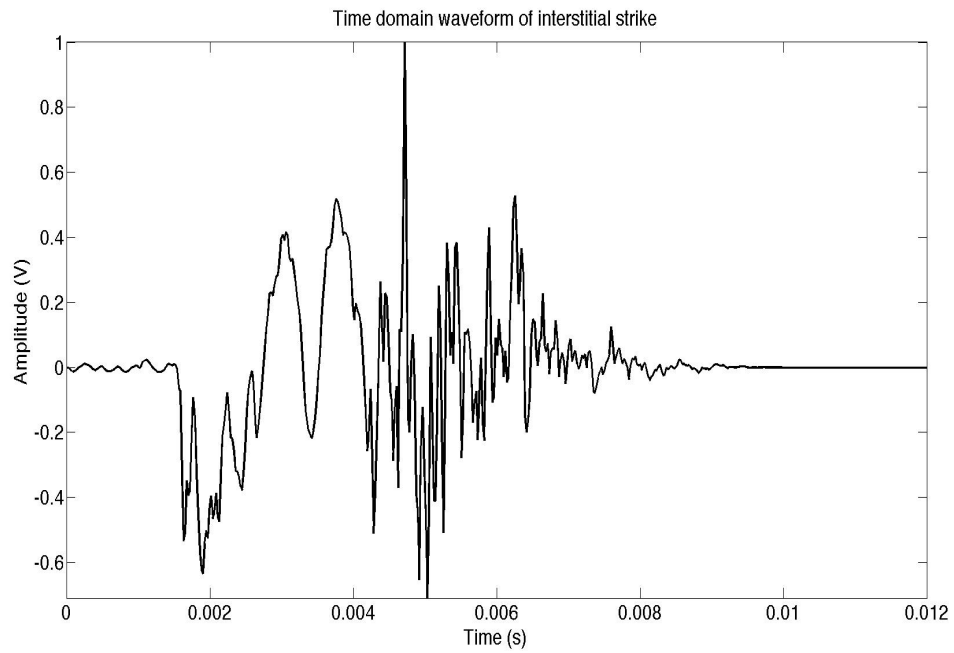
being the result of an error in the calculation of the decay time constant, τ , as described by Equation 5.5. This error was only identified after conducting the listening tests, and will be further addressed in Section 6.3.

5.1.2 Estimation of the Excitation Signal

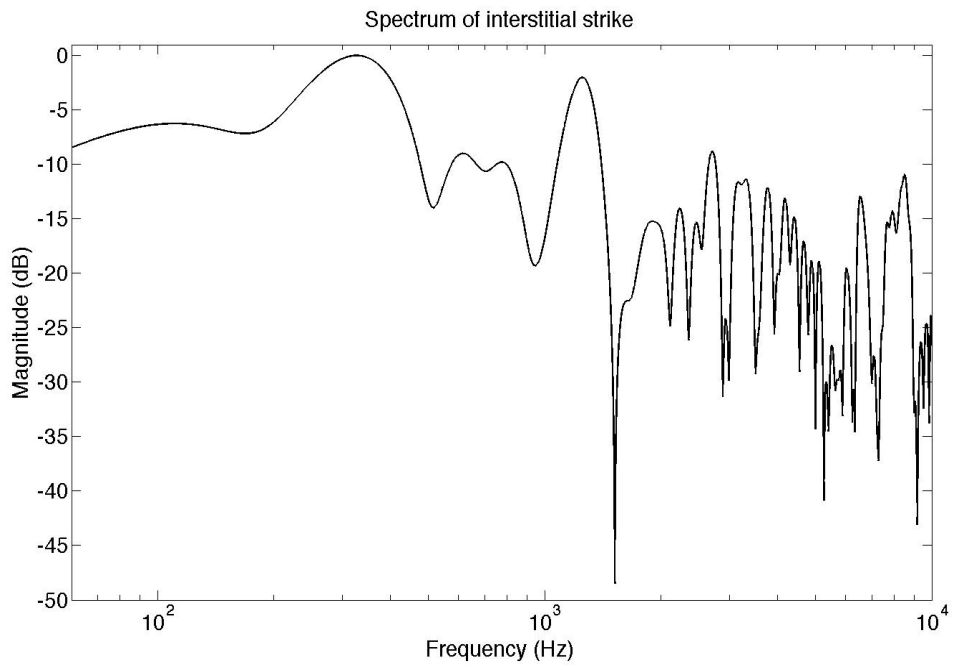
Attack transients are essential for the discrimination and identification of various musical instruments [59]. Whilst transient analysis is beyond the aims of this project, the attack stage of the signature handpan sound is highly dependent upon the nature of the excitation signal. The NFEM was designed for use in this project in order to measure and estimate the impulse response of each of the handpan's note-fields.

An experimental method of estimating the excitation signal, $x_{ex}[n]$ in Equation 5.1, was implemented by employing magnetic absorbing pads to dampen handpan note vibration, and cavity resonance vibration. Thus, the measured signal when striking the internote area of the handpan using the NFEM can be considered approximately equivalent to the excitation signal. It should be noted that in previous research of the steelpan, it was found that excitation due to stick impact often yields a half-sine shaped force [23], so it is also possible to use a half-sine pulse as an approximate excitation signal, however this excitation method was not used for this project. An additional method to extract the approximate excitation signal from the original signal will be detailed in Section 6.3.

The time domain waveform of the measured experimental excitation signal can be seen in Figure 5.3(a) and the broadband nature of the corresponding spectrum is shown in 5.3(b). The signal was cropped at 10 ms, tapered [44] and zero padded to match the length of the estimated impulse response signal. The excitation and impulse response signals were then convolved, resulting in an attack stage with a higher degree of similarity to the original handpan sound. The discrete convolution formula used was shown in Equation 2.13. Since convolution is equivalent to multiplication of spectra [31], any spectral component that is not present in both input signals, will not be present in the output signal. Figure 5.4 displays the attack stage of: (a) the original; (b) the estimated impulse response signal, $h_{allr}[n]$ in Equation 5.1; and (c) the modal synthesis signal, $y_{conv}[n]$ in

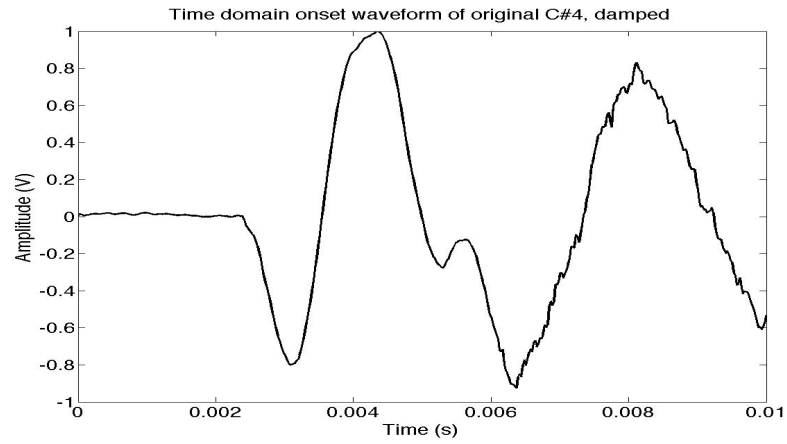


(a)

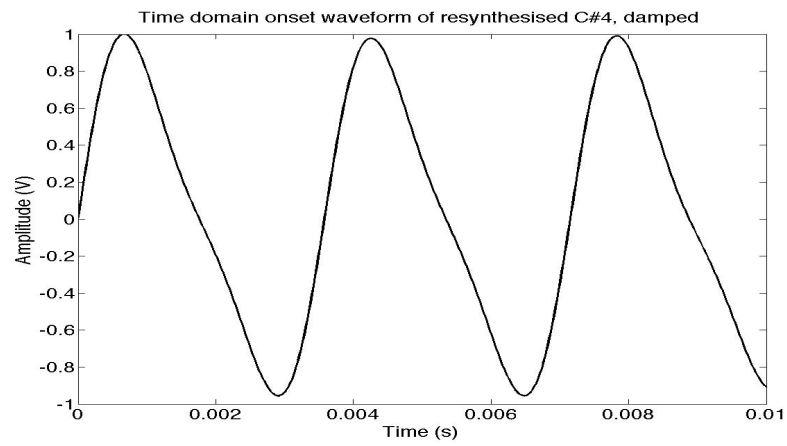


(b)

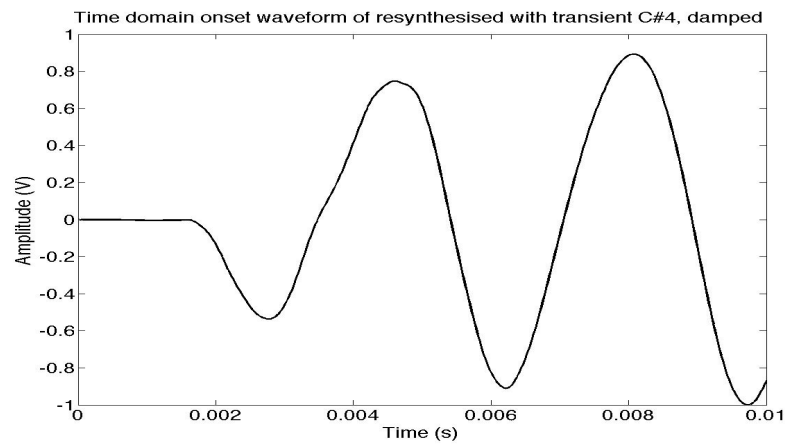
FIGURE 5.3: (a) Time domain waveform; and (b) spectrum of an NFEM strike delivered to the interstitial area of a handpan, with magnetic absorbing pads placed on all note-fields and the port hole. The signal was cropped at 10 ms, tapered [44], and zero padded to match the length of the estimated impulse response signal.



(a)



(b)



(c)

FIGURE 5.4: The attack stage of: (a) the original; (b) the estimated impulse response signal; and (c) the modal synthesis signal of a damped C#₄ note struck in the ‘D’ sweetspot.

Equation 5.1, of a damped C#₄ note struck in the ‘D’ sweetspot. These show the attack stage of 5.4(c) to be more similar to the original signal following convolution with the excitation signal.

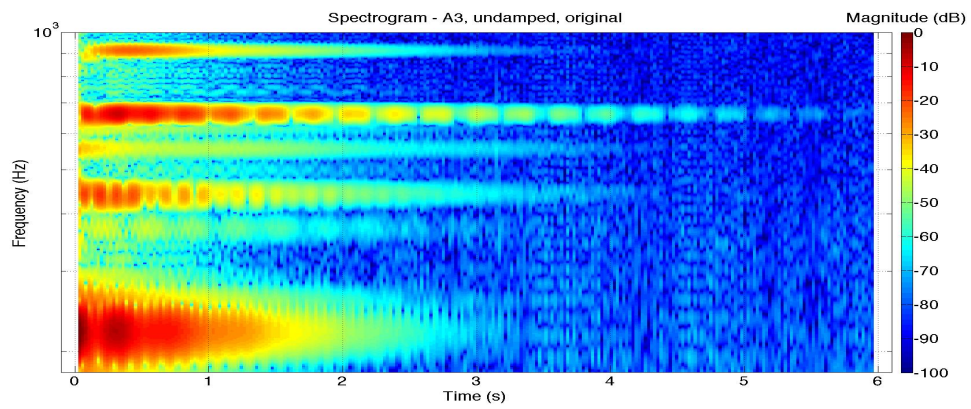
5.1.3 Beating Correction

As seen in Section 4.2.3, the handpan sound can exhibit beating, which manifests as amplitude modulations on individual or multiple modes at different modulation depths and rates. The analysis stage has treated the handpan as a linear system where no high resolution methods have been used to identify closely spaced peaks in the spectrum. These closely spaced peaks, which are thought to be present in the measured signal due to note coupling, lead to beating which thus far has not been accounted for in the synthesis model. A method has been implemented to introduce a basic correction factor for note coupling, which leads to beating. The need for this correction factor is likely due to the relatively large bin width of 21.5 Hz (as stated in Section 4.2) produced by the selected analysis parameters.

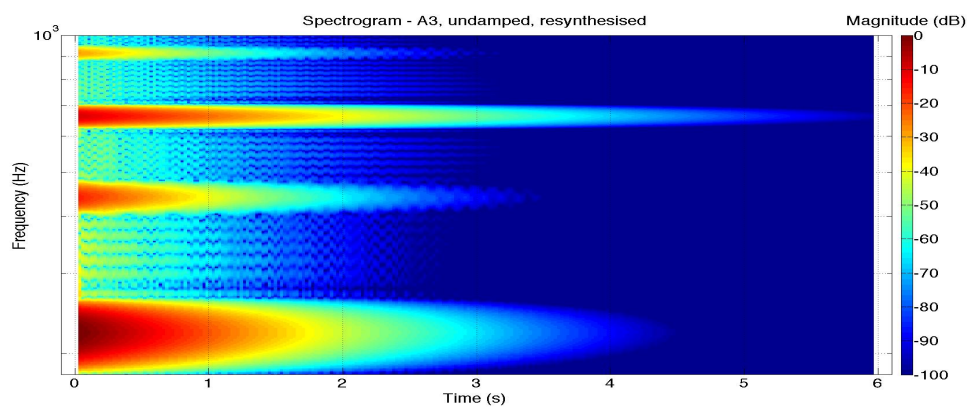
The method for calculating the beating rate for relevant vibrational modes was shown in Section 4.2.3. This parameter was then used to introduce a basic correction factor to the synthesised signal. To include these characteristic beating phenomena in the synthesised signal, it is possible to exploit the fact that the linear superposition of two simple harmonic vibrations with similar frequencies leads to periodic amplitude vibrations [22]:

$$\omega_2 = \omega_1 + \Delta\omega \quad (5.8)$$

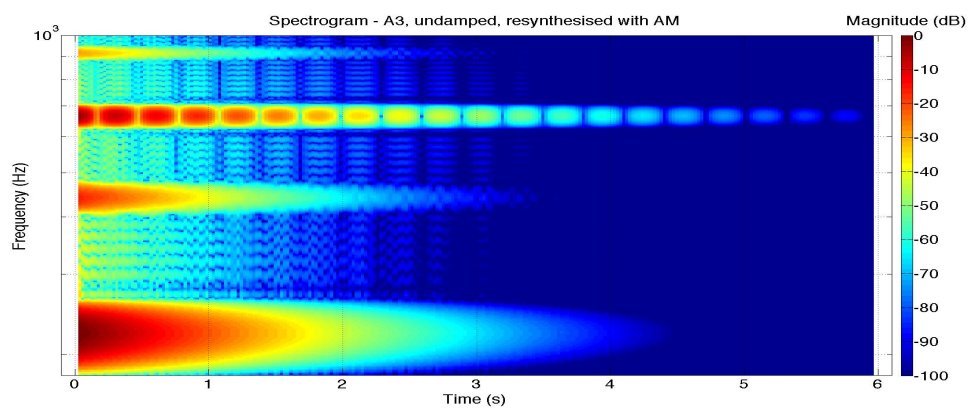
If ω_1 and ω_2 in Equation 5.8 are the angular frequencies of each oscillator and $\Delta\omega$ is the angular frequency difference between the two, then the resultant amplitude envelope of linearly superimposing both oscillators will have an amplitude modulation frequency of $\frac{\Delta\omega}{2\pi}$. Thus, in order to model the signature handpan amplitude modulations, a beating correction oscillator was added to the impulse response signal, prior to convolution with the excitation signal. Despite observing beating on several signature vibrational modes



(a)



(b)



(c)

FIGURE 5.5: Spectrograms of the undamped A_3 signal struck in the ‘D’ sweetspot: (a) original; (b) modal synthesis; and (c) modal synthesis with beating correction signals. The beating mode’s frequency value shown in (c) is 662 Hz, with a modulation rate of approximately 3.3 Hz. The beating correction oscillator’s frequency value was set to 665.3 Hz.

for an individual undamped handpan measurement, only a single oscillator was used to introduce beating correction for an individual vibrational mode due to time constraints and difficulty in implementing an automatic beating detection algorithm for signature modes.

Figure 5.5 displays Spectrograms of the undamped A_3 signal struck in the 'D' sweetspot: (a) original; (b) modal synthesis; and (c) modal synthesis with beating correction signals. These synthesised signals were created using four detected signature vibrational modes. The beating mode's frequency value shown in 5.5(c) is 662 Hz, with a modulation rate of approximately 3.3 Hz. The beating correction oscillator's frequency value was set to 665.3 Hz. Comparing the 662 Hz frequency bin in both 5.5(a) and 5.5(c) shows a high degree of beating rate similarity.

5.2 Subjective Listening Test

Subjective listening tests are considered the most reliable way of measuring the quality of audio systems [60]. Numerous test methodologies exist, such as the MUlti Stimulus test with Hidden Reference and Anchor (MUSHRA), and the triple stimulus, hidden reference test [61]. The methodologies differ in numerous aspects such as the amount and type of stimuli, continuous or discrete scale ratings, and question order randomization schemes. In order to assess the quality of the synthesised handpan sounds, a listening test was designed in order to judge the degree of similarity between the handpan recordings and synthesised versions created using different numbers of signature vibrational modes. These recordings and synthesised signals were the stimuli used in a series of questions presented to participants. The results of this test should go some way toward estimating the minimum number of signature vibrational modes required for synthesis of the handpan sound.

Two training questions followed by eighteen actual questions were presented to the subjects, each question containing five different stimuli. Three groups of synthesised handpan sounds were investigated: damped, undamped and undamped beating corrected (with beating correction oscillator). All signals used in the listening test were produced



from strikes delivered to the 'D' sweetspot of the corresponding note-field. Three note registers (low, mid, high) were tested for the damped notes of two different handpans. Thus the handpan note-field signals investigated in this listening test are as follows:

1. Instrument 3: D3, damped.
2. Instrument 3: D4, damped.
3. Instrument 3: A4, damped.
4. Instrument 1: A3, damped.
5. Instrument 1: D4, damped.
6. Instrument 1: F#4, damped.
7. Instrument 3: D4, undamped.
8. Instrument 1: A3, undamped.
9. Instrument 1: A3, undamped with beating correction oscillator.



A range of stimuli for synthesised handpan signals were constructed. 1, 2, 3 or 4 of the estimated signature modes were used in the damped case, whereas 2, 4, 7 or 10 were used in the undamped case. The difference in number of modes for both configurations is justified by reviewing the results in 4.4.1, which clearly show that undamped signals have more distinct signature peaks than their corresponding damped signals. The fifth stimuli for both configurations was the hidden reference, which is an identical copy of the original audio signal. Participants were asked to rate the similarity of each of the presented audio signals to the reference audio on a continuous scale of 0-10 (with measurement accuracy of a single decimal point). A score of 0 indicated that the corresponding audio sample was perfectly dissimilar to the reference audio, whilst a score of 10 indicated that the audio sample was perfectly similar to the reference audio. The score of each scale was not presented next to the audio signal, which encouraged participants to rate the audio signals relative to the score of the other scales, rather than the presented number next to the scale.



Rate the similarity of each of the following five AUDIO samples (0-10 scale) when compared to the REFERENCE AUDIO.



A score of 0 indicates that the AUDIO sample is perfectly DISSIMILAR to the REFERENCE AUDIO. A score of 10 indicates that the AUDIO sample is perfectly SIMILAR to the REFERENCE AUDIO.



REFERENCE AUDIO  



0 1 2 3 4 5 6 7 8 9 10

AUDIO  

AUDIO  

AUDIO  

AUDIO  

AUDIO  

Please provide any additional comments below



FIGURE 5.6: The listening test's interface for a single question showing the question description, reference audio, five audio samples, continuous scales, and text-box for any additional comments.

The listening test's interface for a single question is displayed in Figure 5.6, showing the question description, reference audio, five stimuli (audio samples), continuous scales, and text-box for any additional comments. An example of the subject information statements are displayed in Appendix I.

An important goal for the subjective listening test is that the data are objective, which means that a statistically similar data set and subsequent conclusions can be reproduced [61]. The statistical design of the listening test should ensure that the conclusions are actually related to the variables under investigation rather than unknown or uncontrolled

variables. To ensure independence of observations, each of the nine questions testing similarity of original and synthesised note-field sounds was presented twice. Additionally, the order of question presentation and stimuli was randomised for every test subject. All tests were conducted in the same listening room, with identical headphones, computer, seating and lighting conditions. Ethical approval was required prior to commencing the listening tests. The ethical approval form is displayed in Appendix I.

5.2.1 Preparation of Audio

The synthesised audio samples required additional processing prior to implementation of the subjective listening tests. These preparations included the addition of appropriate background noise and normalisation. The difference in background noise between the original and synthesised signals is noticeable when comparing Figure 5.5 (a) and 5.5(b). A similar level of background noise must be added to the synthesised signal in order to avoid overtly large differences between the original and synthesised handpan sounds. Due to the fact that the background noise level was slightly different for each original audio signal, a section of background noise was cropped immediately before or after the original handpan audio signal and added to the synthesised signal. Additionally, normalising was also required to bring the original and synthesised audio signals to the same loudness level. This was achieved by calculating the RMS value for the original and synthesised signals and scaling each signal appropriately to achieve the desired global RMS level.

5.2.2 Results

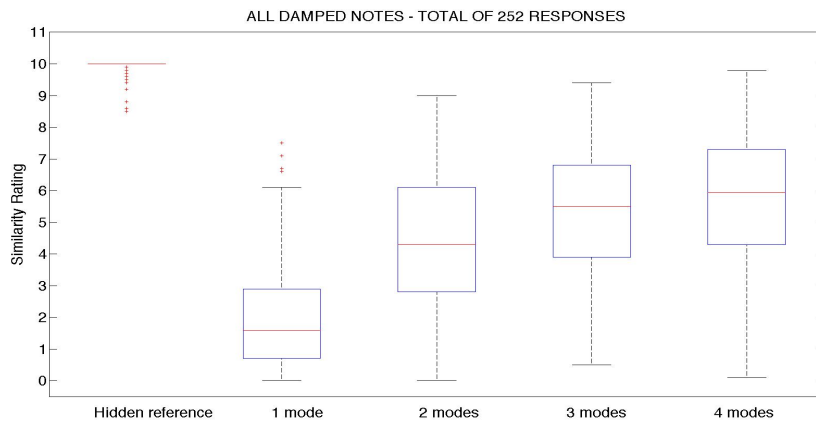
A total of 23 subjects participated in the listening tests. Only data from 21 subjects was used to conduct an analysis of the results, due to the high number of outliers present in responses of the two subjects. The complete set of collected data for all 23 subjects can be found in the accompanying DVD¹. MATLAB's `boxplot` function was used to analyse the results of the subjective listening test. This function takes a matrix of data

¹Directory on DVD: `EyalMSc/Listening_test/list_test_res.csv`.

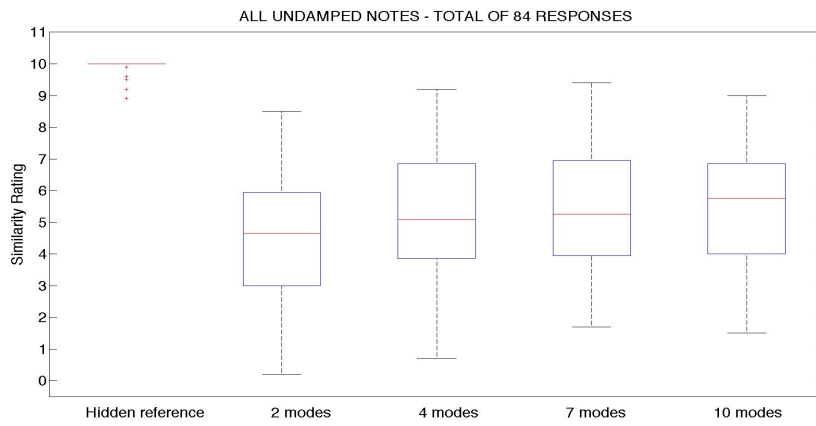
and produces graphs that show attributes like the median and variances for each column of data. Figure 5.7 displays the boxplots produced for: (a) damped (252 responses); (b) undamped (84 responses); and (c) undamped with beating correction (42 responses) signals respectively.

As mentioned previously, a total of 21 subject responses were used to produce these results. Several participants noted in the additional comments sections of their tests that some of the synthesised examples were lacking a similar attack stage to the reference audio, as well as additional higher frequency content. Examining 5.7(a), which contains the boxplots produced for all damped note signals (a total of 252 responses for 12 questions), shows a clear increase in the median similarity rating with increased amount of signature modes. Examining 5.7(b), which contains the boxplots produced for all undamped note signals (a total of 84 responses for 4 questions), also shows a slight increase in median similarity rating with increased amount of signature modes, however this is not as significant for the results in 5.7(a). Examining 5.7(c), which contains the boxplots produced for all undamped, beating corrected signals (a total of 42 responses for 2 questions) shows an increase in median similarity rating for all stimuli, compared to 5.7(b). For instance, the median rating for the 4 mode stimulus in 5.7(b) is 5.1, whereas the median value is 6.75 for 5.7(c). This suggests that the beating characteristics present in some of the handpan signals is a signature component and must be included in order to synthesise the handpan sound. Additionally, this suggests that addition of the beating correction oscillator in the modal synthesis model reduces the number of signature modes required to achieve higher similarity ratings.

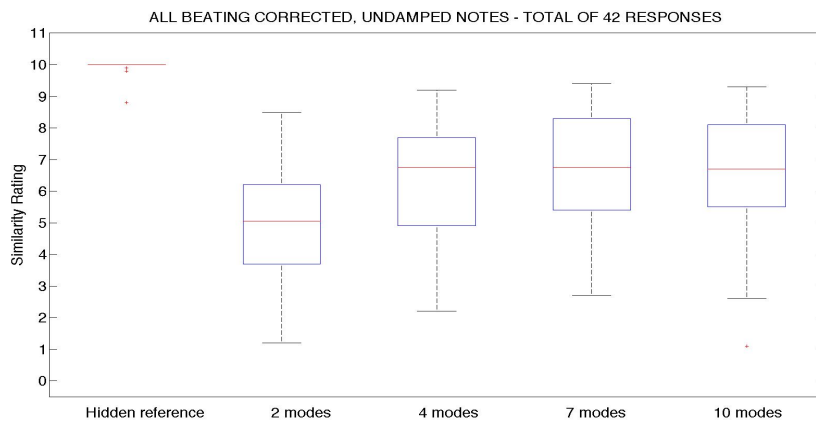
Figure 5.8 displays the boxplots produced for Instrument 3: (a) damped (126 responses for 6 questions); and (b) undamped (42 responses for 2 questions). The damped signals show a clear increase in median similarity for increased amount of synthesised signature modes, however the undamped signals show no such indication. Figure 5.9 displays the boxplots produced for Instrument 1: (a) damped (126 responses for 6 questions); and (b) undamped (42 responses for 2 questions). Once again, the damped signal's boxplots show a clear indication of increase in median similarity with respect to increase in the amount of signature modes used for synthesis. Unlike the undamped boxplots of Instrument 3 in 5.8(b), these also show an increase in median similarity rating, which seems to reach a



(a)

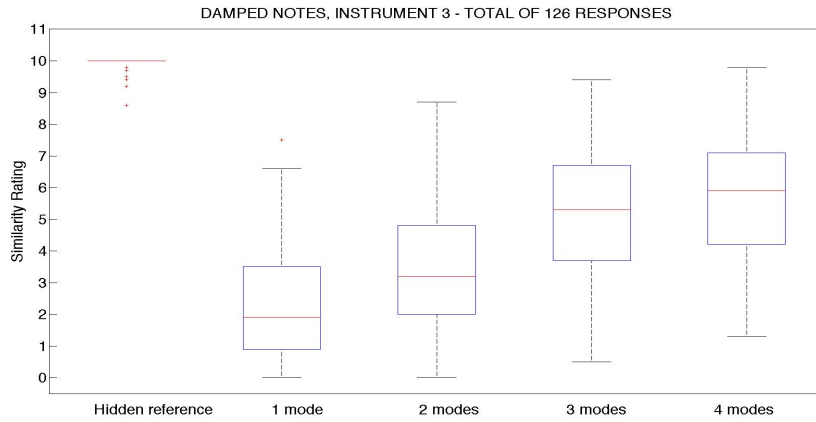


(b)

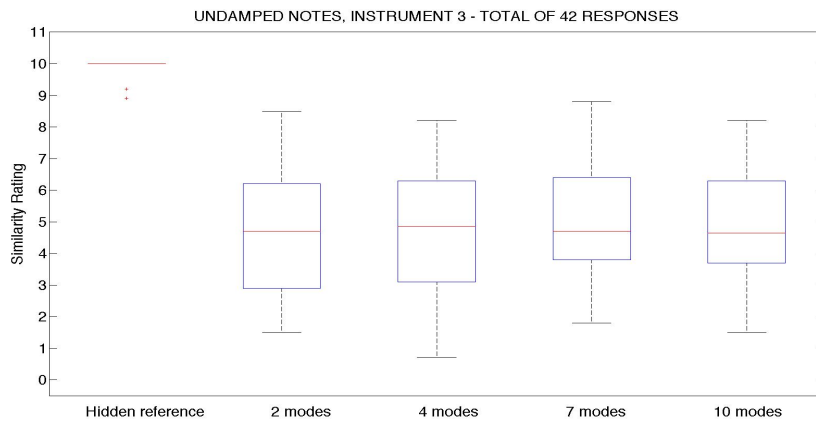


(c)

FIGURE 5.7: Boxplots produced for: (a) damped (252 responses); (b) undamped (84 responses); and (c) undamped with beating correction (42 responses) synthesised signals.



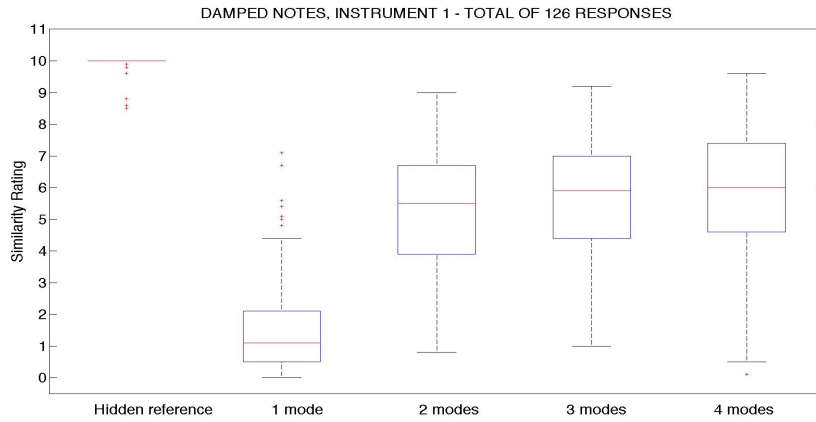
(a)



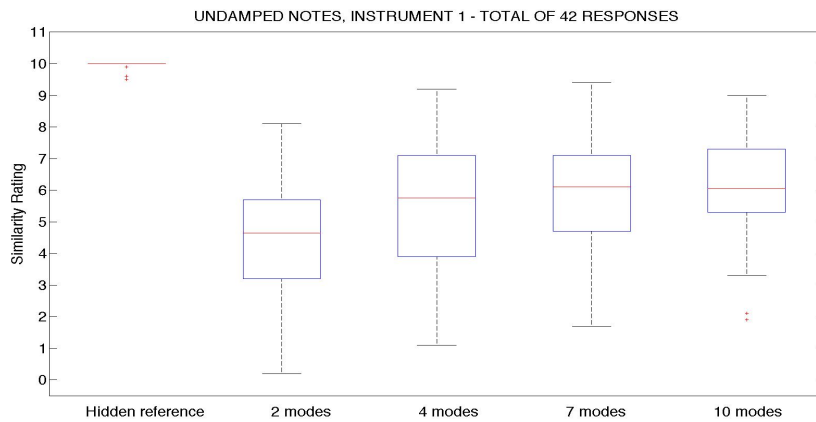
(b)

FIGURE 5.8: Boxplots produced for Instrument 3: (a) damped (126 responses); and (b) undamped (42 responses) signals.

maximum of 6.1 for the 7 mode stimulus. This suggests that the analysis and synthesis methods used for this project might be more suitable for use with some handpan makes more than others. Combined with the conclusions deduced from Figure 5.7 and Figure 5.8, it seems that the number of vibrational modes required to sufficiently synthesise the handpan sound is approximately 4-7 signature modes, not including beating correction oscillators.



(a)



(b)

FIGURE 5.9: Boxplots produced for Instrument 1: (a) damped (126 responses); and (b) undamped (42 responses) signals.

5.2.3 Discussion

The listening tests and results detailed in this section go some way towards estimating the minimum number of vibrational modes required to synthesise the handpan sound. Synthesis of the handpan sound using the least amount of required modes is desirable because this reduces computational and economic expenses of the system, which makes real-time synthesis more plausible and cost effective.

The median values for similarity ratings are relatively low for all results. As mentioned previously in Section 4.4, the most reliable T60 estimates were produced for detected

peaks that decayed in a mostly linear fashion. Thus, most of the questions presented in the listening test were based on damped measurements, which usually resulted in more reliable T60 decay time estimates compared to the undamped measurements. Furthermore, the T60 decay times for synthesised modes were not of a high degree of similarity when compared to the T60 decay times of the original signals, except for the highest magnitude vibrational mode. This is the result of an error in the calculation of the decay time constant, τ , as described by Equation 5.5. Further detail of this calculation error will be presented in Section 6.3. Finally, the fact that not all beating vibrational modes in a single measured handpan sound were modelled, rather only a single vibrational mode, might be a cause for low results. Examining (a) in Figure 5.5, it can be clearly seen that the 440 Hz mode also exhibits beating, whereas the synthesised audio signals only used a single beating correction oscillator as seen in 5.5(c) on the 662 Hz mode. Therefore, it is expected to see greater degrees of similarity reported following more accurate estimation of the T60 decay times, correction of the T60 decay times for synthesised modes, and inclusion of additional beating correction oscillators.

5.2.4 Summary

This chapter has detailed the method used for synthesis of the handpan sound. This modal synthesis approach makes use of a set of exponentially decaying sinusoids, and an experimental excitation signal, which are convolved to produce the synthesised handpan sound signal. The set of exponentially decaying sinusoids represents the estimated note-field impulse response signal. The peak frequencies, initial magnitudes, and T60 decay times calculated in Chapter 4 for individual note-field measurements, were used to create the sinusoids. An experimental method of estimating the excitation signal was implemented by employing magnetic absorbing pads to dampen handpan note vibration, and cavity resonance vibration, followed by striking the internote area of the handpan using the NFEM and measuring the resulting signal. Additionally, a method has been implemented to introduce a basic correction factor for note coupling, which leads to beating. An error in the calculation of the decay time constant, τ , as described by Equation 5.5, and a more accurate method of estimating the initial magnitudes of the

impulse response signal, were identified after conducting the listening tests. Both of these issues will be addressed in Section 6.3. Finally, in order to assess the quality of the synthesised handpan sounds, a listening test was designed in order to judge the degree of similarity between the handpan recordings and synthesised versions created using different numbers of signature vibrational modes. The results of the listening test were presented, which suggest that a minimum of 4-7 vibrational modes are required to synthesise the handpan sound, however this number might be reduced if beating correction oscillators are included in the modal synthesis model.

Chapter 6. Conclusion

This chapter concludes this report with a discussion of the project aims defined in Chapter 1, a review of the project management process, and detail of potential future development of the project work.

6.1 Project Aims

This project was concerned with the design and implementation of an experimental procedure to record, analyse, and synthesise the handpan sound. In order to evaluate the success of achieving the project aims defined in Section 1.1, the level of success related to each aim is evaluated below.

To design and implement an experimental procedure to record the handpan sound, and estimate note coupling.

As described previously in Section 4.1, the repeatability of strikes delivered by the NFEM to an individual note-field in a single strike position was confirmed. This provided the ability to produce and compare the measured sounds in the damped and undamped configurations. The differences between undamped and damped signals were clearly seen in both the time and frequency domain, as shown by the figures in Section 4.4.1. On inspection, the undamped signals contained between 3-6 more peaks in the 100 Hz-1.3 kHz region than their corresponding damped signals. The degree of coupling was greater for Instrument 1 than Instrument 3, which was evident due to the higher number of peaks (above +10 dB in the relevant frequency region).

To demonstrate identification of the signature handpan sound including vibrational modes for individual notes, corresponding decay rates, and beating characteristics.

Section 4.2 detailed the identification method of the handpan's signature vibrational modes, decay rates, and beating characteristics. This was done by analysing a single EDR frame to extract each mode's frequency value and T60 decay times. Beating (amplitude modulation) rates were calculated by analysing the magnitude envelope of signature vibrational modes. Section 4.4 displayed spectrograms of the undamped and damped handpan sound. On inspection, the beating depth of signature vibrational modes in the undamped spectrogram was reduced in the corresponding damped spectrogram. This supports the hypothesis that some of the signature beating characteristics are due to coupling of note-fields with slightly mismatched tuning of signature vibrational modes. Despite this, some beating characteristics were also observed in spectrograms of damped signals. These could be due to non-linear behaviour within the note area, a slight mismatch in tuning of different sections of the individual note-field, interaction of the note-field with the internote area or one of the "problematic frequencies" of the handpan cavity [33], mentioned in Section 2.1.6.

To estimate the minimum number of vibrational modes required for synthesis of the handpan sound.

The results of a subjective listening test presented in 5.2.2 showed an increase in median similarity rating with increase in number of signature modes (up to 7 modes), apart from the undamped synthesis signals of Instrument 3. These suggest that the experimental measurement, analysis, and synthesis methods used in this project have managed to capture, identify, and reproduce signature components of the handpan sound. The results also showed the highest median similarity ratings for synthesis with 4-7 signature modes and a beating correction oscillator. Therefore, the estimated minimum number of vibrational modes required to synthesise the handpan sound is between 4-7 signature modes. It is likely that greater degrees of similarity will be reported upon implementing a more accurate estimation of the T60 decay times, correction of the T60 decay times for synthesised modes, and inclusion of additional beating correction oscillators.

6.2 Project Management

Due to the nature of the research, which involved the production of media including audio, images, and video, it was decided to run a private blog to share updates with the supervisor. A total of twenty blog posts were produced over eight months (10/06/14-01/02/15), which presented and analysed the development of the NFEM, analysis and synthesis algorithms, and the subjective listening test. All these allowed regular correspondence and updates, as well as frequent generation of short term goals allowing consistent progress to be made throughout the project. Reading permissions to the private blog can be granted upon email request to the author [62].

6.3 Future Development

This section presents potential further development of the project work, including ideas that could be completed to immediately build upon the project work as it currently stands, as well as future work beyond the existing scope of the project that represents further avenues of research following the results of this project.

6.3.1 Further Work

Despite identification of the handpan's signature frequency components, decay rates, and beating characteristics, the methods developed in this project can benefit from further work. This further work is displayed here in order of highest to lowest priority:

- Correction of T60 decay times for synthesised modes.

Section 5.1.1, detailed the synthesis of the decay stage of the handpan sound, identifying the dissimilarity of the synthesised and original T60 decay times, with exception of the highest magnitude detected peak. This was identified as being an error in the calculation

of the decay time constant, τ , as described by Equation 6.1:

$$\tau = \frac{T60}{\log_{10}(1 \cdot 10^{-3})} \quad (6.1)$$

where the decay time constant τ is given by the estimated T60 decay time for the signature mode. The error stems from the fact that the scaling factor of $\log_{10}(1 \cdot 10^{-3})$ was used to determine τ for all signature modes of a given measurement, whereas the scaling factor should have varied depending on the initial magnitude of each individual mode. Equation 6.2 shows calculation of the correct scaling factor for each individual mode:

$$s_{par} = \frac{A_{max} \cdot 10^{-3}}{A_{par}} \quad (6.2)$$

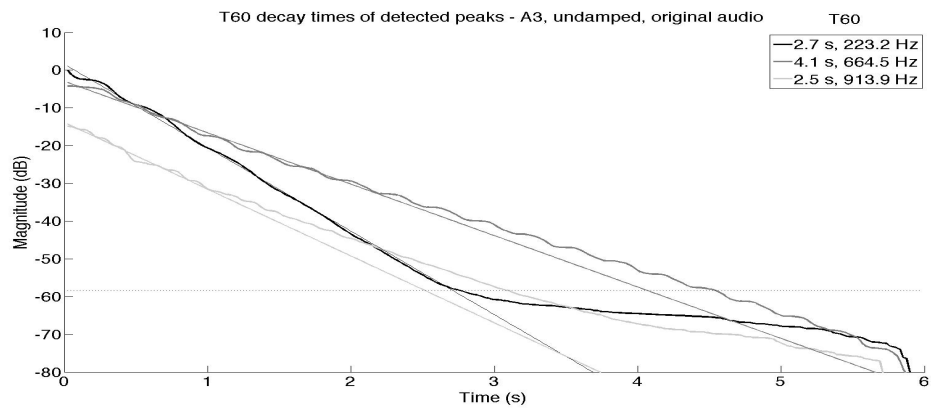
Where s_{par} is the desired scaling factor for the current mode, A_{max} is the initial value of the highest magnitude mode, and A_{par} is the initial magnitude value of the current mode for synthesis. Both A_{max} and A_{par} were converted from dB values as shown in Equation 5.3. Thus the modified equation to calculate the exponential decay time constant, τ , for a given vibrational mode is shown in Equation 6.3:

$$\tau = \frac{T60}{\log_{10}(s_{par})} \quad (6.3)$$

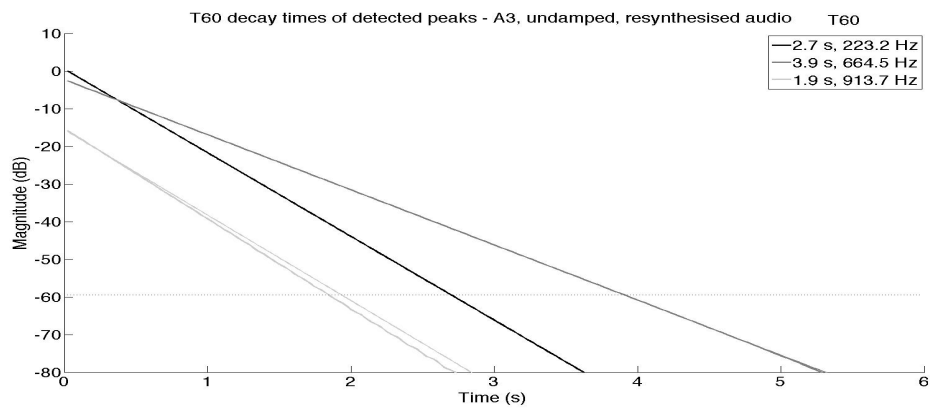
Figure 6.1 shows the decay curves of detected peaks, estimated straight line fits, and calculated T60 decay times for: (a) the original signal; (b) the erroneous impulse response signal; and (c) the corrected impulse response signal of an undamped A_3 handpan signal. Figures 6.1(a) and 6.1(b) were previously shown in Figure 5.2 and are repeated here for clarity. The T60 decay times of 6.1(a) and 6.1(c) are of a higher degree of similarity than 6.1(a) and 6.1(b). T60 decay times for all three signals displayed in Figure 6.1 are shown in Table 6.1.

Audio signal	Mode 1, Freq (Hz)	Mode 1, T60 (s)	Mode 2, Freq (Hz)	Mode 2, T60 (s)	Mode 3, Freq (Hz)	Mode 3, T60 (s)
(a) Original	223.2	2.7	664.5	4.1	913.9	2.5
(b) Erroneous IR	223.2	2.7	664.5	3.9	913.7	1.9
(c) Corrected IR	223.2	2.7	664.5	4.2	913.7	2.6

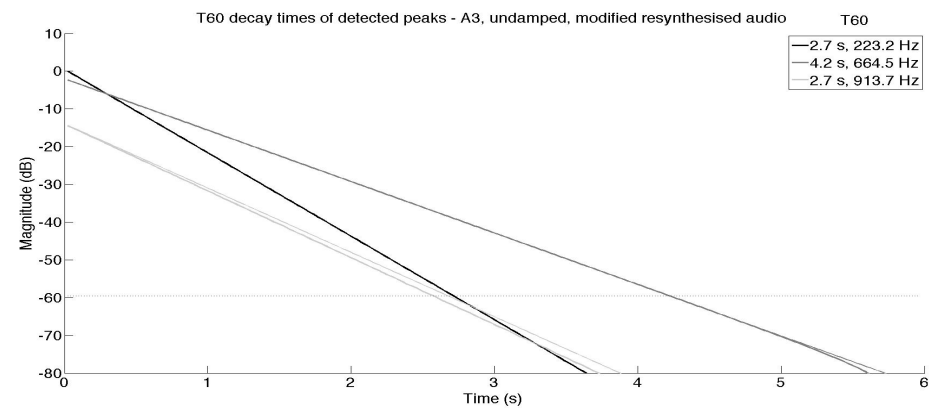
TABLE 6.1: T60 decay times for all three signals displayed in Figure 6.1.



(a)



(b)



(c)

FIGURE 6.1: Decay curves of detected peaks, estimated straight line fits, and calculated T60 decay times for: (a) the original signal; (b) the erroneous impulse response signal; and (c) the corrected impulse response signal of an undamped A₃ handpan signal struck in the ‘D’ sweetspot. (a) and (b) were previously shown in Figure 5.2. T60s of (a) and (c) are of a higher degree of similarity than (a) and (b).

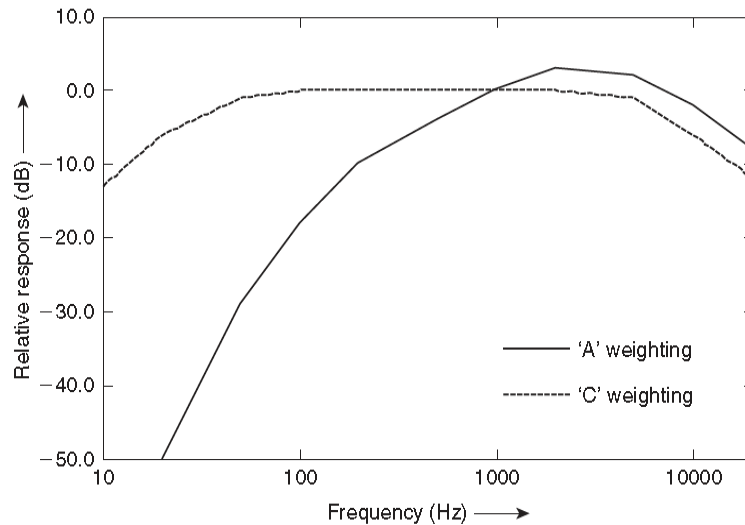


FIGURE 6.2: 'A' and 'C' frequency weightings. 'A' is most appropriate for low amplitude sounds, whilst 'C' is for high amplitude sounds. From [19]

- Improvement of estimated impulse response signal, and initial magnitudes of detected peaks.

A potentially more accurate method for estimating the impulse response signal can be implemented by deconvolving the experimental excitation signal and the measured note-field signal [51], resulting in improved estimation of the initial magnitudes, frequency values, and T60 decay times of each signature vibrational mode. This could be achieved by deconvolving the estimated excitation signal, displayed in Figure 5.3, with the original signal, effectively extracting the estimated impulse response signal.

- Improvement of signature mode detection.

It is well known that sound pressure level does not directly relate to the perceived loudness of a sound [19]. The method of signature vibrational mode detection detailed in Section 4.2, did not take into account the variation of perceived loudness for different frequencies or noise bandwidth. Figure 6.2 displays two types of commonly used frequency weightings, which might be used to increase the accuracy of detection of the handpan's signature modes.

Additionally, a high resolution method, such as ESPRIT [45, 46] can also be used for detection and estimation of modes with closely spaced frequencies and their corresponding damping factors. This high resolution analysis would eliminate the need for the beating correction oscillator detailed in Section 5.1.3. Though using ESPRIT would have provided a higher resolution analysis and therefore more accurate parameter estimation, this high resolution analysis would involve more computations compared to the Fourier methods and spectral analysis techniques detailed in Section 2.2.1 [63]. Thus, using ESPRIT might have been too complex and time consuming to implement within the scope of this work.

- Improvement of the synthesised attack stage, and estimated excitation signal.

Section 5.1.2 detailed the process of convolving the estimated excitation signal with the estimated impulse response signal. As a result of this, the attack stage of the synthesised signal was of a higher degree of similarity to the original handpan signal. Responses from informal listening tests suggest that higher similarity ratings might have been reported following linear summation of the output modal synthesis signal, $y_{rconv}[n]$ in Equation 5.1, with the experimental excitation signal. Audio examples of the result of this summation are available on the data DVD¹. An alternative method for potentially improving the accuracy of the estimated excitation signal, is to deconvolve the signature modes identified in the analysis stage from the original signal, thus extracting a residual signal [51]. This residual can be considered an appropriate signal to represent the excitation in the modal synthesis model.

- Modification of the NFEM.

As mentioned in Section 4.1, successive strikes delivered to an individual note-field in a single strike position using the NFEM were determined to be sufficiently similar for the purposes of this project. The further work to build upon this project would benefit from a method that produces similar strikes delivered to different positions on an individual note-field, as well as similar strikes delivered across different note-fields. This will allow

¹Can be found in the following directory on the DVD: **EyalMSc/Audio/Synthesis/Conclusions**.

a more accurate comparison of measured sound and energy levels across note-fields and instruments. This might be achieved by producing a more flexible method of positioning the NFEM distance and angle relative to the target note-field to increase the similarity of the NFEM's rubber tip velocity when striking the note-field.

The electrical contact method could be used to measure the contact time of the NFEM with the note-field when striking. This is done by attaching foil to the rubber tip and measuring contact time with the metallic (conductive) surface of the handpan [23]. Additionally, velocity transducers could be used in order to measure the velocity of the foil-covered rubber tip, upon exciting the note areas of the handpan. This would assist in producing repeatable strikes across different note areas or sections of an individual note. Finally, this project would benefit from modification of the NFEM to produce at least two levels of strike strength, for example: soft and strong. Analysis of measurements for all notes in both of these playing strengths would give further insight regarding the nature of non-linear note, and note coupling phenomenon.

- Modification of the measurement system.

A measurement microphone was used to record the handpan sounds for this project, as detailed in Section 3.1.4. The experimental method to measure and estimate the signature handpan sound and degree of note coupling might benefit from using velocity transducers in addition to acoustic measurements [23]. As an example, velocity transducers could be placed to measure transverse motion for all note areas simultaneously. This would give insight into the nature of energy transfer from the targeted note to other substructures of the instrument. This is of particular interest when considering the observed onset delay for higher signature modes, like that mentioned previously in Figure 4.10(a). Velocity measurements would also assist in estimating the degree of note coupling between note areas, though electrodynamic vibrator excitation might be more appropriate for this, as the excitation signal can be more accurately modelled or measured.

- Modification of subjective listening tests.

The number of signature vibrational modes required for handpan sound synthesis was estimated at 4-7. Therefore, it would be worth conducting similar listening tests using 4, 5, 6, and 7 synthesis modes to get a better estimation of the minimum number of signature modes required for handpan synthesis.

6.3.2 Future Work

This project has achieved all of the aims defined in Section 1.1, but there is still more work that can be done regarding the analysis and synthesis of the handpan sound. This work could contribute to advancing the field of musical instrument acoustics and synthesis, as well as assist handpan makers in their process of creating higher quality instruments.

- Analysis of the handpan's signature note-field attack stage.

As detailed in Section 5.1.2, attack transients are essential for the discrimination and identification of various musical instruments [59]. Therefore, it is highly desirable to analyse the handpan transient as accurately as possible. The analysis might be achieved by a combination of multi-resolution analysis and adaptive thresholding of the measurements produced in this project in order to facilitate separation of the attack and decay stages [64].

- Analysis of the handpan's interstitial sound.

Section 2.1.6 detailed various handpan playing techniques, such as the percussive strikes delivered to the interstitial area. The sound produced due to striking this area is a short duration transient, and as such analysis of this sound will require a method of transient analysis. It is thought that the timbral qualities of the interstitial strike will depend upon which note-fields are in the immediate surrounding of the interstitial strike position.

- Finite Element Modelling (FEM) of the handpan.

FEM is a powerful yet computationally expensive method for numerically investigating the behaviour of a given system [16]. FEM has previously been used to investigate the steelpan shell vibration [65], mode confinement in the shell [66], and vibrational modes of individual notes [67]. Several finite element models would be beneficial to advancing the knowledge and understanding of the acoustics of the handpan. These include models of an individual handpan note-field, hemispherical note-side shell, hemispherical port-side shell, and a complete handpan including note-fields and port hole. As mentioned in Section 2.1.6, it is thought that all handpans suffer from certain “problematic frequencies” due to internal reflections in the cavity, which can influence the sound of individual note-fields. An FEM model of the handpan cavity might be used to go some way towards confirming or disproving this hypothesis.

- Development of a virtual handpan instrument.

Several Virtual Studio Technology (VST) handpan instruments have been developed recently such as the Alien Drum [68], and Pan Drums [69]. These are sample based synthesisers meaning that they require large file banks, however achieve realistic results. A modal synthesis based virtual handpan instrument would provide a higher degree of control over individual aspects of the sound than sample based instruments, and would reduce the amount of file storage required to function. As an example, the sustain times of individual modes could be lengthened in real time, which is not possible on a sample based instrument unless additional processing is applied. Based on the results of the listening test conducted in this project it is possible that a virtual handpan instrument, controlled in real-time could be designed with a modal synthesis based algorithm using approximately 4-7 oscillators, not including an excitation signal, and beating correction oscillators as described in Section 5.1.3.

Appendices

Appendix A : Data DVD Content

This appendix details the general contents of the accompanying data DVD, and key points on the best way to review the contents.

The contents of the accompanying data DVD are as follows:

1. **EyalMSc/EyalMSc.pdf** - A .pdf version of this document.
2. **EyalMSc/README.txt** - This document details the contents of the data DVD, as well as provides key points on how to best review the data.
3. **EyalMSc/Audio/** - A total of 399 audio files including all measurements, listening test audio files, and four audio files of musical compositions performed on the instruments investigated in this project.
4. **EyalMSc/Code/** - Contains all MATLAB code used to complete the analysis, synthesis, and production of thesis figures.
5. **EyalMSc/Listening_test/** - Contains data from all listening test subjects.
6. **EyalMSc/Video/** - Contains a single video, which demonstrates the experimental procedure to record the signature handpan sound in an anechoic chamber.

Key Points for Reviewing the Data DVD

These are the main points one should be aware of, prior to reviewing the content of the accompanying data DVD:

1. All .m files located in the /Code/ directory should compile and run properly from this directory. AandS.m is the main file that should be used to run the analysis/synthesis system. All other .m files in this directory are related to thesis work or production of figures. Auxiliary code is located in the /Aux/ directory.
2. The /Audio/Measurements/ directory contains all of the recordings made throughout the project. When reviewing the files, it is important to note the following in the file names:
 - the note name (e.g. G3).
 - handpan configuration (noiso = undamped, iso = damped).
 - note field strike position (sdimple = dimple strike, soctave = octave strike, sfifth = perfect fifth strike).
 - strike number (e.g. 2).

/Audio/Synthesis/ contains all files used to conduct the listening tests. The following should be noted:

- the note name (e.g. A3).
 - handpan configuration (noiso = undamped, iso = damped).
 - file type (o = original, and 1/2/3/4/7/10 is the number of signature modes used for Synthesis) (e.g. sdimple = dimple strike, soctave = octave strike).
 - AM indicates files with Beating Correction applied to a single vibrational mode.
3. The /Listening_test/ directory contains .csv files that display results from all subjects in the listening test. list_test_res.csv contains a complete set of responses and question numbers. list_test_res_MAT.csv was used in MATLAB to perform the boxplot analysis. This file contains an edited set of only 21 (out of 23) responses, with no question numbers.

Appendix B : Hang Note Analysis

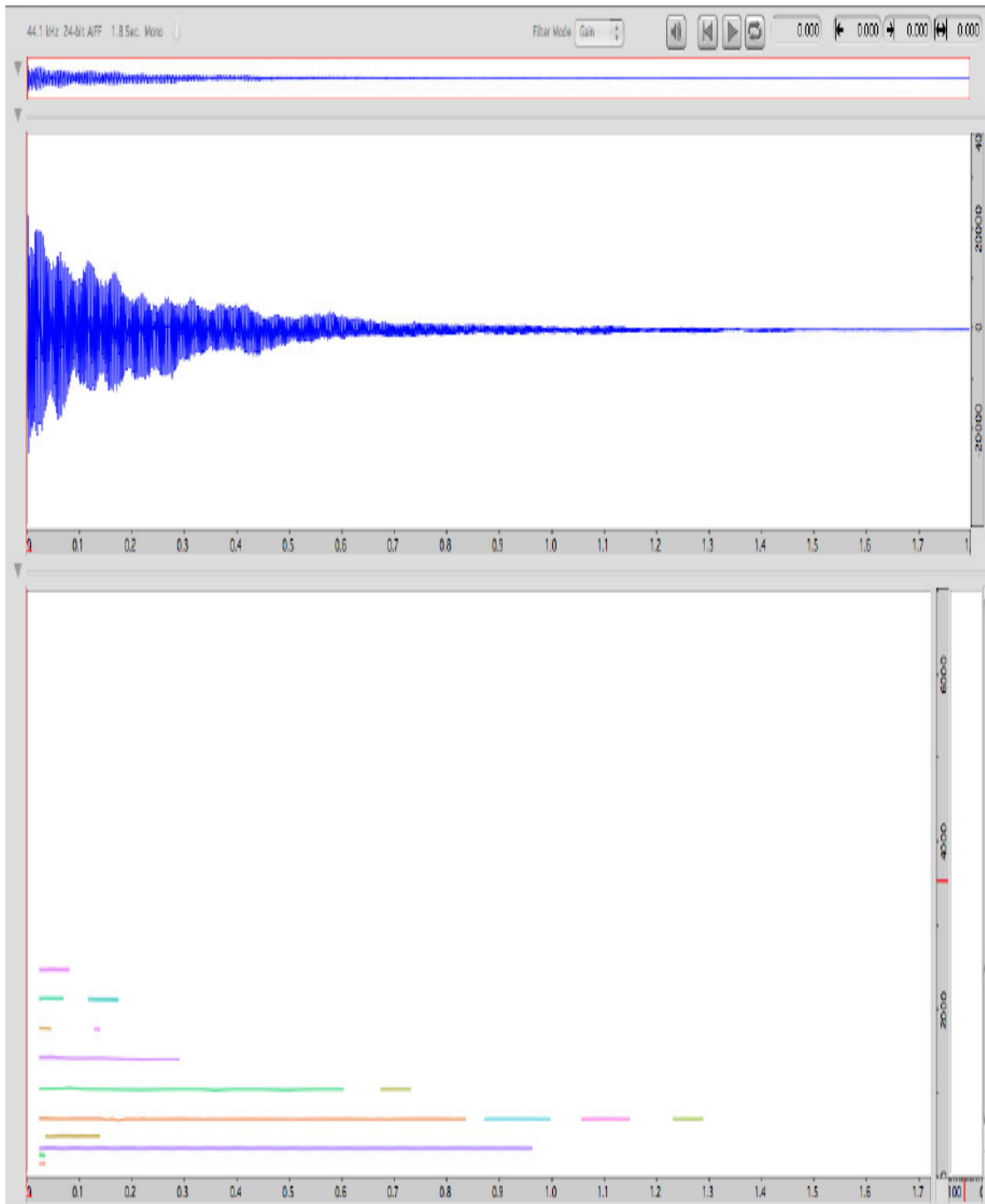


FIGURE 6.3: Waveform and spectrogram analysis of a Hang note played at a strong level.
Adapted from [15]

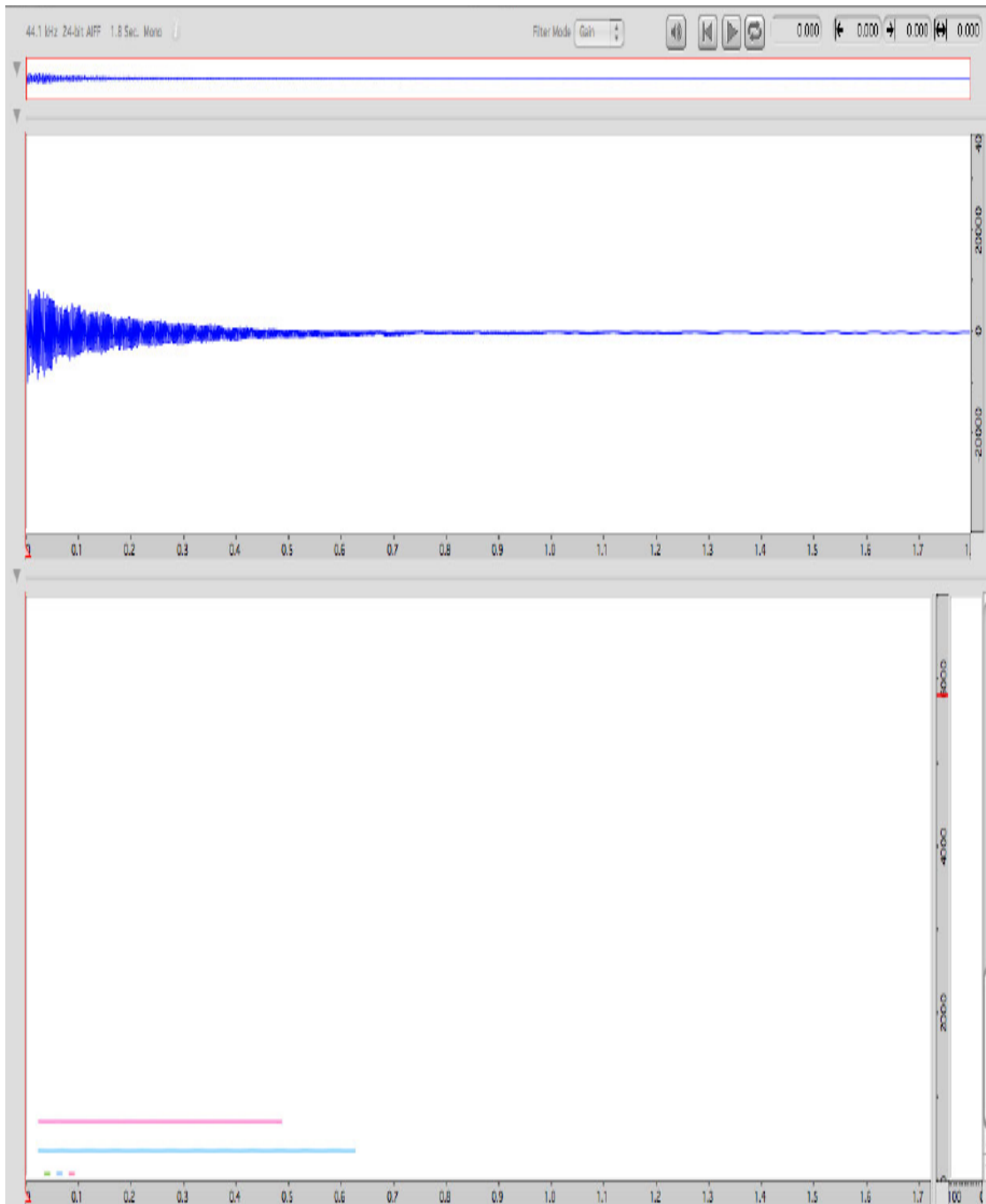


FIGURE 6.4: Waveform and spectrogram analysis of a Hang note played at a soft level. Comparing to Figure 6.3 clearly shows how an increase in playing strength also increases the amount of measured partials and decay times. Amplitude modulations on individual partials are also evident (such as for the higher frequency partials of 6.3). Adapted from [15]

Appendix C : Musical Note Frequencies

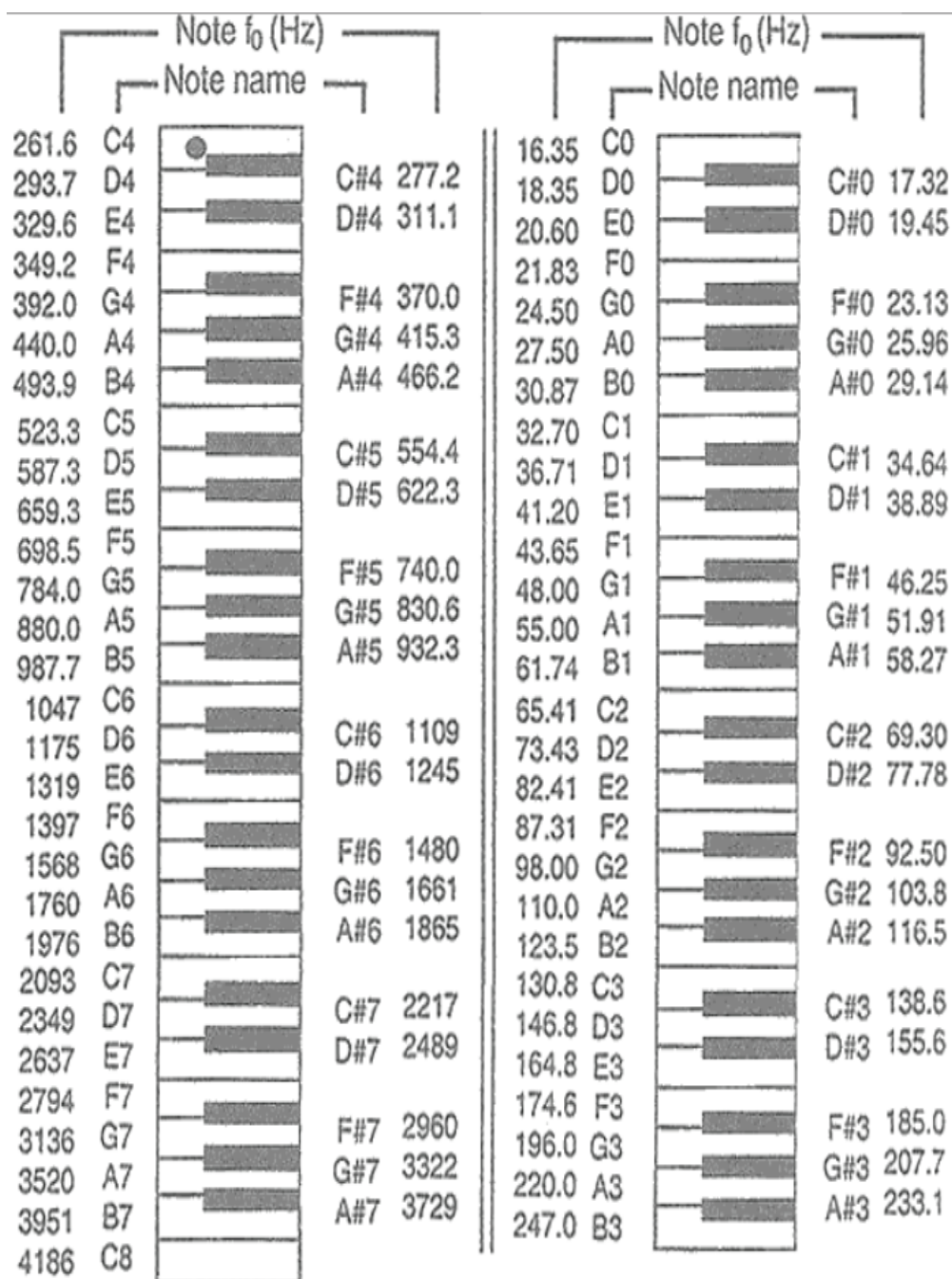


FIGURE 6.5: Musical note names and corresponding frequencies. From [70]

Appendix D : Strike Cross-Correlation

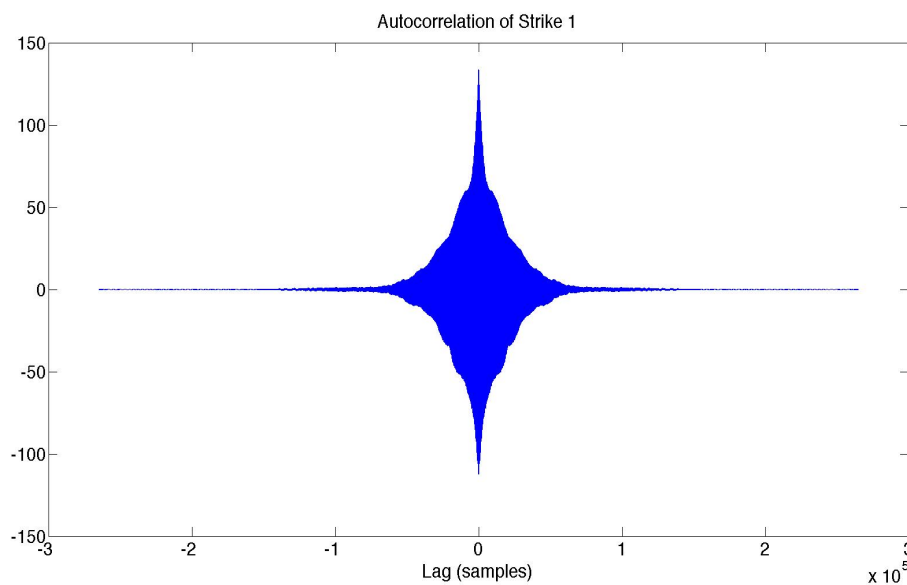


FIGURE 6.6: Autocorrelation of Strike 1, from Figure 4.1, delivered to the 'D' sweetspot of an undamped F#₃ note. Peak calculated at lag sample number 0.

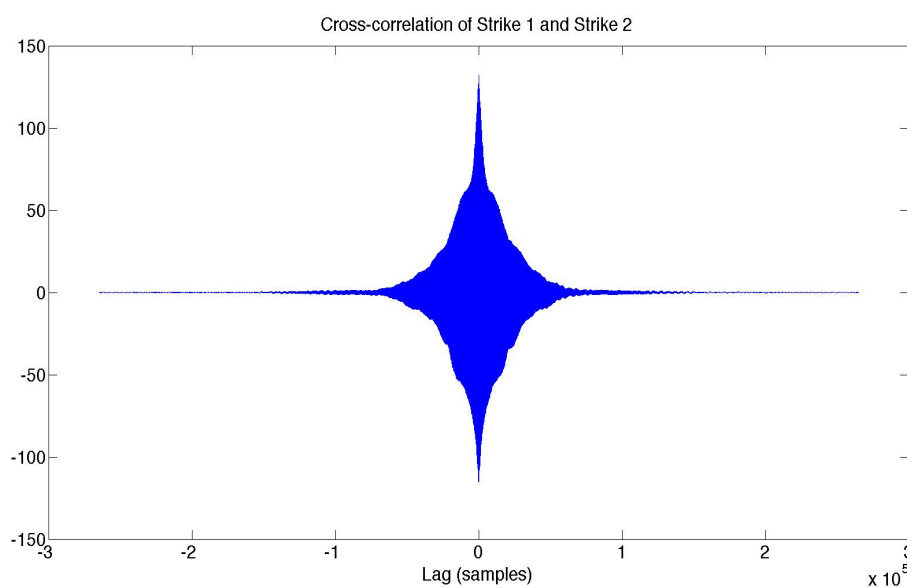


FIGURE 6.7: Cross-correlation of Strike 1 and Strike 2, from Figure 4.1, delivered to the 'D' sweetspot of an undamped F#₃ note. Peak calculated at lag sample number 30.

Appendix E : Signature Vibrational Modes

Note-field	Pk.1 mag. (dB), frequency (Hz), frequency ratio	Pk.2 mag. (dB), frequency (Hz), frequency ratio	Pk.3 mag. (dB), frequency (Hz), frequency ratio	Pk.4 mag. (dB), frequency (Hz), frequency ratio
B ₂	-2.49 126.4 1	-5.09 250.3 1.98	-9.53 616.8 4.88	-10.5 744.4 5.89
F# ₃	-2.85 186.9 1	-9.44 556.9 2.98	-13.6 374.6 2	-18.2 746.4 3.99
A ₃	-2.18 221.8 1	-4.36 663.2 2.99	-15.6 440.2 1.98	-16.4 912.4 4.11
B ₃	-1.85 248.8 1	-5.07 499 2.01	-13 744.1 2.99	-22.6 126.1 0.5
C# ₄	-1.55 280.4 1	-18.1 557.5 1.99	-24.2 437.9 1.56	-27.5 373.5 1.33
D ₄	-0.249 589.8 2	-7.96 295.3 1	-21.4 1178 3.99	-26.7 880.7 2.98
E ₄	-1.61 334.3 1	-3.46 664.5 1.99	-13.6 438.5 1.31	-14.1 283.9 0.85
F# ₄	-1.68 743.5 1.98	-10.6 375 1	-22.5 438.1 1.17	-23 1486 3.96

TABLE 6.2: Highest magnitude peaks, corresponding frequency values, and ratios (relative to the fundamental frequency) of all eight undamped note-fields of Instrument 1 struck in the 'D' sweetspot. Peaks are sorted in order of descending magnitude from left to right.

Note-field	Pk.1 mag. (dB), frequency (Hz), frequency ratio	Pk.2 mag. (dB), frequency (Hz), frequency ratio	Pk.3 mag. (dB), frequency (Hz), frequency ratio	Pk.4 mag. (dB), frequency (Hz), frequency ratio
C ₃	-1.94 134.3 1	-13.6 397.1 2.96	-16.8 731 5.44	-16.9 266.3 1.98
G ₃	-3.16 197.3 1	-4.41 787.2 3.99	-10.3 394.9 2	-24.8 134.4 0.68
Ab ₃	-1.29 211.7 1	-24.9 419.7 1.98	-25.5 625.4 2.95	-28.9 258.1 1.22
B ₃	-1.69 253.2 1	-11.7 501.2 1.98	-26 751.4 2.97	-27.5 134.1 0.52
C ₄	-1.26 262.3 1	-4.66 529.5 2.02	-22.7 1049 4	-28.9 135 0.51
D ₄	-0.966 591.6 1.99	-2.1 297 1	-16.4 882.7 2.97	-19.5 1182 3.98
Eb ₄	-1.94 626.8 2	-1.97 313.6 1	-19.6 1253 4	-24.6 395 1.26
G ₄	-2.03 787.4 1.99	-4.68 395.6 1	-16.6 1181 2.99	-28 1968 4.97

TABLE 6.3: Highest magnitude peaks, corresponding frequency values, and ratios (relative to the fundamental frequency) of all eight undamped note-fields of Instrument 2 struck in the 'D' sweetspot. Peaks are sorted in order of descending magnitude from left to right.

Note-field	Pk.1 mag. (dB), frequency (Hz), frequency ratio	Pk.2 mag. (dB), frequency (Hz), frequency ratio	Pk.3 mag. (dB), frequency (Hz), frequency ratio	Pk.4 mag. (dB), frequency (Hz), frequency ratio
D ₃	-1.89 147.5 1	-7.32 296.2 2.01	-13.5 588.6 3.99	-16 1271 8.62
A ₃	-1.71 220.4 1	-3.08 662 3	-8.44 441.8 2	-12.6 882.8 4.01
A# ₃	-2.26 703.1 2.98	-3 235.1 1	-8.57 467.8 1.98	-28 149.2 0.63
D ₄	-0.255 589 1.99	-21.8 295.5 1	-26.1 882.6 2.99	-37.7 446.5 1.51
E ₄	-0.7 662.3 1.99	-9.42 990 2.98	-14.5 332 1	-19.4 1322 3.98
F ₄	-1.4 701.5 2	-19.8 588.1 1.67	-22 351.6 1	-23.5 1054 3
G ₄	-2 393.9 1	-10.6 786.5 2	-11.6 1178 2.99	-26.7 661.9 1.68
A ₄	-0.702 883.2 1.99	-3.63 442.8 1	-8.69 1325 2.99	-29 590 1.33

TABLE 6.4: Highest magnitude peaks, corresponding frequency values, and ratios (relative to the fundamental frequency) and of all eight undamped note-fields of Instrument 3 (post-tuned) struck in the 'D' sweetspot. Peaks are sorted in order of descending magnitude from left to right.

Note-field	Pk.1 mag. (dB), frequency (Hz), frequency ratio	Pk.2 mag. (dB), frequency (Hz), frequency ratio	Pk.3 mag. (dB), frequency (Hz), frequency ratio	Pk.4 mag. (dB), frequency (Hz), frequency ratio
G ₃	-2.5 201 1	-17.6 398.4 1.98	-20.2 591.4 2.94	-26.9 791.8 3.94
C ₄	-3.69 528.5 1.97	-4.29 267.6 1	-19.4 793 2.96	-25.6 200 0.74
D ₄	-2.4 302 1	-16.7 598.9 1.98	-25.4 490.3 1.62	-31.1 201.6 0.67
E ₄	-2.07 339.4 1	-10.9 670.4 1.98	-26.5 999.3 2.94	-26.8 200.7 0.59
F ₄	-1.14 709.3 1.98	-6.79 358.7 1	-14.9 453.3 1.26	-18.1 1425 3.97
G ₄	-2.26 399.4 1	-3.95 795.5 1.99	-19.3 485.2 1.21	-25.4 201 0.5
A ₄	-2.32 453.3 1	-13.6 896.2 1.98	-21.2 499 1.1	-30.1 201.1 0.44
B ₄	-2.13 499.5 2.49	-30.6 394.2 1.96	-31.5 200.7 1	-33.1 997.5 1.99
C ₅	-1.96 529.3 1.3	-10.8 1057 2.59	-34.6 407.4 1	-35.2 199.6 0.37

TABLE 6.5: Highest magnitude peaks, corresponding frequency values, and ratios (relative to the fundamental frequency) of all nine undamped note-fields of Instrument 4 (pre-tuned) struck in the ‘D’ sweetspot. Peaks are sorted in order of descending magnitude from left to right.

Note-field	Pk.1 mag. (dB), frequency (Hz), frequency ratio	Pk.2 mag. (dB), frequency (Hz), frequency ratio	Pk.3 mag. (dB), frequency (Hz), frequency ratio	Pk.4 mag. (dB), frequency (Hz), frequency ratio
G ₃	-2.8 591.2 2.99	-3.26 197.7 1	-7.8 394.1 1.99	-8.92 785.5 3.97
C ₄	-1.95 525.1 2	-7.76 262.3 1	-13.6 787.5 3.01	-30.6 198 0.76
D ₄	-0.651 591.5 2	-0.714 883.1 2.98	-13.4 296.2 1	-24.7 395.7 1.34
E ₄	-3.37 662 2	-7.87 331.7 1	-11.4 1323 3.99	-21.1 990.7 2.99
F ₄	-0.113 700.7 1.99	-9.39 351.4 1	-17.9 1051 2.99	-20.3 445.2 1.27
G ₄	-1.95 786 1.99	-7.98 394.2 1	-15.6 467.3 1.19	-23.1 525.5 1.33
A ₄	-3.05 882.7 1.99	-3.62 442.7 1	-18.2 1324 2.99	-24.3 2206 4.98
Bb ₄	-2.91 467.2 1	-7.23 936.4 2	-13.1 1403 3	-17.9 525.9 1.13
C ₅	-2.18 525.6 1	-14.3 1052 1.99	-22.9 467.1 0.88	-37.1 1322 2.5

TABLE 6.6: Highest magnitude peaks, corresponding frequency values, and ratios (relative to the fundamental frequency) of all nine undamped note-fields of Instrument 4 (post-tuned) struck in the ‘D’ sweetspot. Peaks are sorted in order of descending magnitude from left to right.

Appendix F : T60 decay times

Note-field	Pk.1 T60 (s),	Pk.2 T60 (s),	Pk.3 T60 (s),
B ₂	2.8	2.1	4.1
F# ₃	2.5	4.7	3.2
A ₃	2.7	4.1	2.5
B ₃	4	5.1	8.9*
C# ₄	3	4	1.7
D ₄	5.9	2.6	2.3
E ₄	2.8	4.6	2
F# ₄	3.8	4	1.8

TABLE 6.7: T60 decay times for all undamped note-fields of Instrument 1 struck in the 'D' sweetspot, which correspond to the three highest magnitude detected peaks in Table 6.2. *Inaccurate estimation

Note-field	Pk.1 T60 (s),	Pk.2 T60 (s),	Pk.3 T60 (s),
C ₃	3.4	4.7	2.4
G ₃	2.7	5	2.6
Ab ₃	2.7	3	3.8
B ₃	2.8	4.3	1.6
C ₄	3	2.3	1.8
D ₄	5.9	3.5	3.7
Eb ₄	5.6	2.9	1.7
G ₄	2.9	4.2	2.2

TABLE 6.8: T60 decay times for all undamped note-fields of Instrument 2 struck in the 'D' sweetspot, which correspond to the three highest magnitude detected peaks in Table 6.3.

Note-field	Pk.1 T60 (s),	Pk.2 T60 (s),	Pk.3 T60 (s),
D ₃	2.2	2.3	2.6
A ₃	2.3	3.3	3.5
A# ₃	1.8	3.1	2.4
D ₄	3.9	2.4	2.8
E ₄	2.1	4	2.9
F ₄	4	2.5	1.6
G ₄	2.6	3.3	3
A ₄	3.2	3.3	1.4

TABLE 6.9: T60 decay times for all undamped note-fields of Instrument 3 (pre-tuned) struck in the ‘D’ sweetspot, which correspond to the three highest magnitude detected peaks in Table 4.1.

Note-field	Pk.1 T60 (s),	Pk.2 T60 (s),	Pk.3 T60 (s),
D ₃	2.1	2.9	2.3
A ₃	2.2	4.3	2.4
A# ₃	4.9	1.9	3.6
D ₄	1.7	1.7	1.9
E ₄	4.7	3.3	1.9
F ₄	2.8	1.8	2.1
G ₄	2.8	3.6	2.6
A ₄	3.7	3	2.3

TABLE 6.10: T60 decay times for all undamped note-fields of Instrument 3 (post-tuned) struck in the ‘D’ sweetspot, which correspond to the three highest magnitude detected peaks in Table 6.4.

Note-field	Pk.1 T60 (s),	Pk.2 T60 (s),	Pk.3 T60 (s),
G ₃	1.9	2	2.6
C ₄	2.8	1.2	2.3
D ₄	2.1	2.5	1.7
E ₄	2	2.6	1.8
F ₄	3.4	2.3	1.8
G ₄	2.2	2.5	2
A ₄	2.1	1.9	1.7
B ₄	2.2	1.5	1.1
C ₅	2.6	1.9	0.87

TABLE 6.11: T60 decay times for all undamped note-fields of Instrument 4 (pre-tuned) struck in the ‘D’ sweetspot, which correspond to the three highest magnitude detected peaks in Table 6.5.

Note-field	Pk.1 T60 (s),	Pk.2 T60 (s),	Pk.3 T60 (s),
G ₃	2.5	1.9	2.1
C ₄	2.8	2	2.6
D ₄	2.9	2.9	1.5
E ₄	2.7	1.7	1.7
F ₄	2.9	1.8	1.8
G ₄	2	2.4	1.8
A ₄	2.5	2	1.7
Bb ₄	1.9	2.3	1.3
C ₅	2.3	1.8	1.3

TABLE 6.12: T60 decay times for all undamped note-fields of Instrument 4 (post-tuned) struck in the ‘D’ sweetspot, which correspond to the three highest magnitude detected peaks in Table 6.6.

Appendix G : Beating Rate Estimation

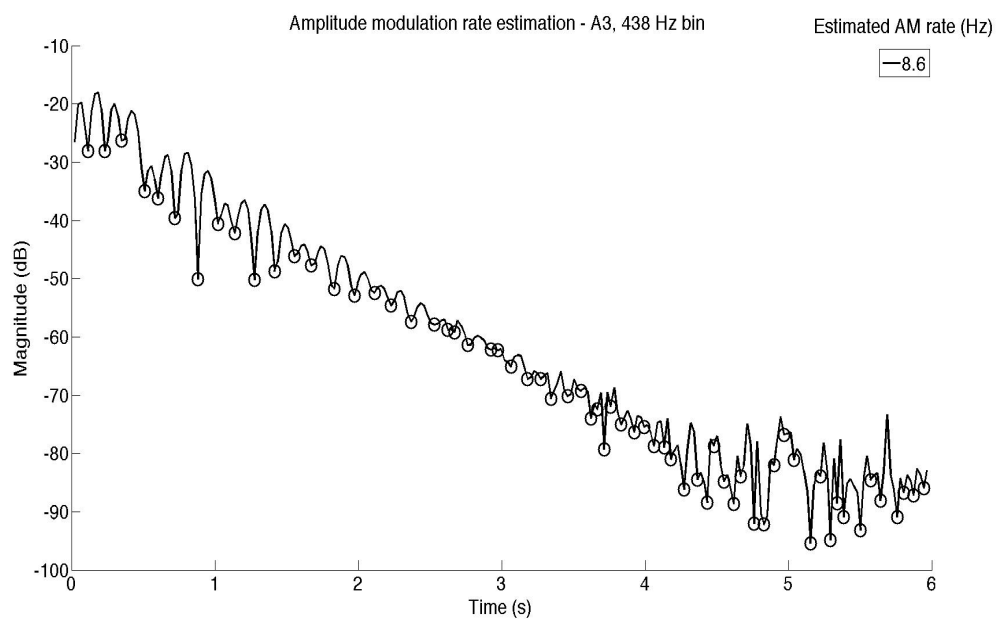


FIGURE 6.8: The 438 Hz amplitude envelope from a spectrogram of the undamped A_3 note-field signal struck in the 'D' sweetspot, with local minima marked with circles.

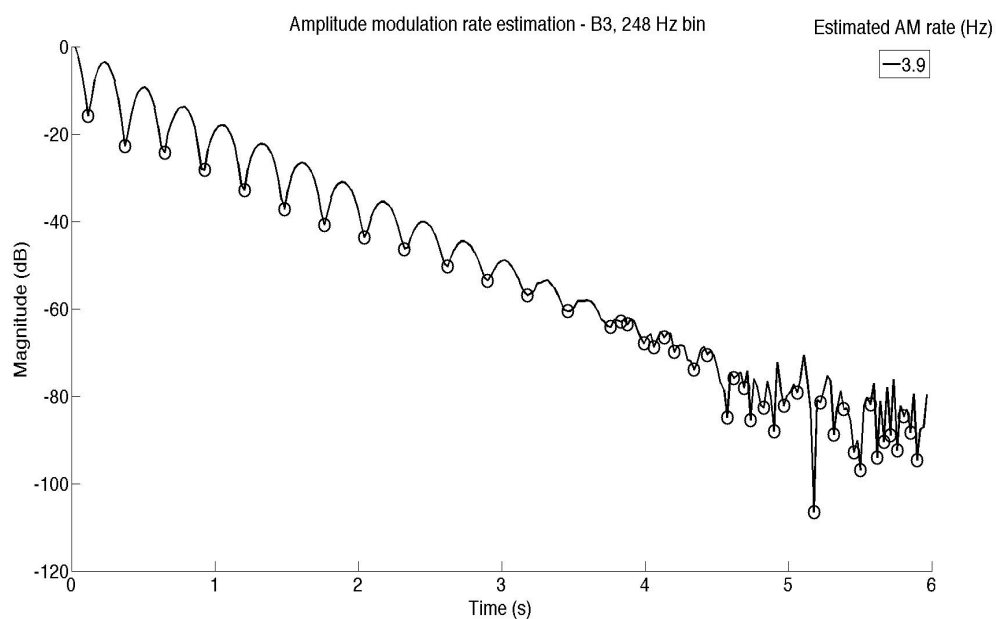


FIGURE 6.9: The 248 Hz amplitude envelope from a spectrogram of the undamped B_3 note-field signal struck in the 'D' sweetspot, with local minima marked with circles.

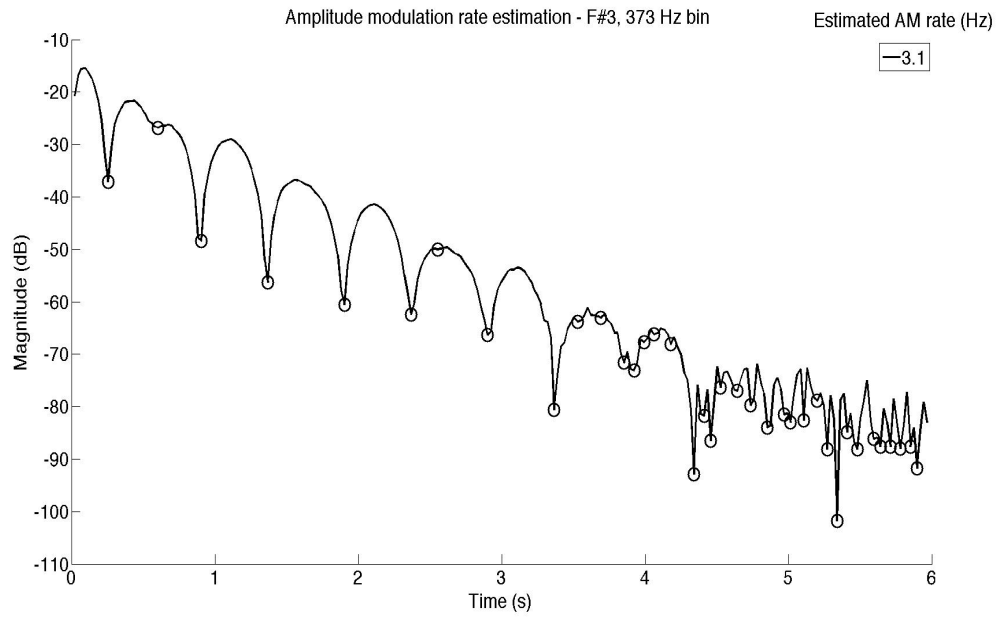


FIGURE 6.10: The 373 Hz amplitude envelope from a spectrogram of the undamped F#₃ note-field signal struck in the ‘D’ sweetspot, with local minima marked with circles.

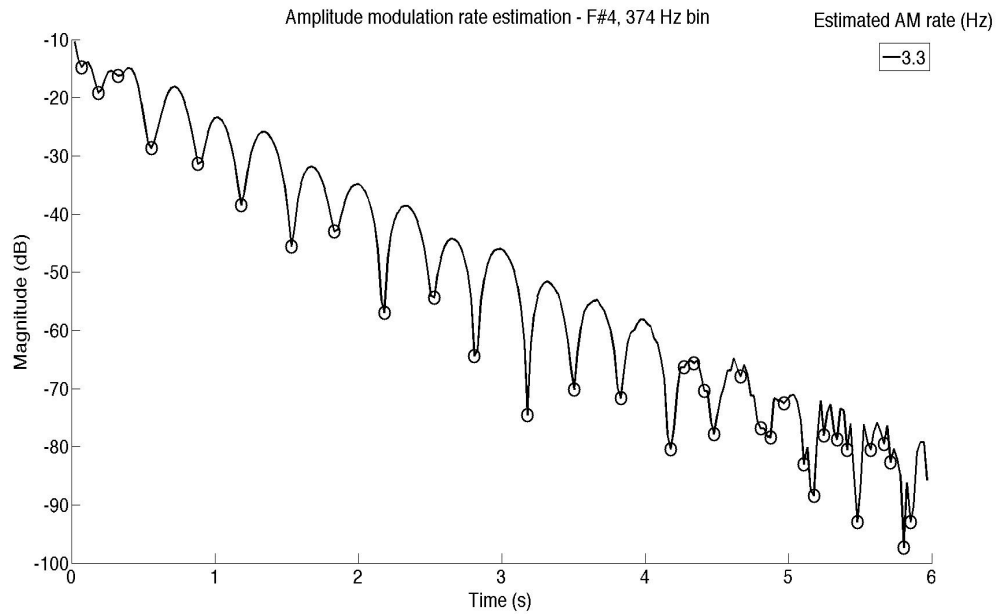


FIGURE 6.11: The 374 Hz amplitude envelope from a spectrogram of the undamped F#₄ note-field signal struck in the ‘D’ sweetspot, with local minima marked with circles.

Appendix H : Multiple Instruments

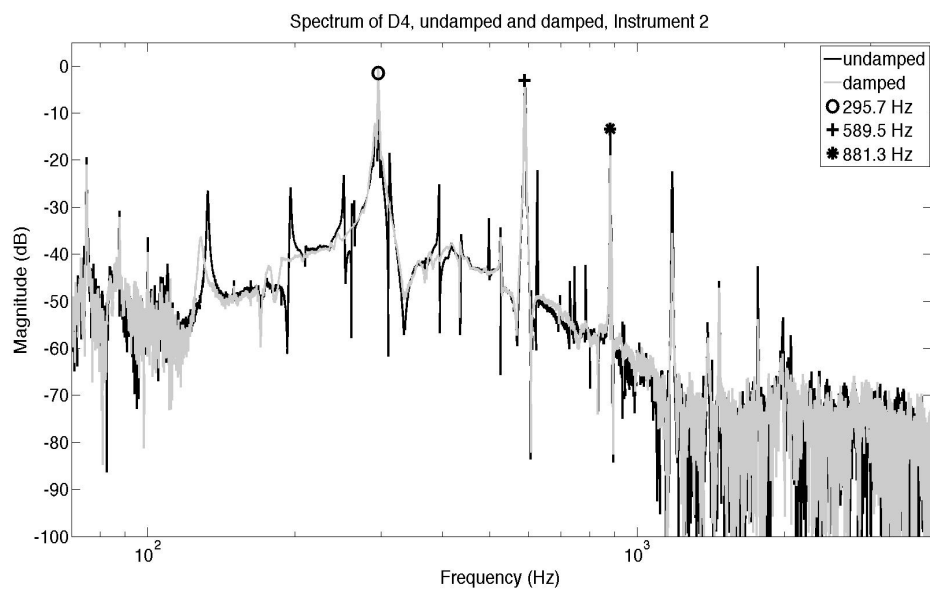


FIGURE 6.12: Spectra of the undamped and damped D₄ note-field for Instrument 2 struck in the 'D' sweetspot.

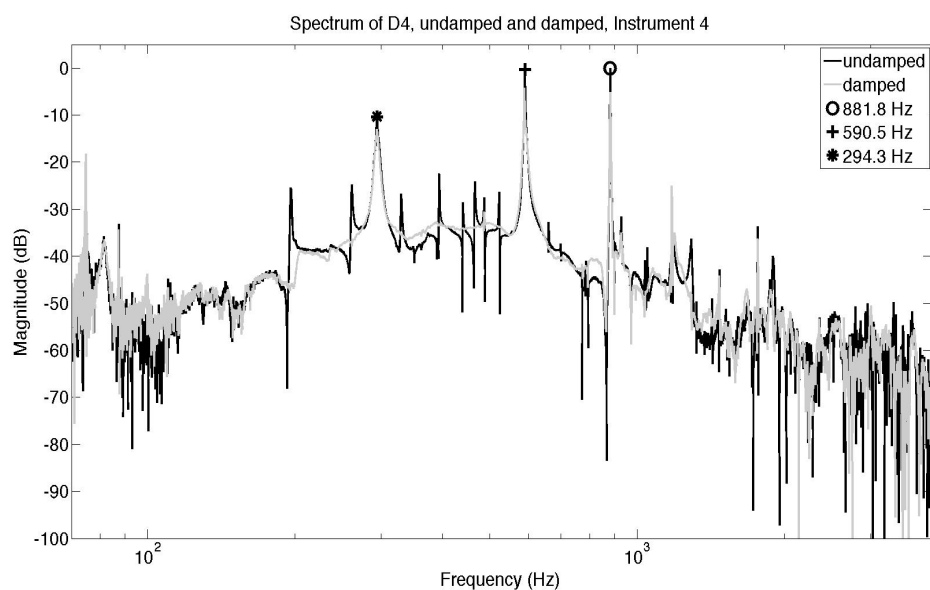


FIGURE 6.13: Spectra of the undamped and damped D₄ note-field for Instrument 4 struck in the 'D' sweetspot.

Appendix I : Listening Test

Physical
Sciences
Ethics
Committee

FAST-TRACK ETHICAL APPROVAL FORM (STUDENTS)

This fast-track system is for taught students only. Research students and staff must complete the full Ethical Approval Form.

If you answer **YES** to any of the following you must complete either this Fast-track ethical approval form, to be signed off by your supervisor, or a full Ethical approval application, to be approved by the Physical Science Ethics Committee (allow at least two weeks for this process).

Note that the outcome of the Fast-track system may result in you needing to complete a full ethical approval application.

Does your project involve any of the following?

Human participants (adults or children)	YES	<input checked="" type="checkbox"/>	NO	<input type="checkbox"/>
Human material (e.g. tissue or fluid samples)	YES	<input type="checkbox"/>	NO	<input checked="" type="checkbox"/>
Human data (e.g. surveys and questionnaires on issues such as lifestyle, housing and working environments, attitudes and preferences)	YES	<input checked="" type="checkbox"/>	NO	<input type="checkbox"/>
Vertebrates, especially mammals and birds	YES	<input type="checkbox"/>	NO	<input checked="" type="checkbox"/>
Any other organisms not previously mentioned	YES	<input type="checkbox"/>	NO	<input checked="" type="checkbox"/>
Military or defence context	YES	<input type="checkbox"/>	NO	<input checked="" type="checkbox"/>
Funding sources with potential to adversely affect existing relationships or bring the University or Department into disrepute.	YES	<input type="checkbox"/>	NO	<input checked="" type="checkbox"/>
Restrictions on dissemination	YES	<input type="checkbox"/>	NO	<input checked="" type="checkbox"/>
Overseas countries under regimes with poor human rights record or identified as dangerous by the Foreign & Commonwealth Office	YES	<input type="checkbox"/>	NO	<input checked="" type="checkbox"/>
Applications that could potentially involve unethical practice, including potential dual-use applications which could be unethical	YES	<input type="checkbox"/>	NO	<input checked="" type="checkbox"/>

Students: you should discuss the ethical considerations of your project with your project supervisor and, if necessary, fill in a full ethics form to be submitted to the Physical Sciences Ethics Committee.

Supervisors: Please ensure you are familiar with the University's 'Code of practice and principles for good ethical governance' in order to guide your student effectively. Please seek

THE UNIVERSITY of York

FIGURE 6.14: The ethical approval process required prior to commencing the listening tests. Page 1.

guidance from the Departmental Ethics Officer if you are uncertain about any ethical issue arising from this application.

FAST-TRACK ETHICAL APPROVAL FORM (STUDENTS)

Project Information:

Student Name: Eyal Alon

Course Title: MSc by Research

Tick one box:

Undergraduate project Postgraduate project

Undergraduate module assignment Postgraduate module assignment

Other (Please state.....)

Title of project: Analysis and Simulation of the acoustics of the handpan

Project supervisor / module leader name: Dr. Damian Murphy

Protocol:

	<i>If you answer yes to any of the following, this must be explicit in any supporting literature (e.g. consent forms, information sheets and questionnaires)</i>	YES	NO	N/A
1	Will you describe the procedures to participants in advance, so that they are informed about what to expect?	✓		
2	Will you tell participants that their participation is voluntary?	✓		
3	Will you inform the participants of the purpose / background of the study?	✓		
4	Will you obtain written consent for participation?	✓		
5	If the research is observational, will you ask participants for their consent to being observed?			✓
6	Will you tell participants that they may withdraw from the research at any time and for any reason?	✓		
7	With questionnaires and interviews will you give participants the option of omitting questions they do not want to answer?			✓
8	Will you tell participants that their data will be treated with full confidentiality and that, if published, it will not be identifiable as theirs?	✓		

a): If you answer NO to any of the following you must submit a full ethical approval form

FIGURE 6.15: The ethical approval process required prior to commencing the listening tests. Page 2.

Physical
Sciences
Ethics
Committee

Protocol:

b): If you answer **YES** to any of the following you must submit a full ethical approval form.

		YES	NO	N/A
9	Is your study designed to be challenging/disturbing (physically or psychologically)?		✓	
10	Will you deliberately mislead your participants?		✓	
11	Does your study involve taking bodily samples?		✓	
12	Is your study physically invasive?		✓	
13	Is there any obvious or inevitable adaptation of your research findings to ethically questionable aims?		✓	
14	Could the methodologies or findings of your study damage the reputation of the University of York?		✓	

Health and Safety:
Please identify any risks to the participants and state any precautions you will take to ensure their health and safety:

1. Hearing damage - proper calibration of individual listening levels prior to commencing survey.

Participants: If you answer **YES** to any of the following you must submit a full ethical approval form. If you have ticked **YES** to 15 and your participants are **patients**, in addition to the full ethical application you must follow the Guidelines for Ethical Approval of NHS Projects.

THE UNIVERSITY of York

FIGURE 6.16: The ethical approval process required prior to commencing the listening tests. Page 3.

Physical
Sciences
Ethics
Committee

		YES	NO	N/A	
15	Does your project involve work with animals		✓		
16	Will any of the participants be from one of the following vulnerable groups? Note that you may also need to obtain satisfactory DBS clearance (or equivalent for overseas students)	Children under 18			
		People with learning difficulties			
		People who are unconscious or severely ill		✓	
		NHS patients			
		Other vulnerable groups (specify)			

Data Protection: If you answer **NO** to any of the following you must submit a full ethical approval form

		YES	NO	N/A
17	Any personal / sensitive data will be stored in password protected folders on computers.	✓		
18	Any hard copies of personal data (including consent forms) will be stored in a secure place.	✓		
19	Only the student and supervisors will have access to the data generated from the study. (The supervisor may share the anonymised data with other researchers at the University of York)	✓		
20	The data will be preserved beyond the study in line with University policy and will be placed in the custody of the supervisor at the end of the project.	✓		
21	All data will be anonymised prior to analysis. Please state your method of anonymisation: Survey results files will be numbered and saved in a password protected file folder. Consent forms will be numbered accordingly	✓		

FOR THE STUDENT TO COMPLETE:

Please complete and sign the following section and submit to your supervisor alongside any supporting documentation (this includes consent forms, information sheets and questionnaires where necessary).

Provide a brief summary of the participants and procedures of your project (max 100 words)

THE UNIVERSITY of York

FIGURE 6.17: The ethical approval process required prior to commencing the listening tests. Page 4.

Physical
Sciences
Ethics
Committee

Participants must have a background in Music Technologies and critical listening, for this listening test. It will take under 20 minutes to complete. Each question will be answered by rating the similarity of the synthesised audio files to the reference audio file.

I have considered the ethical implications of this project and have identified no significant ethical implications requiring a full ethics submission to the Physical Sciences Ethics Committee

I have included all relevant paperwork (e.g. consent form, information sheet, questionnaire/interview schedules) with this application

Signed..... *[Signature]* Print name Eyal Alon Date 16/01/15
(Student)

FOR THE SUPERVISOR TO COMPLETE:
By signing this form you are taking responsibility for the ethical conduct of this project

The student has taken all reasonable steps to ensure ethical practice in this study and I can identify no significant ethical implications requiring a full ethics submission to the Physical Sciences Ethics Committee

I have checked and approved all relevant paperwork required for this proposal

STATEMENT OF ETHICAL APPROVAL

This project has been considered using the Physical Sciences Ethics Committee Fast-track ethical approval procedure, agreed by the Physical Sciences Ethics Committee of the University of York, and is now approved.

Signed..... DT Murphy Print name Damian Murphy Date 19/1/2015
(Supervisor/Module leader)

THE UNIVERSITY of York

FIGURE 6.18: The ethical approval process required prior to commencing the listening tests. Page 5.

Thank you for agreeing to participate in this listening test! The test will last around 20 minutes. Your participation in this test is voluntary. You may withdraw from the test at any time and for any reason by notifying the principal investigator. The data gathered in this test will be treated with full confidentiality and if published, will not be identifiable as yours.

Prior to the test beginning, the principal investigator will adjust the headphone volume to a level that is comfortable for you and within safe limits. Please do not adjust the volume once the test is underway.

This test is investigating the similarity of synthesised handpan sounds to a reference sound. You will be played a number of synthesised handpan sounds and asked to rate how similar they sound to the reference sound.

You will be presented with 18 questions (there will also be two training questions at the start to familiarise you with the procedure).

For each question, you will be presented with five audio samples. Please play them as many times as you would like. You will then be asked to rate the similarity of each of the five samples to the reference sound on a continuous scale of 0 to 10. There is also a comment box at the bottom of every page if you would like to justify your answers or comment on anything - please note that leaving a comment is optional!

On the next page you will be asked to provide your age and gender. This information is to ensure that a suitable population sample is used. All test responses will be stored anonymously on a University of York computer for research purposes only.

Please ensure you have read and understood the following statements before continuing:

- I have read and understood the test explanation and agree to comply with all instructions given during the test.
- I give my consent for my answers in this survey to be used for research purposes, including (but not limited to) publication in journals and presentation at conferences and public engagement events. I agree that I will not seek to restrict the use of the results provided my anonymity is preserved.
- I understand that I am free to withdraw from the test at any time and for any reason.

Please tick the box below to confirm that you have read the above statements and agree to them.

I agree to the statements above.

Please tick the box below to confirm that you are over 18.

I confirm that I am over 18.

>>

FIGURE 6.19: The subject information statements were filled by each participant prior to completing the listening test. Page 1.

References

- [1] F. Rohner. Letter of appreciation to Samsung Electronics Ltd. Co., [Accessed: 25/04/15], . URL <http://www.hang.ch/en/news/category/news>.
- [2] F. Rohner and S. Schärer. Newsletter PANArt, May 19th, [Accessed: 25/04/15], . URL <http://www.hangblog.org/newsletter-panart-may-19th-2010/>.
- [3] F. Rohner and S. Schärer. History, Development and Tuning of the HANG. *ISMA 2007*, .
- [4] swissinfo.ch - Jessica Dacey. Life-changing, a chimera or just a drum?, [Accessed: 25/04/15]. URL <http://www.swissinfo.ch/eng/life-changing--a-chimera-or-just-a-drum-/38515012>.
- [5] M. Delago. Manu Delago - Projects, [Accessed: 25/04/15]. URL <http://www.manudelago.com/eng/projects.htm>.
- [6] F. Rohner. PANArt's offer to the metal sound sculptors, [Accessed: 25/04/15], . URL <http://www.hang.ch/en/news/category/panarts-offerte-an-blechklangplastiker>.
- [7] What is a Halo? What is a Genesis, Cirrus, and Stratus, [Accessed: 25/04/15]. URL http://www.pantheonsteel.com/FAQ.aspx#What_is_the_Halo__exactly_.
- [8] C. Foulke. CFoulke, [Accessed: 25/04/15]. URL <http://www.cfoulke.com>.
- [9] Zen Handpans. Zen Handpans, [Accessed: 25/04/15]. URL <http://zenhandpans.com>.
- [10] Saraz. Saraz Handpans, [Accessed: 25/04/15]. URL <http://sarazhandpans.com>.

- [11] Symphonic Steel. Symphonic Steel Hand Pan Creation, [Accessed: 25/04/15]. URL <http://www.symphonicsteel.com>.
- [12] Dave's Island Instruments. Dave's Island Instruments - Handpans, [Accessed: 25/04/15]. URL <http://www.davesislandinstruments.com/Catalog.aspx?CategoryID=94>.
- [13] florianbetz. HandPan.org - Pantam Questions about Name, [Accessed: 25/04/15]. URL <http://www.handpan.org/forum/viewtopic.php?f=26&t=12382>.
- [14] T.D. Rossing A. Morrison U. Hansen F. Rohner and S. Schärer. ACOUSTICS OF THE HANG: A hand-played steel instrument. *ISMA 2007*.
- [15] D. Wessel A. Morrison and T.D. Rossing. Sound of the HANG. *Proceedings of Meetings on Acoustics*, 4(1):035002, 2008, [Accessed: 25/04/15]. URL <http://scitation.aip.org/content/asa/journal/poma/4/1/10.1121/1.3068630>.
- [16] V. Välimäki J. Pakarinen C. Erkut and M. Karjalainen. Discrete-time modelling of musical instruments. *Reports on Progress in Physics*, 69(1):1, 2006, [Accessed: 25/04/15]. URL <http://stacks.iop.org/0034-4885/69/i=1/a=R01>.
- [17] OnMusic Dictionary. Hornbostel-Sachs, 2015, [Accessed: 25/04/15]. URL <http://dictionary.onmusic.org/terms/1731-hornbostel-sachs>.
- [18] T.D. Rossing. *Science of Percussion Instruments*. World Scientific Publishing Co Pte Ltd, 2000. ISBN 9810241585.
- [19] D.M. Howard and J. Angus. *Acoustics and Psychoacoustics*. Focal, 2009. ISBN 9780240521756, [Accessed: 25/04/15]. URL <http://books.google.co.il/books?id=qgsst20QYJEC>.
- [20] Wikipedia. Hang (instrument) — Wikipedia, The Free Encyclopedia, [Accessed: 25/04/15], . URL [http://en.wikipedia.org/w/index.php?title=Hang_\(instrument\)&oldid=640832394](http://en.wikipedia.org/w/index.php?title=Hang_(instrument)&oldid=640832394).

- [21] Wikipedia. Struck idiophone — Wikipedia, The Free Encyclopedia, [Accessed: 25/04/15], . URL http://en.wikipedia.org/wiki/Struck_idiophone#Directly_struck_.28111.29.
- [22] N.H. Fletcher and T.D. Rossing. *The Physics of Musical Instruments*. Springer, 1998. ISBN 9780387983745, [Accessed: 25/04/15]. URL <http://books.google.co.uk/books?id=9CRSRYQ1RLkC>.
- [23] A. Achong. *Secrets of the Steelpan*. Xlibris Corporation, 2013. ISBN 9781483634845.
- [24] T.D. Rossing and N.H. Fletcher. Nonlinear vibrations in plates and gongs. *The Journal of the Acoustical Society of America*, 73(1), 1983.
- [25] K.A. Legge and N.H. Fletcher. Nonlinearity, chaos, and the sound of shallow gongs. *The Journal of the Acoustical Society of America*, 86(6), 1989.
- [26] A. Chaigne C. Touze and O. Thomas. Nonlinear vibrations and chaos in gongs and cymbals. *Acoustical Science and Technology*, 26(5):403–409, 2005. doi: 10.1250/ast.26.403.
- [27] A. Achong. THE STEELPAN AS SYSTEM OF NON-LINEAR MODE-LOCALIZED OSCILLATORS, I: THEORY, SIMULATIONS, EXPERIMENTS AND BIFURCATIONS. *Journal of Sound and Vibration*, 197(4):471 – 487, 1996. ISSN 0022-460X. doi: <http://dx.doi.org/10.1006/jsvi.1996.0543>,{[Accessed:25/04/15]}. URL <http://www.sciencedirect.com/science/article/pii/S0022460X9690543X>.
- [28] U.J. Hansen and T.D. Rossing. The Caribbean Steelpan, and some Offsprings. *Forum Acusticum 2005*.
- [29] T.D. Rossing and U.J. Hansen. Vibrational mode shapes in caribbean steelpans: Part ii: cello and bass. *Applied Acoustics*, 65(12):1233 – 1247, 2004. ISSN 0003-682X. doi: <http://dx.doi.org/10.1016/j.apacoust.2004.04.009>,{[Accessed:25/04/15]}. URL <http://www.sciencedirect.com/science/article/pii/S0003682X04001070>.

- [30] J. Wolfe. Helmholtz Resonance, [Accessed: 25/04/15]. URL <http://newt.phys.unsw.edu.au/jw/Helmholtz.html>.
- [31] U. Zoelzer. *Dafx: Digital Audio Effects*. John Wiley & Sons, Inc., New York, NY, USA, 2002. ISBN 0471490784.
- [32] HandPan.org - The place for HandPan Players, [Accessed: 25/04/15]. URL <http://www.handpan.org/forum/index.php>.
- [33] broussel2. HandPan.org - Basic sound structure of a handpan, [Accessed: 25/04/15]. URL <http://www.handpan.org/forum/viewtopic.php?f=6&t=11424&start=0&hilit>.
- [34] Justin@SRH. HandPan.org - Sacred Rhythm Prototype Handpans, [Accessed: 25/04/15]. URL <http://www.handpan.org/forum/viewtopic.php?f=23&t=9670&start=24>.
- [35] C. Foulke. Singing Steel Enthusiast - Projects, [Accessed: 25/04/15], 2012. URL <http://www.handpanfan.com/Projects.html>.
- [36] D. Kuckhermann. World Percussion - THE PANART HANG (DRUM) AND HANDPANS, [Accessed: 25/04/15]. URL <http://worldpercussion.net/instruments/panart-hang-and-handpans/>.
- [37] YouTube - Colin Foulke. Preview - Intermediate to Advanced Handpan Techniques DVD Tutorial, [Accessed: 25/04/15]. URL <https://www.youtube.com/watch?v=qs-wnRpWnAo>.
- [38] J.O. Smith. Mathematics of the Discrete Fourier Transform (DFT), [Accessed: 25/04/15], . URL <http://ccrma.stanford.edu/~jos/mdft/>.
- [39] J.O. Smith. Physical Audio Signal Processing, [Accessed: 25/04/15], . URL <https://ccrma.stanford.edu/~jos/pasp/>.
- [40] J.O. Smith. Spectral Audio Signal Processing, [Accessed: 25/04/15], . URL <https://ccrma.stanford.edu/~jos/sasp/>.

- [41] LDS-group. Understanding FFT Windows, Universität Würzburg, [Accessed: 25/04/15]. URL <http://www.physik.uni-wuerzburg.de/~praktiku/Anleitung/Fremde/AN014.pdf>.
- [42] G. Heinzel, A. Rudiger, and R. Schilling. Spectrum and spectral density estimation by the Discrete Fourier transform (DFT), including a comprehensive list of window functions and some new flat-top windows. pages Max–Planck–Institut für Gravitationsphysik, 2002.
- [43] J.O. Smith and X. Serra. *PARSHL: An analysis/synthesis program for non-harmonic sounds based on a sinusoidal representation*. CCRMA, Department of Music, Stanford University, 1987.
- [44] J. Wells. Reading the Sines: Sinusoidal Identification and Description using the Short Time Fourier Transform. *Music Technology Forum: Time-Frequency Analysis for Audio*, pages 1–12, apr 2004.
- [45] R. Roy and T. Kailath. ESPRIT-estimation of signal parameters via rotational invariance techniques. *IEEE Transactions on Acoustics, Speech, and Signal Processing*, 37(7):984–995, July 1989.
- [46] J. Carrou, F. Gautier, and R. Badeau. Theoretical and experimental investigations of harp’s sympathetic modes. *Proc. of International Congress on Acoustics (ICA)*, 2007.
- [47] S. Bilbao. *Numerical Sound Synthesis: Finite Difference Schemes and Simulation in Musical Acoustics*. Wiley, 2009. ISBN 9780470749029, [Accessed: 25/04/15]. URL <http://books.google.ca/books?id=3q5nGRd4UysC>.
- [48] X. Serra and J.O. Smith. Spectral modeling synthesis: A sound analysis/synthesis system based on a deterministic plus stochastic decomposition. *Computer Music Journal*, pages 12–24, 1990.
- [49] V. Välimäki and T. Takala. Virtual musical instruments — natural sound using physical models. *Organised Sound*, 1(02):75–86, 2000.

- [50] J.O. Smith. Virtual Acoustic Musical Instruments: Review and Update . *Centre for Computer Research in Music and Acoustics (CCRMA)*, .
- [51] P. Cook. *Real Sound Synthesis for Interactive Applications*. A K Peters/CRC Press, 2002.
- [52] M. Lagrange, G. Scavone, and P. Depalle. Time-domain Analysis/Synthesis of the Excitation Signal in a Source/Filter Model of Contact Sounds. *Proceedings of the 14th International conference on auditory display*, 2008.
- [53] Z. Ren, H. Yeh, and M. Lin. Example-Guided Physically Based Modal Sound Synthesis. *ACM Transactions on Graphics (TOG) 2013*. URL http://gamma.cs.unc.edu/AUDIO_MATERIAL/.
- [54] A. Morrison and T.D. Rossing. The extraordinary sound of the hang. *Physics Today*.
- [55] Earthworks - High definition microphones. M30 - 30kHz omni measurement microphone, [Accessed: 25/04/15]. URL <http://www.earthworksaudio.com/microphones/m-series/m30/>.
- [56] U. Kronman. *Steel pan tuning: a handbook for steel pan making and tuning*. Musikmuseets skrifter. Musikmuseet, 1992, [Accessed: 25/04/15]. URL <http://books.google.co.uk/books?id=PGMJJAQAAMAAJ>.
- [57] M. Beale. sumsqr.m, [Accessed: 25/04/15]. URL http://uk.mathworks.com/matlabcentral/fileexchange/47767-libpls-1-95-zip/content/libPLS_1.95/sumsqr.m.
- [58] MathWorks. Matlab Documentation - polyfit, [Accessed: 25/04/15]. URL <http://uk.mathworks.com/help/matlab/ref/polyfit.html>.
- [59] F. Keiler, C. Karadogan, U. Zölzer, and A. Schneider. Analysis of Transient Musical Sounds by Auto-Regressive Modeling. *Proc of 6th Int Conf on Digital Audio Effects (DAFx'03)*, 2003.

- [60] ITU. Method for the subjective assessment of intermediate quality level of coding systems, [Accessed: 25/04/15]. URL http://www.itu.int/dms_pubrec/itu-r/rec/bs/R-REC-BS.1534-1-200301-S!!PDF-E.pdf.
- [61] S. Bech and N. Zacharov. *Perceptual audio evaluation-Theory, method and application*. John Wiley & Sons, 2007.
- [62] E. Alon. Eyal's MSc Blog, [Accessed: 25/04/15]. URL <http://eyalmsc.blogspot.co.uk>. Please send email to author (ea553@york.ac.uk) to be included on the blog readers list.
- [63] J. Laroche and J.L. Meillier. Multichannel excitation/filter modeling of percussive sounds with application to the piano. *IEEE TRANSACTIONS ON SPEECH AND AUDIO PROCESSING*, 2, 1994.
- [64] C. Duxbury, M. Davies, and M. Sandler. Separation of transient information in musical audio using multiresolution analysis techniques. In *Proceedings of the COST G-6 . . .*, 2001.
- [65] D. Gay. Finite Element Modelling of Steelpan Shell Vibration. pages 1–19, October 2002.
- [66] S.E. Maloney, C.Y. Barlow, and J. Woodhouse. A study of mode confinement in Caribbean steel drums. *15th International Congress on sound and vibration*, 2008.
- [67] J. Bridge. THE VIBRATIONAL MODES OF THE NOTES OF THE TENOR STEELPAN- A FINITE ELEMENT STUDY. pages 1–8, January 2006.
- [68] 8dio.com. The New Alien Drum VST, [Accessed: 25/04/15]. URL <http://8dio.com/instrument/alien-drum/>.
- [69] Soniccouture. Pan Drums, [Accessed: 25/04/15]. URL <http://www.soniccouture.com/en/products/26-percussion/g29-pan-drums/>.
- [70] C Fielding. College of Santa Fe Auditory Theory, [Accessed: 26/04/15]. URL http://www.feilding.net/sfuad/musi3012-01/images/lectures/equal_temperament.gif.